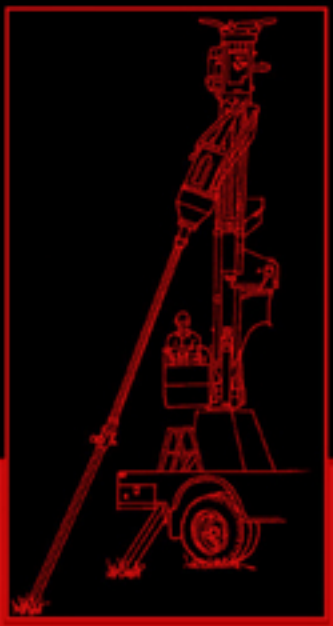

Second Edition

EARTH ANCHORS

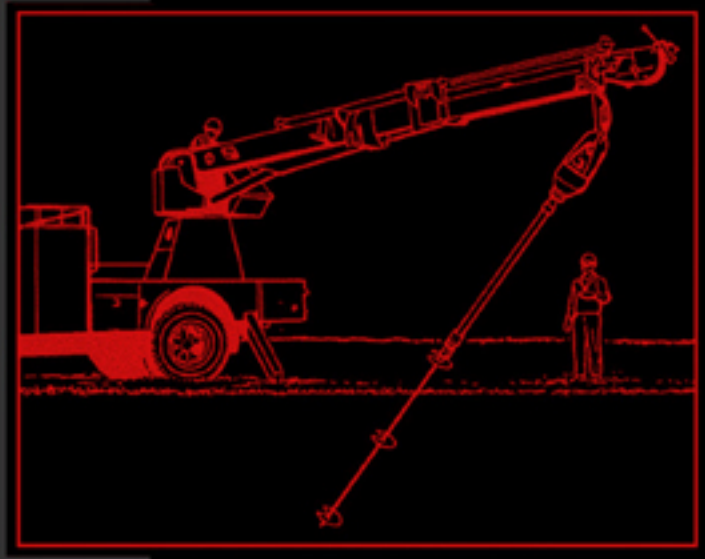

Braja M. Das
Sanjay Kumar Shukla

EARTH ANCHORS

Second Edition

Braja M. Das
Sanjay Kumar Shukla

J.ROSS PUBLISHING

ISBN 978-1-60427-077-8

Printed and bound in the U.S.A. Printed on acid-free paper
10 9 8 7 6 5 4 3 2 1

Library of Congress Cataloging-in-Publication Data

Das, Braja M., 1941-
Earth anchors / by Braja M. Das and Sanjay Kumar Shukla. — Second edition.
pages cm
Includes bibliographical references and index.
ISBN 978-1-60427-077-8 (hardcover : alk. paper) 1. Foundations. 2. Anchorage (Structural engineering) I. Shukla, Sanjay Kumar. II. Title.
TA775.D226 2013
624.1′5—dc23

2013010895

Direct all inquiries to J. Ross Publishing, Inc., 300 S. Pine Island Road, Suite #305, Plantation, Florida 33324.

Phone: (954) 727-9333
Fax: (561) 892-0700
Web: www.jrosspub.com

TABLE OF CONTENTS

PREFACE

Anchors are primarily used in the construction of foundations for earth-supported and earth retaining structures. The fundamental reason for using earth anchors in construction is to transmit the outwardly directed load to the soil at a greater depth and/or farther away from the structure. Although earth anchors have been used in practice for several hundred years, proper theoretical developments for purposes of modern engineering design have taken place only during the past 40 to 45 years or so. This book summarizes most theoretical and experimental works related to the development of proper relationships for ultimate and allowable holding capacities of earth anchors.

The first edition of this book was published with a 1990 copyright by Elsevier Science Publishers B.V., Amsterdam, The Netherlands, in the Developments in Geotechnical Engineering Series (No. 50). It was reprinted with a 2007 copyright by J. Ross Publishing in their Classics Series. Sanjay Kumar Shukla is the co-author of this second edition. The book now has a total of ten chapters. In this edition, the following major changes have been made:

- Horizontal plate anchors in sand are presented in Chapter 2 and horizontal plate anchors in clay in Chapter 3.
- Helical anchors are now presented in two chapters: anchors in sand in Chapter 6 and anchors in clay in Chapter 7. A discussion on single-helix screw anchors in sand has been added to Chapter 6.
- Two new chapters have been added: suction and caisson anchors (Chapter 9) and geo-anchors (Chapter 10).
- A summary section has been included for each chapter.

- Self-assessment multiple-choice questions, followed by answers, are given at the end of each chapter.

In all chapters, the discussions have been limited to the failure mechanisms in the soil and procedures to calculate the ultimate and allowable loads. No attempt has been made to describe the construction procedures for installation of the anchors. Modifications to the contents of the book in future editions will, of course, be necessary with future developments and changes in the state-of-the-art. We hope this book will be helpful to designers and researchers working in the area of earth anchors.

Thanks are due to Janice Das for preliminary editing and providing other help during the preparation of the text. The authors are grateful to Tom Bowling of Entura Hydro Tasmania of Australia for several meaningful suggestions during the preparation of this text. Thanks are also due to Sandy Pearlman, the project editor, who did an outstanding job in putting the entire manuscript together in a very short period of time. We truly appreciate the help of Steve Buda of J. Ross Publishing for undertaking the task of publishing this edition of the book.

Braja M. Das
Sanjay Kumar Shukla

THE AUTHORS

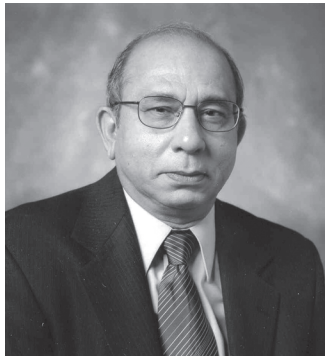

Professor Braja M. Das is Dean Emeritus of the College of Engineering and Computer Science at California State University, Sacramento. He received his M.S. in civil engineering from the University of Iowa and his Ph.D. in the area of geotechnical engineering from the University of Wisconsin. He is the author of several geotechnical engineering texts and reference books and has authored more than 250 technical papers in the area of geotechnical engineering. His primary areas of research include shallow foundations, earth anchors, and geosynthetics. He is a Fellow and Life Member of the American Society of Civil Engineers, a Life Member of the American Society for Engineering Education, and an Emeritus Member of the Chemical and Mechanical Stabilization Committee of the Research Board of the National Research Council (Washington, D.C.). He was previously a member of the editorial board of the *Journal of Geotechnical Engineering* (ASCE), a member of the *Lowland Technology International* journal (Japan), associate editor of the *International Journal of Offshore and Polar Engineering* (ISOPE), and co-editor of the *Journal of Geotechnical and Geological Engineering* (Springer, The Netherlands). Presently, he is the Editor-in-Chief of the *International Journal of Geotechnical Engineering* (Maney Publishing, U.K.).

Dr. Sanjay Kumar Shukla is an Associate Professor and Program Leader of the Discipline of Civil Engineering at the School of Engineering, Edith Cowan University, Perth, Australia. He graduated in 1988 with a first-class degree with distinction in civil engineering from the Ranchi University, Ranchi, India and received his M.Tech. and Ph.D. degrees in 1992 and 1995, respectively, in civil engineering from the Indian Institute of Technology, Kanpur, India. He is a Fellow of Engineers Australia, a Life Fellow of the Institution of Engineers (India) and Indian Geotechnical Society, and a member of the American Society of Civil Engineers and the International Geosynthetics Society. He has more than 20 years of teaching, research, and consultancy experience in the field of geotechnical and geosynthetic engineering. He serves on the editorial boards of the *International Journal of Geotechnical Engineering* and the *Indian Geotechnical Journal* and is the Scientific Editor of the *Journal of Mountain Science.* He has authored and edited 4 books and 12 book chapters. He is also an author of 117 research papers and technical articles, including 73 refereed journal publications.

1

EARTH ANCHORS: GENERAL

Earth anchors are constructed to resist the loads which cause instability to structures such as foundations, earth retaining structures, and slopes. During the last three to four decades, the experimental and mathematical research works relating to earth anchors have accelerated, and the results of those works have been published in various technical journals and conference proceedings. This chapter introduces the very basic description of earth anchors and most of their types commonly used in geotechnical engineering structures. A comprehensive review of the specific anchor types and their engineering aspects is presented systematically in the following chapters.

1.1 INTRODUCTION

Anchors used in soil and rock, commonly called *earth anchors,* are primarily designed and constructed to resist outwardly directed loads imposed on structures such as foundations, earth retaining structures, and slopes. These outwardly directed loads are transmitted to the soil and rock at a greater depth by the anchors.

Buried anchors have been used for thousands of years to stabilize structures. Tents are the oldest structures which were stabilized by using anchors or stakes. Until the middle of the 19th century, anchors were primarily used for stabilizing fairly lightweight structures. With the design and construction of large suspen-

sion bridges, very large loads were transmitted to the bridge foundations. In order to support these loads, permanent anchoring systems in rock medium were gradually developed and constructed.

With the development and construction of special lightweight structures such as lattice transmission towers and radar towers, design of special tension anchoring systems for foundations became necessary, primarily because the wind load created reactions that were greater than the self-weight of the structures.

Earth anchors of various types are now used for uplift resistance of transmission towers, utility poles, aircraft moorings, submerged pipelines, and tunnels. Anchors are also used for tieback resistance of earth retaining structures, waterfront structures, at bends in pressure pipelines, and when it is necessary to control thermal stress.

The earlier forms of anchors used in soil for resisting vertically directed uplifting loads were *screw anchors.* Figure 1.1 shows two different configurations of screw anchors. These anchors were simply twisted into the ground up to a pre-estimated depth and then tied to the foundation. They were used either singly or in groups.

In general, at the present time, earth anchors can be divided into seven basic categories: *plate anchors, direct embedment anchors, helical anchors, grouted anchors, anchor piles* and *drilled shafts, suction caisson* and *drag anchors,* and *geo-anchors.* Some authors refer to plate anchors as direct embedment anchors.

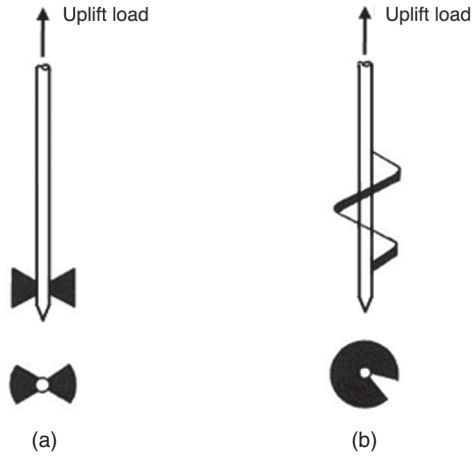

FIGURE 1.1 Two different configurations of screw anchors

1.2 PLATE ANCHORS

Plate anchors may be made of steel plates, precast concrete slabs, poured concrete slabs, timber sheets, and so forth. They may be horizontal to resist vertically directed uplifting load, inclined to resist axial pullout load, or vertical to resist horizontally directed pullout load, as shown in Figures 1.2a to 1.2c. These anchors can be installed by excavating the ground to the required depth and then backfilling and compacting with good quality soil. They may be referred to as *backfilled plate anchors* (Figure 1.3a). In many cases, plate anchors may be installed in excavated trenches, as shown in Figure 1.3b. These anchors are then attached to tie-rods, which may either be driven or placed through augered

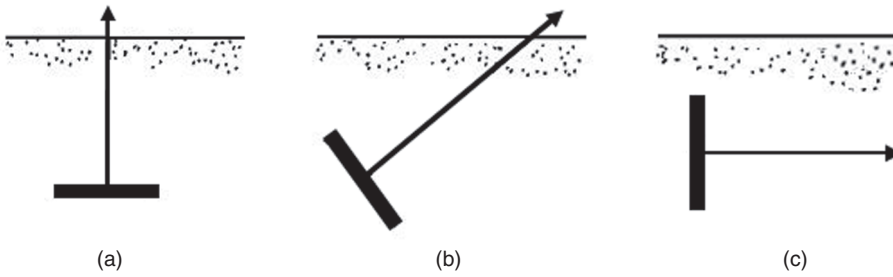

FIGURE 1.2 Plate anchors: (a) horizontal plate anchor, (b) inclined plate anchor, and (c) vertical plate anchor

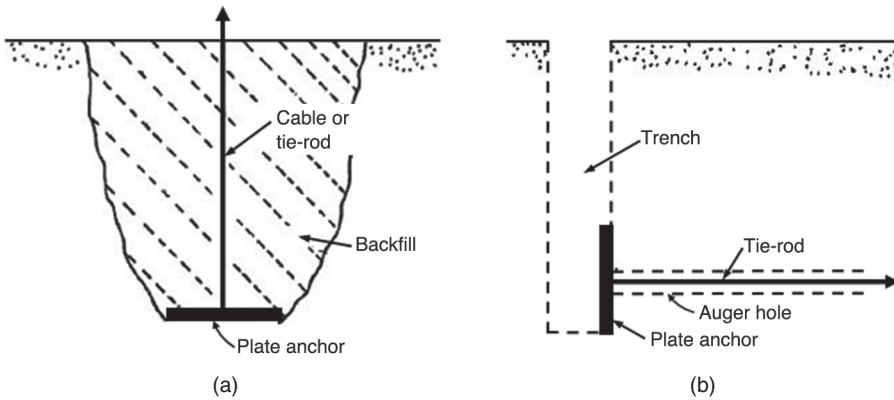

FIGURE 1.3 Installation of plate anchors: (a) backfilled plate anchor and (b) direct bearing plate anchor

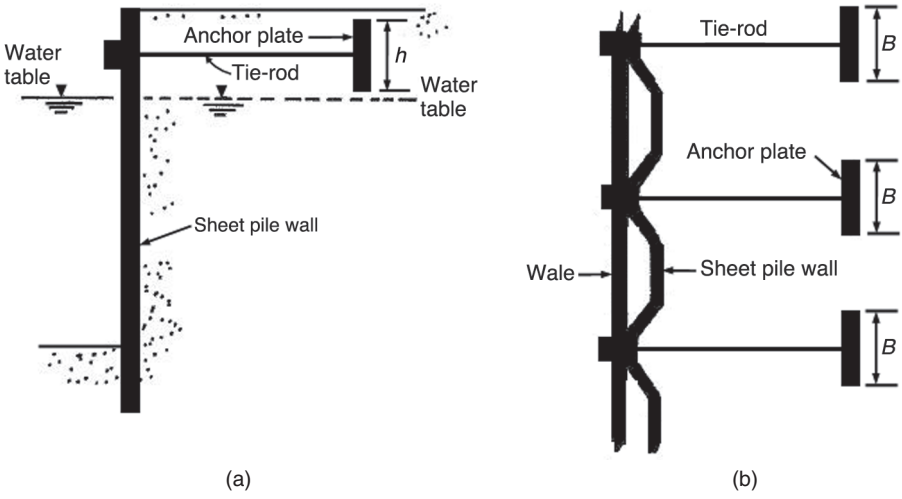

FIGURE 1.4 Use of vertical plate anchor in sheet pile wall: (a) section and (b) plan

holes. Anchors placed in this way are referred to as *direct bearing plate anchors.* In the construction of sheet pile walls, primarily used for waterfront structures, vertical backfilled or direct bearing plate anchors are common. Figure 1.4a shows the cross section of a sheet pile wall with a vertical anchor. The vertical anchors of height h and width B and spaced with a center-to-center spacing of S are tied to the sheet pile wall, as shown in Figure 1.4b.

In many cases, horizontal anchor beams along with batter piles can also be used in the construction of sheet pile walls (Figure 1.5).

1.3 DIRECT EMBEDMENT ANCHORS

Direct embedment anchors are similar in nature to direct bearing plate anchors (Figure 1.6). They may be triangular or take any other penetrative shape, and they are installed vertically by driving with a rod to a desired depth. After the desired depth is reached, the rod is withdrawn and the cable is tensioned to rotate the anchor through an angle of 90° into its final position.

1.4 HELICAL ANCHORS

Helical anchors consist of a steel shaft with one or more helices attached to it (Figure 1.7). An anchor made by suitably connecting a prefabricated steel screw

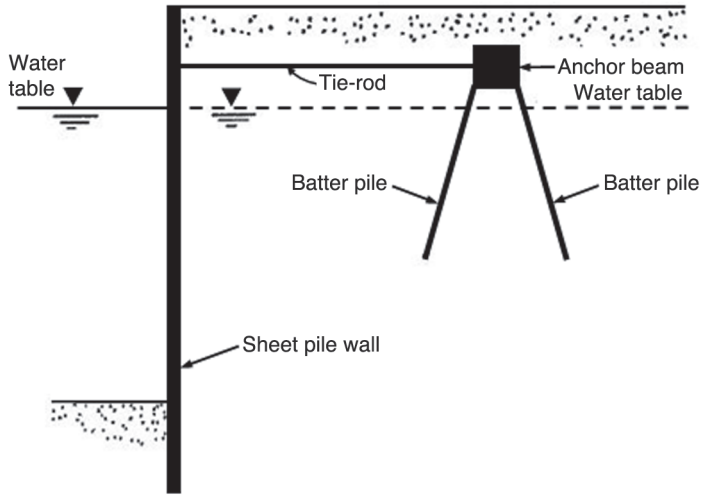

FIGURE 1.5 Use of horizontal anchor beam with batter piles in sheet pile wall

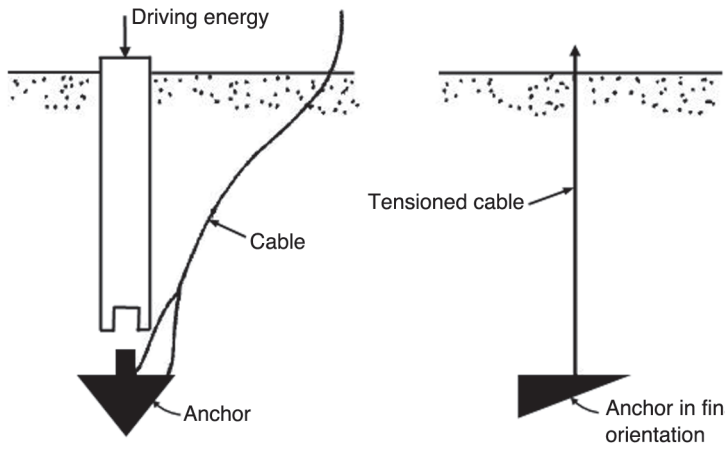

FIGURE 1.6 Direct embedment anchor (redrawn after Kulhawy, 1985)

helix element to a steel shaft is called a *single-helix (screw) anchor,* which is one form of helical anchor. A single-helix (screw) anchor can also be made as helically shaped circular steel plates welded to a steel rod. Another form of helical anchors is a *multi-helix anchor,* in which the circular plates are welded at a predetermined suitable spacing.

For multi-helix anchors, the pitch and center-to-center spacing of the helices can be varied so that the upper helices follow the lower ones. This helps reduce

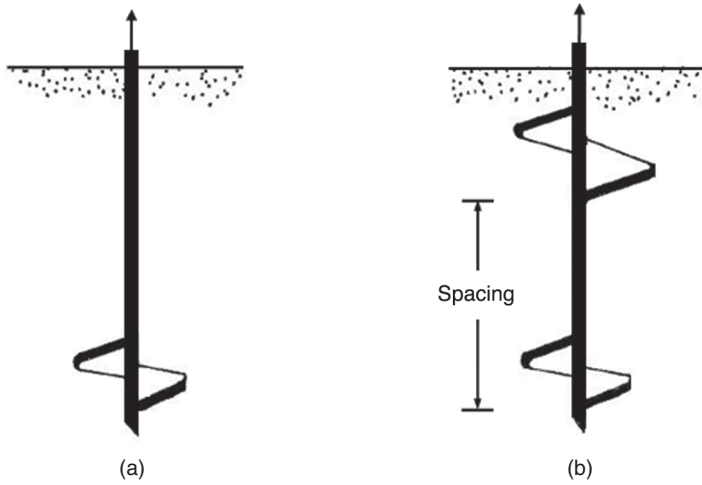

FIGURE 1.7 Helical anchors: (a) single helix and (b) multi-helix

the disturbance in the soil. Figures 1.8 and 1.9 are photographs of helical anchors with one and two helices, respectively. The schematic diagram and a photograph of the installation of a helical anchor are shown in Figures 1.10 and 1.11, respectively. These anchors are driven into the ground in a rotating manner using truck- or trailer-mounted augering equipment where the soil condi-

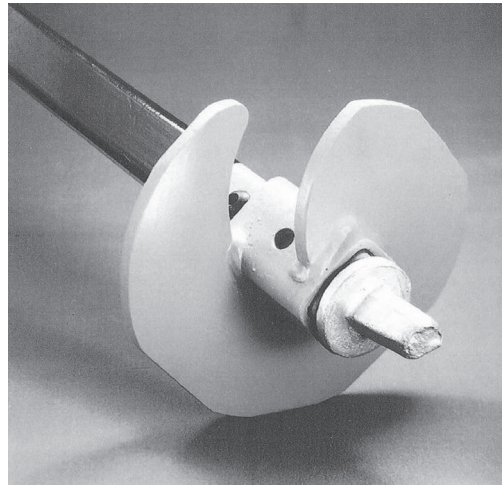

FIGURE 1.8 Helical anchor with one helix (Courtesy of A.B. Chance Co., Centralia, Missouri)

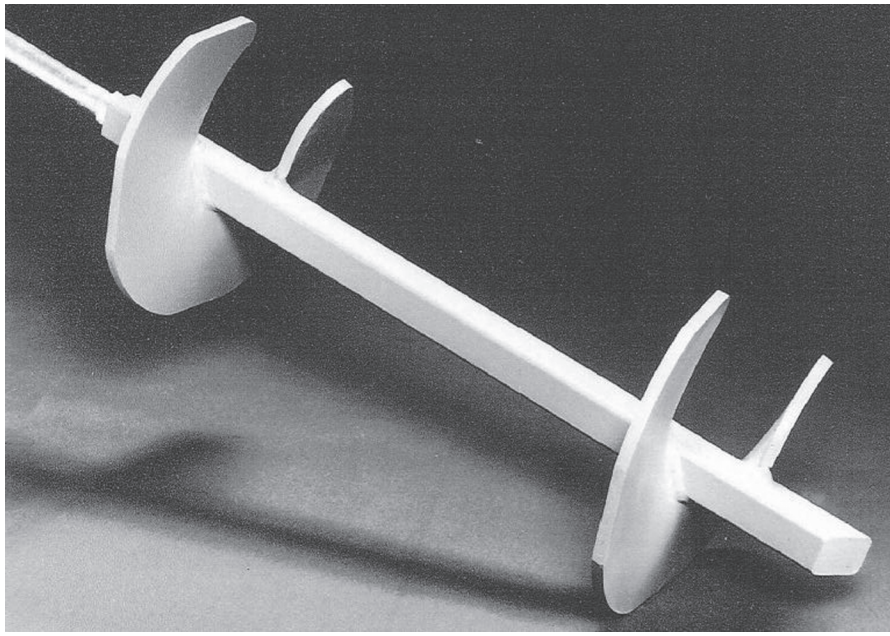

FIGURE 1.9 Helical anchor with two helices (Courtesy of A.B. Chance Co., Centralia, Missouri)

tions permit. An axial load is applied to the shaft while rotating to advance it into the ground. When installing these augers in soils mixed with gravel and large boulders, care should be taken to avoid possible damage to the helices.

Helical anchors can resist tensile loads on the foundation; however, at the same time, they can also supply additional bearing capacity to the foundation (under downward-loading condition) developed at the helix-soil interface.

Helical anchors are becoming increasingly popular in the construction of electric transmission tower foundations in the United States. They may be installed in either a vertical or an inclined position.

1.5 GROUTED ANCHORS

Grouted anchors primarily consist of placing a steel bar or steel cable into a predrilled hole and then filling the hole with cement grout. Figure 1.12 shows various types of grouted anchors, brief explanations of which are given below:

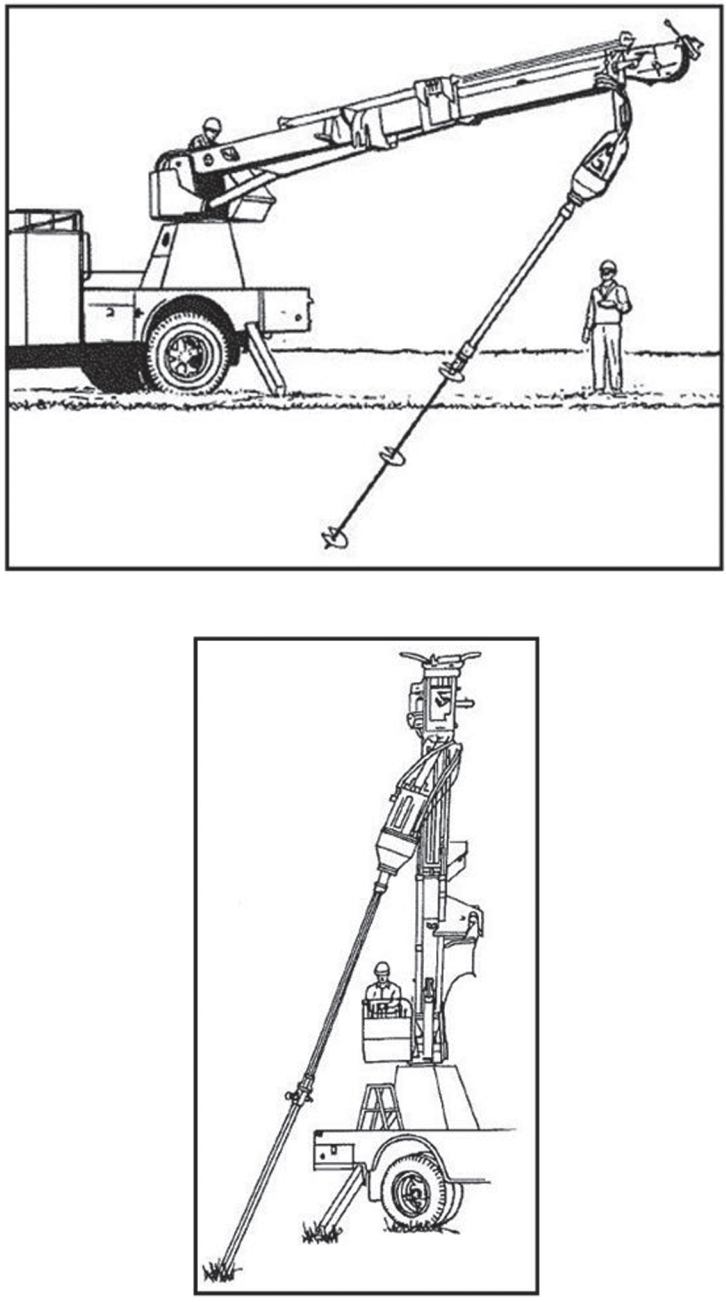

FIGURE 1.10 Installation of helical anchor (Courtesy of A.B. Chance Co., Centralia, Missouri)

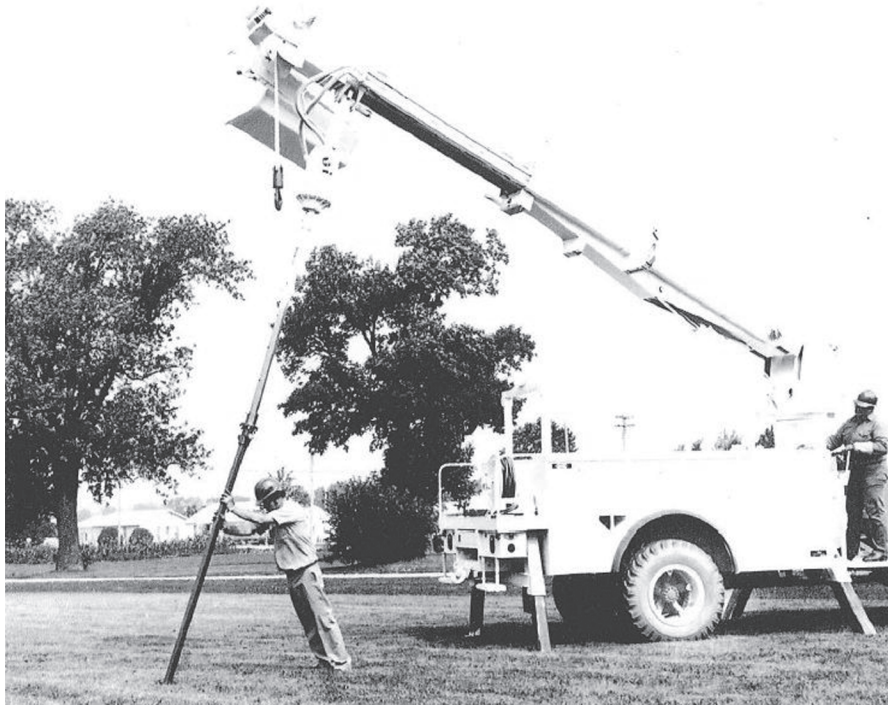

FIGURE 1.11 Installation of helical anchor (Courtesy of A.B. Chance Co., Centralia, Missouri)

1. *Gravity*. For this type of anchor, the grout is poured into the hole from the ground surface without any pressure (Figure 1.12a).
2. *Low pressure*. For this type of anchor, the grout is injected into the hole at pressures up to the overburden pressure (Figure 1.12b). This process ideally increases the effective anchor diameter by penetrating the *in situ* pores or fractures in the ground and/or by compacting the surrounding soil.
3. *High pressure*. For anchors of this type, the grout is injected at high pressure. This pressure increases the effective diameter of the anchor and compacts the loose soil around it. It may also cause hydraulic fracturing in the ground, resulting in a grout-filled system of fissures (Figure 1.12c) and perhaps a larger effective diameter of the system.
4. *Single and multiple bell*. This is primarily a gravity-type anchor; however, single or multiple bells are made in the ground mechanically before grouting (Figures 1.12d and 1.12e).

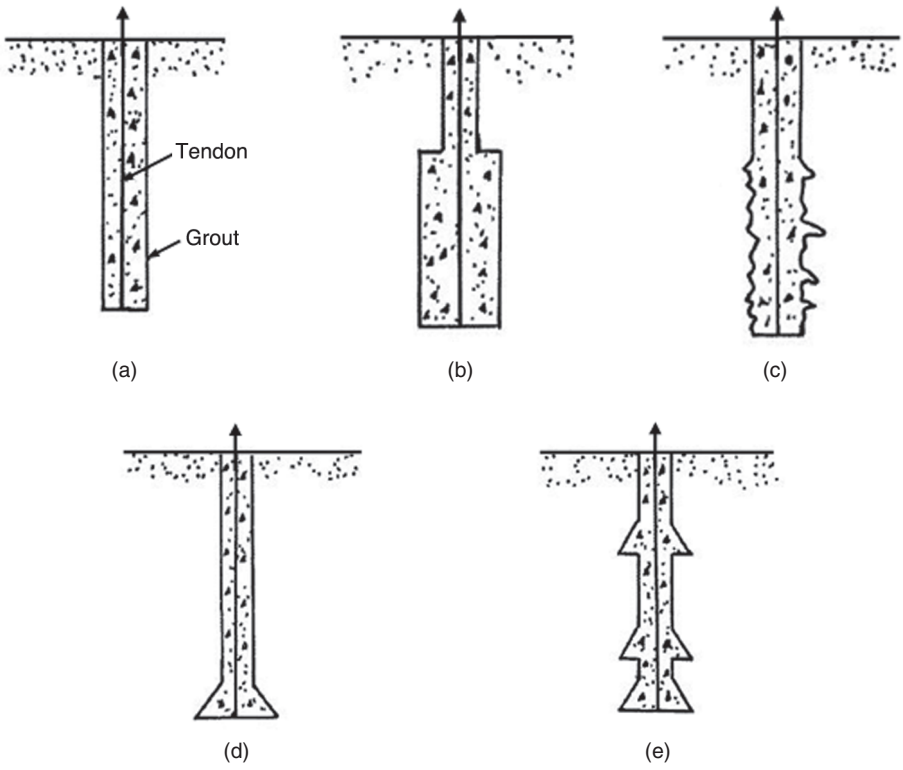

FIGURE 1.12 Grouted anchors: (a) gravity, (b) low pressure, (c) high pressure, (d) single bell, and (e) multiple bell (redrawn after Kulhawy, 1985)

Grouted anchors can be used in many construction projects, such as sheet pile walls (Figure 1.13a), revetment of rock retaining walls (Figure 1.13b), basement floors to resist buoyancy (Figure 1.13c), and foundations of transmission towers to resist overturning.

1.6 ANCHOR PILES AND DRILLED SHAFTS

Piles and drilled shafts (Figure 1.14) can be used in the construction of foundations subjected to uplift where soil conditions are poor or for very heavily loaded foundations. They serve dual purposes; that is, they help support the downward load on the foundation of the structure, and they also resist uplift.

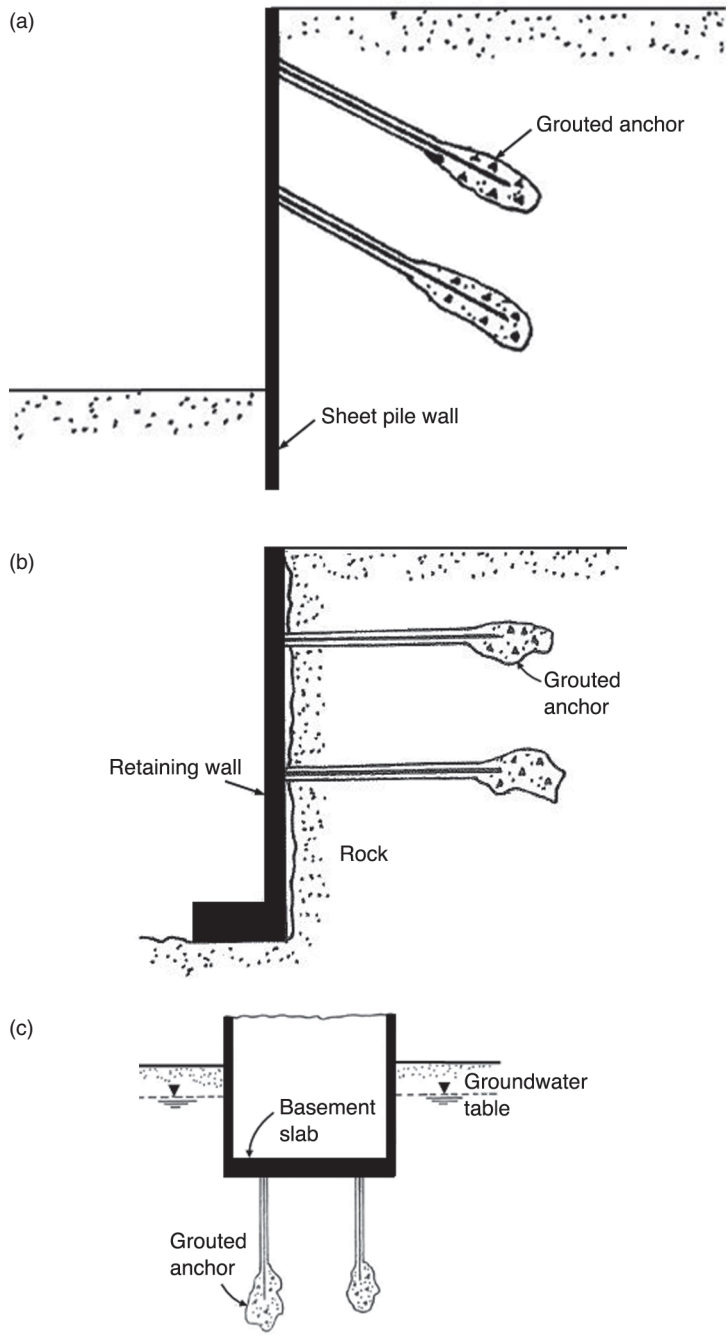

FIGURE 1.13 Use of grouted anchors in (a) sheet pile wall, (b) revetment of rock retaining wall, and (c) floor of basement

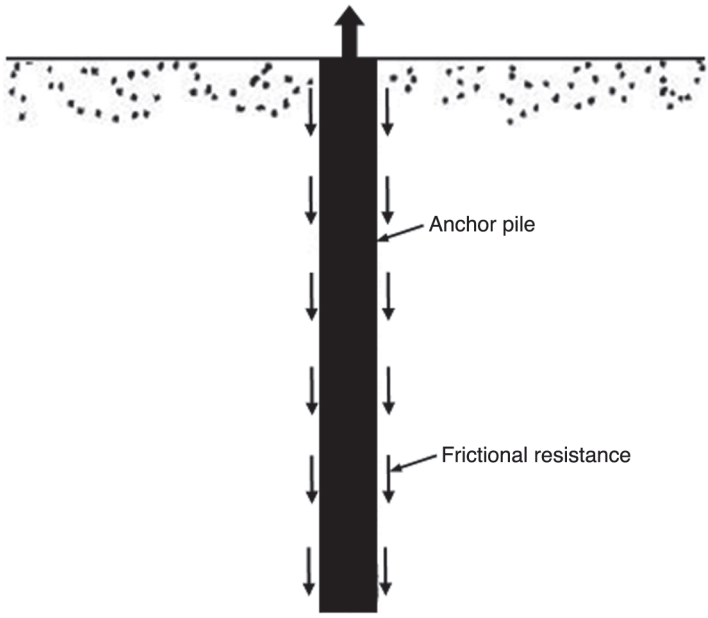

FIGURE 1.14 Anchor pile and drilled shaft subjected to uplifting load

1.7 SUCTION CAISSON AND DRAG ANCHORS

Suction caisson and drag anchors are commonly used to secure mooring systems (steel wire/chain, synthetic rope, steel tendons, etc.) of buoyant platforms to the seabed (Figure 1.15). A suction caisson comprises a large-diameter cylinder, typically in the range of 3 to 8 m, open at the bottom and closed at the top. The length-to-diameter ratio is generally in the range of 3 to 6 (Randolph and Gourvenec, 2011). A traditional drag anchor (also called fixed fluke plate anchor) consists of a broad fluke rigidly connected to a shank. The angle between the shank and the fluke is predetermined, though it may be adjusted prior to anchor placement on the seabed. The traditional drag anchors have a limitation of taking large vertical loads; therefore, vertically loaded anchors (also called drag-in plate anchors) also have been developed.

1.8 GEO-ANCHORS

A geo-anchor consists of a permeable core of coarse sand, gravel, or crushed stone wrapped in one or several layers of high-strength woven geotextile. Geo-

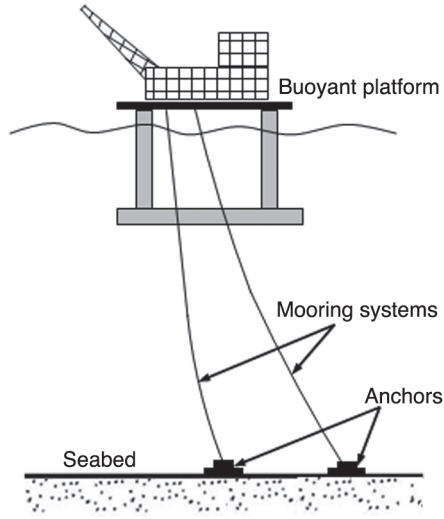

FIGURE 1.15 Buoyant platform anchored to seabed

anchors can be used to increase the stability of steep slopes, to reduce the lateral earth pressures on retaining structures, or to stabilize embankments constructed on soft clay. Figure 1.16 shows the role of geo-anchors in stabilizing a soil slope by their construction in trenches. This type of geo-anchor can be more effective in areas where the annual rainfall is high and the groundwater level is close to the ground level. Another form of geo-anchor is the trench anchor for firmly securing the geosynthetic layer installed as a pond/canal liner or slope surface protection so that geosynthetic movement or pullout does not occur (Shukla and Yin, 2006; Shukla, 2012). Figure 1.17 shows a typical V-trench anchor.

1.9 COVERAGE OF THE TEXT

During the last three to four decades, the pace of experimental and mathematical research works relating to earth anchors has accelerated, and the results of those works have been published in various technical journals and conference proceedings. The purpose of this text is to present in a systematic manner a comprehensive review of some of the past and recent studies. Updated information is provided for evaluation of the holding capacities of *plate anchors oriented in a horizontal, inclined, and vertical manner* in soil; *helical anchors*; *piles subjected to vertical uplift*; *suction caisson* and *drag anchors*; and *geo-anchors.* Limited attempt has been made to provide either the details for the *placement*

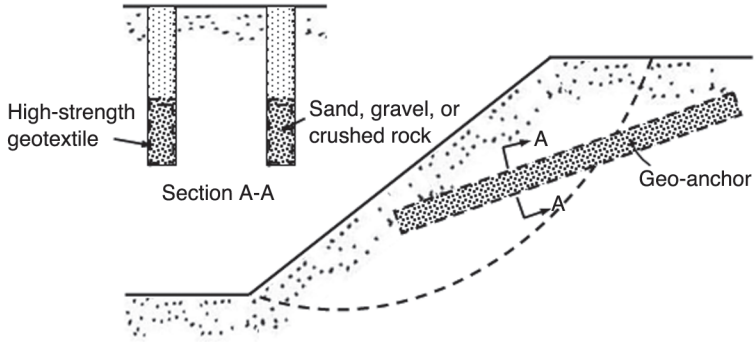

FIGURE 1.16 Geo-anchor in a slope (adapted from Broms, 1993)

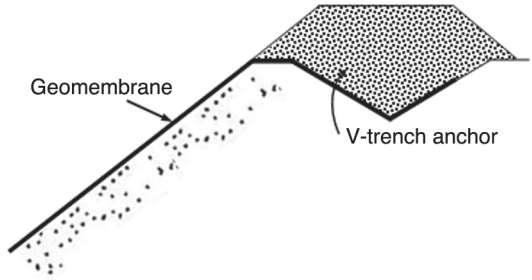

FIGURE 1.17 V-trench anchor (adapted from Shukla and Yin, 2006; Shukla, 2012)

of the anchors in the field or the *construction techniques.* Valuable information in these areas can be obtained from the work of Hanna (1982) and others. No aspects of grouted anchors are covered in this text, since valuable information is available from several other well-organized sources (Hanna, 1982; Littlejohn, 1970). In spite of the accelerated pace of research work on various aspects of anchors at the present time, adequate field verifications are often lacking in several instances. These shortcomings will also be outlined in the text.

1.10 SUMMARY OF MAIN POINTS

1. Earth anchors are primarily designed and constructed to resist outwardly directed loads imposed on structures such as foundations, earth retaining structures, and slopes.

2. The different forms of earth anchors are screw anchors, plate anchors, direct embedment anchors, helical anchors, grouted anchors, anchor piles and drilled shafts, suction caisson and drag anchors, and geo-anchors.
3. Plate anchors are made up of steel plates, precast concrete slab, timber sheets, and so forth; they may be horizontal, vertical, or inclined. They are installed by ground excavation to the required depth and then backfilling or by placing in excavated trenches.
4. Helical anchors consist of a steel shaft with one or more helices attached to it.
5. Grouted anchors primarily consist of placing a steel bar or steel cable into a predrilled hole and then filling the hole with cement grout.
6. Anchor piles and drilled shafts help support the downward load on the foundation of a structure, and they also resist uplift.
7. A suction caisson comprises a large-diameter cylinder, typically in the range of 3 to 8 m, open at the bottom and closed at the top. A traditional drag anchor consists of a broad fluke rigidly connected to a plank.
8. Geotextile-wrapped coarse-grained soil columns and trench anchors are two different forms of geo-anchors.

SELF-ASSESSMENT QUESTIONS

Select the most appropriate answer to each multiple-choice question

1.1. The earliest form of anchor used in soil for resisting vertically directed uplifting load is:
   a. plate anchor
   b. helical anchor
   c. screw anchor
   d. suction caisson anchor

1.2. A vertical plate anchor resists:
   a. horizontally directed pullout load
   b. vertically directed pullout load
   c. axial pullout load
   d. inclined pullout load

1.3. Which of the following anchors is installed by driving into the ground in a rotating manner using truck- or trailer-mounted augering equipment:
   a. plate anchor
   b. helical anchor

c. grouted anchor
d. geo-anchor

1.4. Grouted anchors can be used in:
a. sheet pile walls
b. basement floors
c. foundations of transmission towers
d. all of the above

1.5. Piles and drilled shafts are commonly used in the construction of foundations subjected to uplift:
a. where soil conditions are poor
b. for very heavily loaded foundations
c. both a and b
d. where water is present

1.6. Which of the following anchors is commonly used to secure mooring systems of buoyant platforms to the seabed:
a. suction caisson anchor
b. plate anchor
c. grouted anchor
d. geo-anchor

1.7. The length-to-diameter ratio for suction caisson anchors is generally in the range of
a. 1 to 3
b. 3 to 6
c. 6 to 9
d. 9 to 12

1.8. Geo-anchors in the form of geotextile-wrapped coarse-grained soil columns installed in slopes play the role of:
a. reinforcement
b. drainage
c. both a and b
d. filtration

Answers

1.1: c 1.2: a 1.3: b 1.4: d 1.5: c 1.6: a 1.7: b 1.8: c

REFERENCES

Broms, B.B. (1993). Geo-anchors. *Geotext. Geomembr.,* 12(3):215–234.

Hanna, T.H. (1982). *Foundations in Tension-Ground Anchor,* Trans Tech Publication and McGraw-Hill.

Kulhawy, F.H. (1985). Uplift behavior of shallow soil anchors—an overview. *Proc. Uplift Behavior of Anchor Foundations,* ASCE, 1–25.

Littlejohn, G.S. (1970). Soil anchors. *Proc. Conf. Ground Eng.,* London, 33–44.

Randolph, M. and Gourvenec, S. (2011). *Offshore Geotechnical Engineering,* Spon Press, Taylor and Francis, Abingdon, Oxon.

Shukla, S.K. (2012). *Handbook of Geosynthetic Engineering,* second edition, ICE Publishing, London.

Shukla, S.K. and Yin, J.-H. (2006). *Fundamentals of Geosynthetic Engineering,* Taylor and Francis, London.

2

HORIZONTAL PLATE ANCHORS IN SAND

In the past, several theoretical and semi-empirical methods were developed to predict the ultimate uplifting load of strip, circular, and rectangular anchors embedded in sands. Some of these methods are described in this chapter. Recently some numerical investigations of the behavior of horizontal plate anchors in sands have been reported in the literature; this chapter also summarizes such works briefly.

2.1 INTRODUCTION

As briefly discussed in Chapter 1, horizontal plate anchors are used in the construction of foundations subjected to uplifting load. In the past, a number of increasingly sophisticated theories have been developed to predict the ultimate uplift capacity of horizontal plate anchors embedded in various types of soils. In this chapter, the development of those theories for horizontal plate anchors in sands is discussed.

Figure 2.1 shows a horizontal plate anchor with a width h and a length B ($B \geq h$). The embedment depth of this plate anchor is H measured from the ground surface. The embedment ratio is defined as the ratio of the depth of embedment to the width of the anchor, that is, H/h. If such an anchor is placed at a relatively shallow depth, that is, with a small embedment ratio, the failure surface at ultimate load will extend to the ground surface (Figure 2.2). The angle α at which the failure surface intersects the horizontal ground surface will vary with the type of soil. For loose sand and soft clayey soils, α may be equal to 90°;

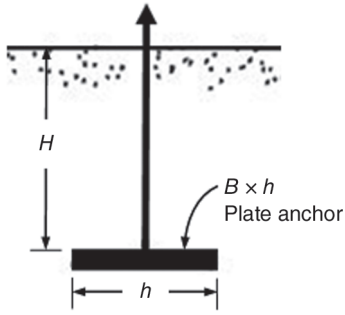

FIGURE 2.1 Geometric parameters of a horizontal plate anchor

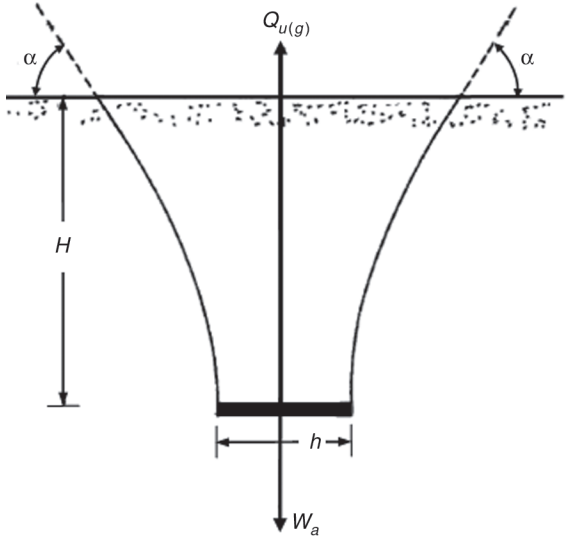

FIGURE 2.2 Shallow horizontal anchor

however, for dense sand and stiff clays, this angle may be close to $45° - \phi/2$ (where ϕ = angle of internal friction of soil). This type of behavior of an anchor is referred to as the *shallow anchor condition.* If the anchor is located at a relatively large embedment ratio, the failure surface in soil at ultimate load does not extend to the ground surface; that is, a local shear failure in soil located around the anchor takes place. This is referred to as the *deep anchor condition.*

For a given anchor, the gross ultimate uplift capacity can be defined as:

$$Q_{u(g)} = Q_u + W_a \tag{2.1}$$

where

$Q_{u(g)}$ = gross ultimate uplift capacity
Q_u = net ultimate uplift capacity
W_a = effective self-weight of the anchor

The net ultimate uplift capacity is the sum of the effective weight of the soil located in the failure zone and the shearing resistance developed along the failure surface.

2.2 EARLY THEORIES

2.2.1 Soil Cone Method

Some of the early theories to determine the net ultimate uplift capacity Q_u were restricted to *shallow circular* plate anchors. Mors (1959) proposed that the failure surface in soil at ultimate load may be approximated as a truncated cone with an apex angle of $\theta = 90° + \phi/2$, as shown in Figure 2.3. The net ultimate

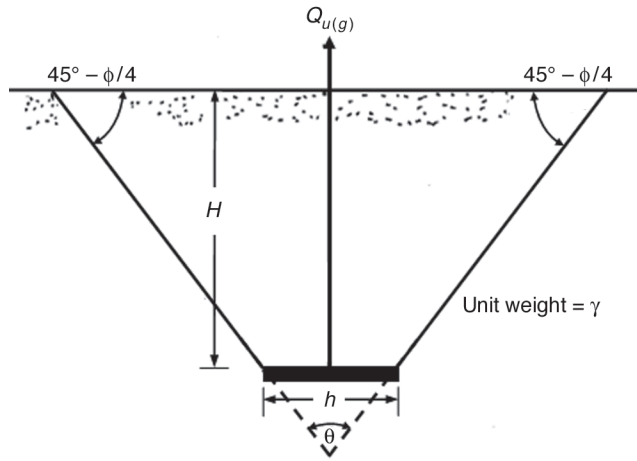

FIGURE 2.3 Mors's theory (1959): soil cone method ($\theta = 90° + \phi/2$, h = diameter of anchor plate)

uplift capacity may be assumed to be equal to the weight of the soil located inside the failure surface. Thus:

$$Q_u = \gamma V \tag{2.2}$$

where

V = volume of soil in the truncated cone
γ = unit weight of soil, and

$$V = \frac{\pi H}{12}\left\{ h^2 + \left[h + 2H \cot\left(45° - \frac{\phi}{4} \right) \right]^2 + h \left[h + 2H \cot\left(45° - \frac{\phi}{4} \right) \right] \right\}$$

or

$$V = \frac{\pi H}{12}\left[3h^2 + 4H^2 \cot^2\left(45° - \frac{\phi}{4} \right) + 6Hh \cot\left(45° - \frac{\phi}{4} \right) \right] \tag{2.3}$$

It needs to be pointed out that the shearing resistance developed along the failure surface has been neglected in Equation 2.2.

A similar theory was also proposed by Downs and Chieurzzi (1966), who suggested that the apex angle θ be taken as being equal to 60°, as shown in Figure 2.4. For this case:

$$Q_u = \gamma V$$

$$= \frac{\pi \gamma H^3}{12} [h^2 + (h + 2H \cot 60°)^2 + h(h + 2H \cot 60°)]$$

$$= \frac{\pi \gamma H^3}{12} (3h^2 + 1.333H^2 + 3.464H) \tag{2.4}$$

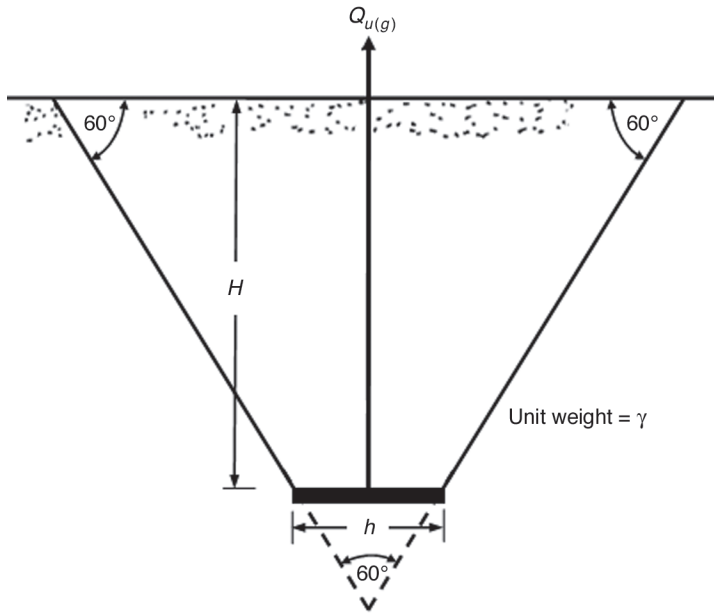

FIGURE 2.4 Downs and Chieurzzi's theory (1966): soil cone method (h = diameter of anchor plate)

2.2.2 Friction Cylinder Method

In many cases in the past, the friction cylinder method was used to estimate the uplift capacity of *shallow circular* anchor plates. In this type of calculation, the friction surface in the soil was assumed to be cylindrical, as shown in Figure 2.5a. For cohesionless soils, the net ultimate load was taken as the sum of the weight of the soil located inside the failure cylinder and the frictional resistance mobilized along the failure surface. Thus:

$$Q_u = \left(\frac{\pi h^2}{4}\right)(H)(\gamma) + \int_0^H (\sigma_0' \tan \phi) dz \tag{2.5a}$$

where

σ_0' = effective overburden pressure at a depth z measured from the ground surface (Figure 2.5b)
ϕ = soil friction angle

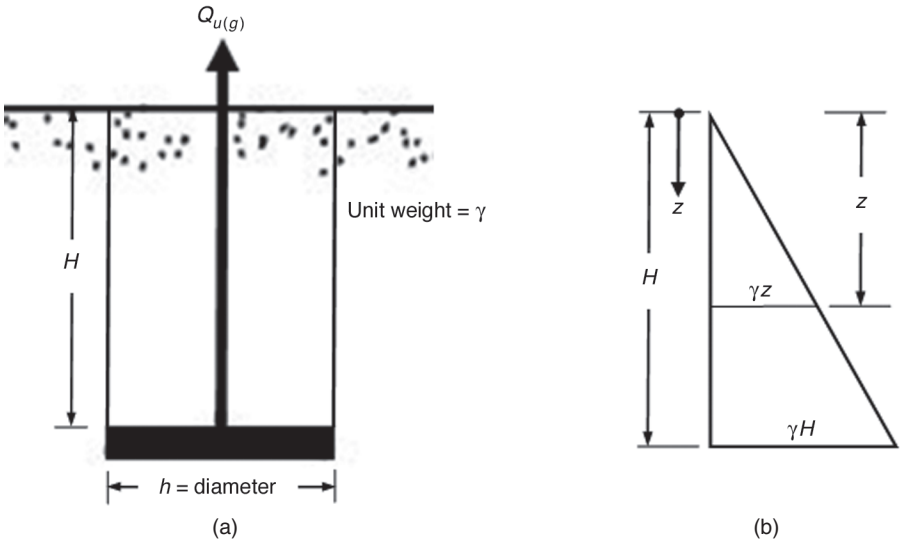

FIGURE 2.5 Friction cylinder method: (a) failure mechanism and (b) variation of effective overburden pressure

With substitution of values, Equation 2.5a becomes:

$$Q_u = \frac{\pi H h^2 \gamma}{4} + \int_0^H (\pi h)(\gamma z \tan \phi) dz$$

$$= \frac{\pi H h^2 \gamma}{4} + \left(\frac{\pi h H^2 \gamma}{4}\right) \tan \phi \qquad (2.5b)$$

In a similar manner, for the saturated cohesive soils:

$$Q_u = \frac{\pi H h^2 \gamma}{4} + (\pi H h) + c_u \qquad (2.6)$$

Surface area of the cylindrical failure surface

where

c_u = undrained cohesion

Ireland (1963) proposed the following relationships for shallow anchors embedded in sands as well as silts and clays:

$$Q_u = \frac{\pi H h^2 \gamma}{4} + \frac{\pi}{2} \gamma h H^2 K_0 \tan \phi \tag{2.7}$$

where

K_0 = coefficient of lateral earth pressure

Ireland (1963) also recommended the following values for K_0 and ϕ:

$$K_0 = \begin{cases} 0.5 \text{ for granular soils} \\ 0.4 \text{ for silts and clays} \end{cases}$$

$$\phi = \begin{cases} 30^\circ \text{ for granular soils} \\ 20^\circ \text{ for silts and clays} \end{cases}$$

2.3 BALLA'S THEORY

Based on several model and field test results in dense soil, Balla (1961) established that for *shallow circular anchors,* the failure surface in soil will be as shown in Figure 2.6. Note from the figure that aa' and bb' are arcs of a circle. The angle α is equal to $45^\circ - \phi/2$. The radius of the circle, of which aa' and bb' are arcs, is expressed as:

$$r = \frac{H}{\sin\left(45^\circ + \frac{\phi}{2}\right)} \tag{2.8}$$

The net ultimate uplift capacity of the anchor is the sum of two components: (a) weight of the soil in the failure zone and (b) the shearing resistance developed along the failure surface. Thus:

$$Q_u = H^3 \gamma \left[F_1\left(\phi, \frac{H}{h}\right) + F_3\left(\phi, \frac{H}{h}\right) \right] \tag{2.9}$$

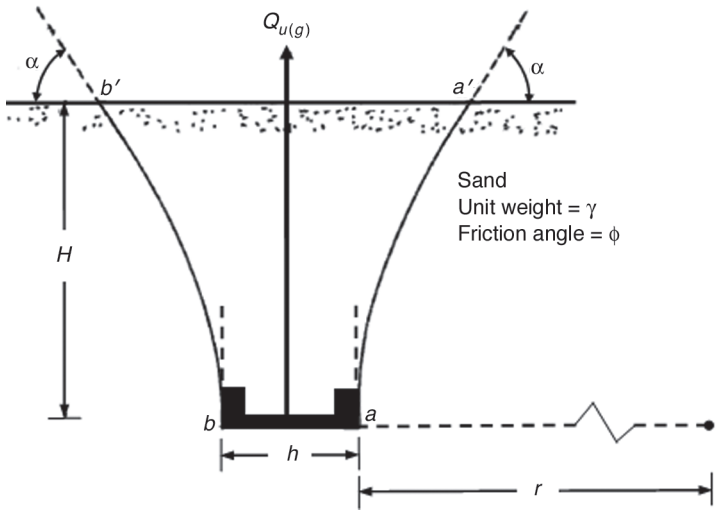

FIGURE 2.6 Balla's theory (1961) for shallow circular anchor plate

The sums of the functions $F_1(\phi, H/h)$ and $F_3(\phi, H/h)$ developed by Balla (1961) are plotted in Figure 2.7 for various values of the soil friction angle ϕ and embedment ratio H/h. The general nature of the plot of Q_u versus H/h will be like that in Figure 2.8.

In general, Balla's theory is in good agreement for the uplift capacity of anchors embedded in dense sand at an embedment ratio of $H/h \leq 5$. However, for anchors located in loose and medium sand, the theory overestimates the net ultimate uplift capacity. The main reason that Balla's theory overestimates the net uplift capacity for $H/h >$ about 5 even in dense sand is because it is essentially a deep anchor condition, and the failure surface does not extend to the ground surface.

The simplest procedure to determine the embedment ratio at which the deep anchor condition is reached may be determined by plotting the nondimensional breakout factor F_q against H/h, as shown in Figure 2.9.

The breakout factor is defined as:

$$F_q = \frac{Q_u}{\gamma AH} \tag{2.10}$$

where

A = area of the anchor plate

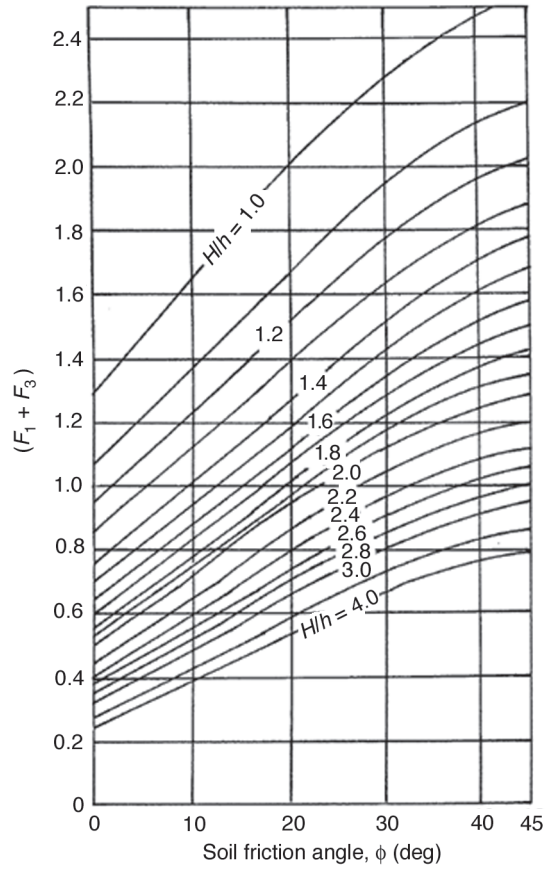

FIGURE 2.7 Variation of $F_1 + F_3$ based on Balla's theory (1961)

The breakout factor increases with H/h up to a maximum value of $F_q = F_q^\star$ at $H/h = (H/h)_{cr}$. For $H/h > (H/h)_{cr}$, the breakout factor remains practically constant, that is, $F_q^\star$. Anchors located at an embedment ratio of $H/h \leq (H/h)_{cr}$ are shallow anchors, and those located at $H/h > (H/h)_{cr}$ are deep anchors.

2.4 BAKER AND KONDNER'S EMPIRICAL RELATIONSHIP

Baker and Kondner (1966) conducted several laboratory model tests, and by using dimensional analysis, they proposed the following relationships:

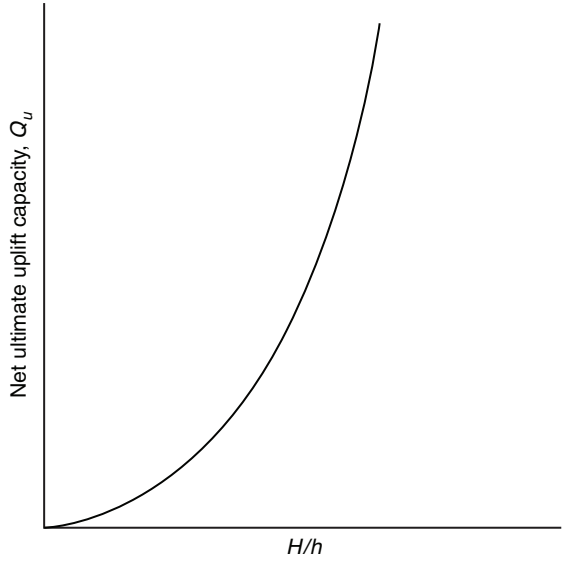

FIGURE 2.8 Nature of variation of Q_u with H/h

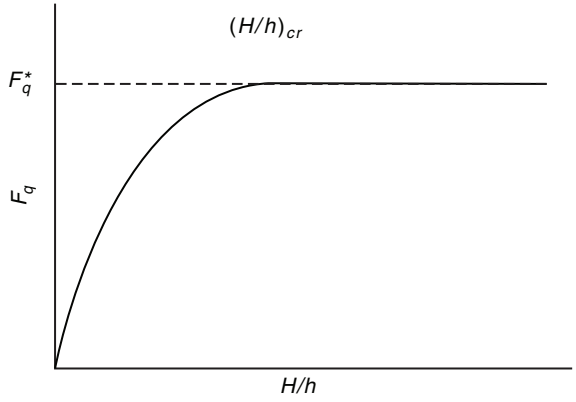

FIGURE 2.9 Nature of variation of F_q with H/h

$$Q_u = c_1 H h^2 \gamma + c_2 H^3 \gamma \quad \text{(for shallow circular anchors)} \tag{2.11}$$

$$Q_u = 170 h^3 \gamma + c_3 h^2 t \gamma + c_4 H h + \gamma \quad \text{(for deep circular anchors)} \tag{2.12}$$

where

t = thickness of the anchor plate
c_1, c_2, c_3, c_4 = constants that are functions of the soil friction angle and the relative density of compaction

For shallow anchors, the model test results of Baker and Kondner agreed well with the theory of Balla (1961). Those tests were conducted in a dense sand with $\phi = 42°$.

2.5 MARIUPOL'SKII'S THEORY

Mariupol'skii (1965) proposed separate mathematical formulations for estimation of the ultimate uplift capacity of shallow and deep circular anchors. According to this theory, for shallow anchors, the progressive failure mechanism commences with compression of the soil located above the anchor plate (Figure 2.10). This compression occurs with a column of soil that has the same diameter as the anchor plate. Hence, the initial force consists of the following components:

1. The effective weight of the anchor
2. The effective weight of the soil column of diameter h and height H
3. The friction and cohesion along the surface of the soil column

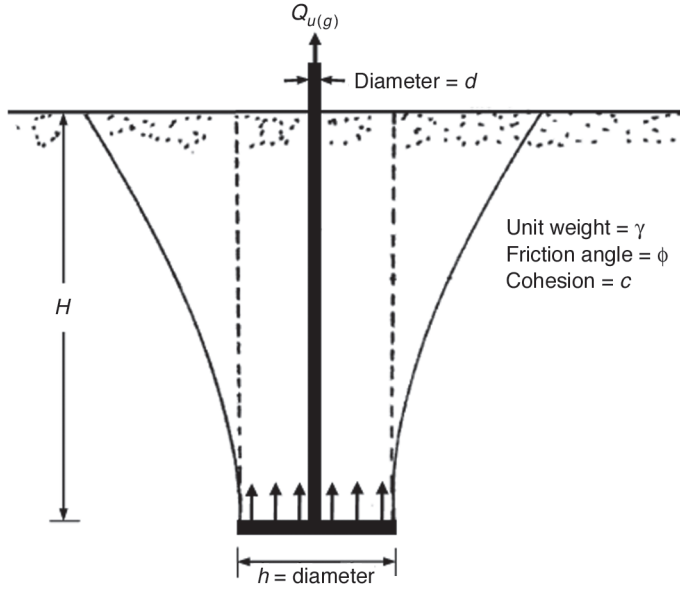

FIGURE 2.10 Mariupol'skii's theory (1965) for shallow circular plate anchor

As pullout progresses, there is continued compaction of soil, and this leads to an increase in the vertical compressive stress. Thus there is a continued increase in the frictional resistance along the surface of the soil column. The increase of the frictional resistance entrains adjacent rings of soil. Ultimately sufficient tensile stress is developed so that failure occurs with the separation of soil in the form of a cone with a curvilinear geneatrix. The net ultimate uplift capacity thus calculated by this theory can be given as:

$$Q_u = \frac{\pi}{4}(h^2 - d^2)\frac{\left\{\begin{array}{l}\gamma H\left[1 - \left(\frac{d}{h}\right)^2 + 2K_0\left(\frac{H}{h}\right)\tan\phi\right] \\ \\ + 4c\left(\frac{H}{h}\right)\end{array}\right\}}{1 - \left(\frac{H}{h}\right)^2 - 2n\left(\frac{H}{h}\right)} \qquad (2.13)$$

where

K_0 = lateral earth pressure coefficient
c = cohesion
n = an empirical coefficient
d = diameter of the anchor shaft

For sand, $c = 0$, so:

$$Q_u = \frac{\pi}{4}(h^2 - d^2)\frac{\left\{\gamma H\left[1 - \left(\frac{d}{h}\right)^2 + 2K_0\left(\frac{H}{h}\right)\tan\phi\right]\right\}}{1 - \left(\frac{H}{h}\right)^2 - 2n\left(\frac{H}{h}\right)} \qquad (2.14)$$

For deep anchors, it was assumed that under the applied load the anchor will reach a limiting condition, after which additional work is required to raise the anchor through a distance L, which is equivalent to the work required to expand a cylindrical cavity of height L and diameter d to a diameter h, as shown in Figure 2.11. Based on this concept, the net ultimate uplift capacity can be expressed as:

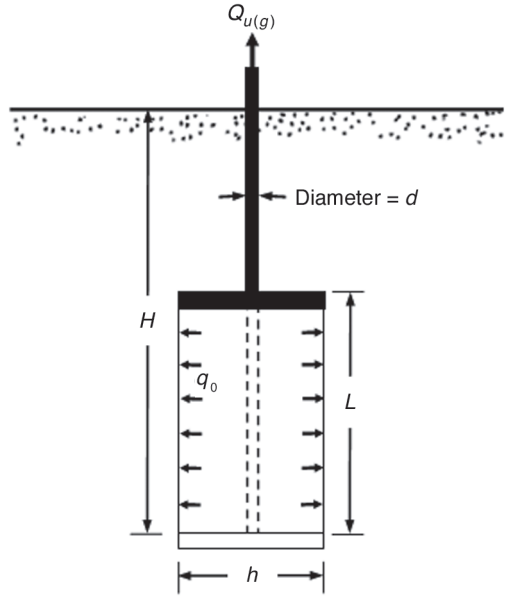

FIGURE 2.11 Mariupol'skii's theory (1965) for deep circular plate anchor

$$Q_u = \left(\frac{\pi q_0}{2}\right)\left(\frac{h^2 - d^2}{2 - \tan\phi}\right) + f(\pi d)\,[H - (h - d)] \qquad (2.15)$$

where

q_0 = radial pressure under which the cavity is expanded
f = unit skin resistance along the stem of the anchor

It was recommended that the lower of the two values (that is, those calculated from either Equation 2.14 or 2.15) be adopted for design. This was primarily because the limit of $H/h = (H/h)_{cr}$ for the deep anchor condition was not clearly established.

2.6 MEYERHOF AND ADAMS'S THEORY

Meyerhof and Adams (1968) proposed a semi-theoretical relationship for estimation of the ultimate uplift capacity of *strip, rectangular,* and *circular* anchors.

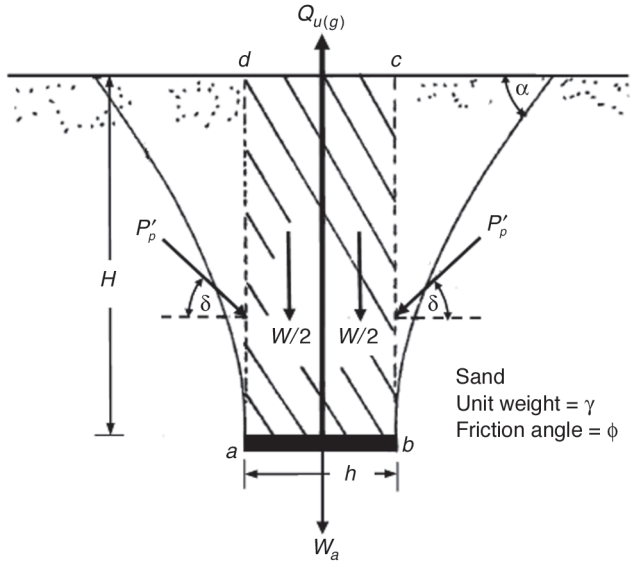

FIGURE 2.12 Failure mechanism from Meyerhof and Adams's theory (1968)

The principles of this theory can be explained by considering a *shallow strip* anchor embedded in sand, as shown in Figure 2.12.

At ultimate load, the failure surface in soil makes an angle α with the horizontal. The magnitude of α depends on several factors, such as the relative density of compaction and the angle of internal friction of the soil, and it varies between $90° - \phi/3$ to $90° - 2\phi/3$, with an average of about $90° - \phi/2$. Let us consider the free body diagram of the soil located in the zone *abcd*. For stability, the following forces per unit length of the anchor need to be considered:

1. The weight of the soil, W
2. The passive force P'_p per unit length along the faces *ad* and *bc*

The force P'_p is inclined at an angle δ to the horizontal. For an average value of $\alpha = 90° - \phi/2$, the magnitude of δ is about $(\frac{2}{3})\phi$.

Note that

$$W = \gamma H h \tag{2.16}$$

$$P'_p = \frac{P'_h}{\cos\delta} = \left(\frac{1}{2}\right)\left(\frac{1}{\cos\delta}\right)(K_{ph}\gamma H^2) \tag{2.17}$$

where

P'_h = horizontal component of the passive force
K_{ph} = horizontal component of the passive earth pressure coefficient

Now, for equilibrium, summing the vertical components of all forces:

$$\sum F_V = 0$$

$$Q_{u(g)} = W + 2P'_p \sin\delta + W_a$$

$$Q_{u(g)} - W_a = W + 2(P'_p \cos\delta)\tan\delta$$

$$Q_u = W + 2P'_h \tan\delta$$

or

$$Q_u = W + 2\left(\frac{1}{2} K_{ph}\gamma H^2\right)\tan\delta = W + K_{ph}\gamma H^2 \tan\delta \qquad (2.18)$$

The passive earth pressure coefficient based on the curved failure surface for $\delta \approx (2/3)\phi$ can be obtained from Caquot and Kerisel (1949). Furthermore, it is convenient to express $K_{ph}\tan\delta$ in the form

$$K_u \tan\phi = K_{ph}\tan\delta \qquad (2.19)$$

where

K_u = nominal uplift coefficient

Combining Equations 2.18 and 2.19, we obtain:

$$Q_u = W + K_u\gamma H^2 \tan\phi \qquad (2.20)$$

The variation of the nominal uplift coefficient K_u with the soil friction angle ϕ is shown in Figure 2.13. It falls within a narrow range and may be taken as equal to 0.95 for all values of ϕ varying from 30° to about 48°.

As discussed in Section 2.3, the nondimensional breakout factor is defined as:

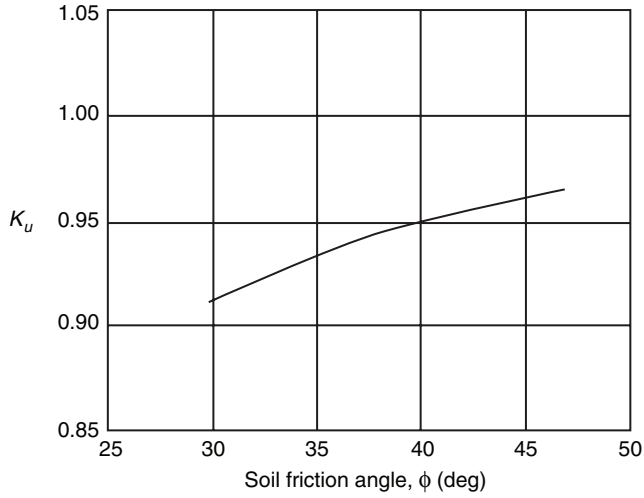

FIGURE 2.13 Variation of K_u with soil friction angle

$$F_q = \frac{Q_u}{\gamma AH}$$

For strip anchors, and area A per unit length is equal to $h \times 1 = h$. Thus, from Das and Seeley (1975a):

$$F_q = \frac{Q_u}{\gamma AH} = \frac{Q_u}{\gamma hH} = W + K_u \gamma H^2 \tan \phi$$

However, $W = \gamma hH$. Therefore:

$$F_q = \frac{\gamma hH + K_u \gamma H^2 \tan \phi}{\gamma hH} = 1 + K_u \left(\frac{H}{h} \tan \phi \right) \tag{2.21}$$

For circular anchors, Equation 2.20 can be modified to the form

$$Q_u = W + \frac{\pi}{2} S_F \gamma hH^2 K_u \tan \phi \tag{2.22}$$

where

W = weight of the soil above the circular anchor = $\left(\frac{\pi}{4} h^2\right) H\gamma$
h = diameter of the anchor
S_F = shape factor

The shape factor can be expressed as:

$$S_F = 1 + m\left(\frac{H}{h}\right) \tag{2.23}$$

where

m = coefficient which is a function of the soil friction angle ϕ

Thus, combining Equations 2.22 and 2.23, we obtain:

$$Q_u = \frac{\pi}{4} h^2 H\gamma + \frac{\pi}{2}\left[1 + m\left(\frac{H}{h}\right)\right]\gamma h H^2 K_u \tan\phi \tag{2.24}$$

The breakout factor F_q can be given as (Das and Seeley, 1975a):

$$F_q = \frac{Q_u}{\gamma A H} = \frac{\frac{\pi}{4} h^2 H\gamma + \frac{\pi}{2}\left[1 + m\left(\frac{H}{h}\right)\right]\gamma h H^2 K_u \tan\phi}{\gamma\left(\frac{\pi}{4} h^2\right) H}$$

$$= 1 + 2\left[1 + m\left(\frac{H}{h}\right)\right]\left(\frac{H}{h}\right) K_u \tan\phi \tag{2.25}$$

For rectangular anchors that have dimensions of $B \times h$, the net ultimate capacity can be expressed as:

$$Q_u = W + \gamma H^2 (2S_F h + B - h) K_u \tan\phi \tag{2.26}$$

The preceding equation was derived with the assumption that the two end portions of length $h/2$ are governed by the shape factor S_F, while the passive

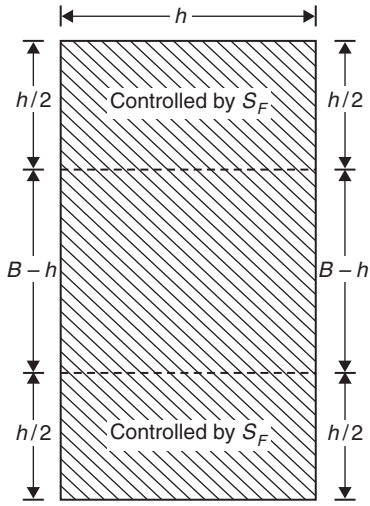

FIGURE 2.14 Assumptions in the derivation of Equation 2.26

pressure along the central portion of length $B - h$ is the same as the strip anchor (Figure 2.14). In Equation 2.26

$$W = \gamma BhH \tag{2.27}$$

and

$$S_F = 1 + m\left(\frac{H}{h}\right) \tag{2.23}$$

Thus:

$$Q_u = \gamma BhH + \gamma H^2 \left\{ 2\left[1 + m\left(\frac{H}{h}\right)\right] h + B - h \right\} K_u \tan\phi \tag{2.28}$$

The breakout factor F_q can be determined as:

$$F_q = \frac{Q_u}{\gamma AH} = \frac{Q_u}{\gamma BhH} \tag{2.29}$$

Combining Equations 2.28 and 2.29, we obtain (Das and Seeley, 1975a):

$$F_q = 1 + \left\{ \left[1 + 2m \left(\frac{H}{h} \right) \right] \left(\frac{h}{B} \right) + 1 \right\} \left(\frac{H}{h} \right) K_u \tan \phi \qquad (2.30)$$

The coefficient m given in Equation 2.23 was determined from experimental observations (Meyerhof and Adams, 1968), and its values are given in Table 2.1. In Figure 2.15, m is also plotted as a function of the soil friction angle ϕ.

Experimental observations of Meyerhof and Adams on circular anchors showed that the magnitude of $S_F K_u = [1 + m(H/h)]K_u$ for a given friction angle

TABLE 2.1 Variation of m (Equation 2.23)

Soil friction angle, ϕ (deg)	m
20	0.05
25	0.1
30	0.15
35	0.25
40	0.35
45	0.5
48	0.6

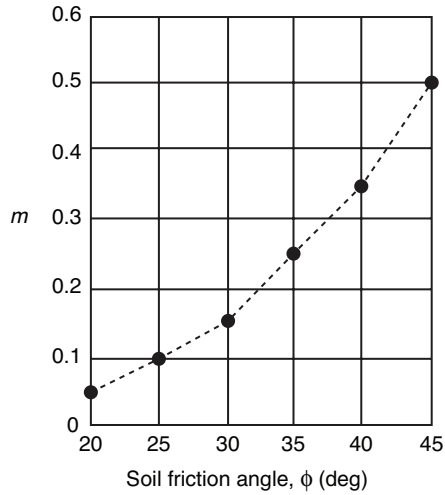

FIGURE 2.15 Variation of m with soil friction angle ϕ

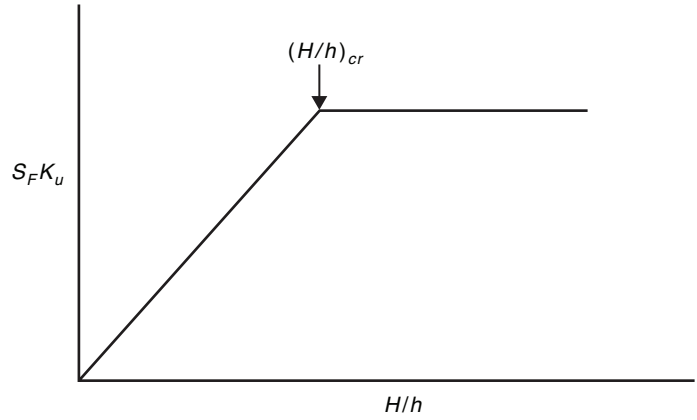

FIGURE 2.16 Nature of variation of $S_F K_u$ with H/h

ϕ increases with H/h to a maximum value at $H/h = (H/h)_{cr}$ and remains constant thereafter, as shown in Figure 2.16. This means that beyond $(H/h)_{cr}$, the anchor behaves as a deep anchor. These $(H/h)_{cr}$ values for square and circular anchors are given in Table 2.2 and also in Figure 2.17.

Thus, for a given value of ϕ for square ($h = B$) and circular (diameter = h) anchors, we can substitute m (Table 2.1) into Equations 2.25 and 2.30 and calculate the breakout factor (F_q) variation with embedment ratio (H/h). The maximum value of $F_q = F_q^\star$ will be attained at $H/h = (H/h)_{cr}$. For $H/h > (H/h)_{cr}$, the breakout factor will remain constant as $F_q^\star$. The variation of F_q with H/h for various values of ϕ made in this manner is shown in Figure 2.18. The variation of the maximum breakout factor $F_q^\star$ for deep square and circular anchors with the soil friction angle ϕ is shown in Figure 2.19.

TABLE 2.2 Critical embedment ratio $(H/h)_{cr}$ for square and circular anchors

Soil friction angle, ϕ (deg)	$(H/h)_{cr}$
20	2.5
25	3
30	4
35	5
40	7
45	9
48	11

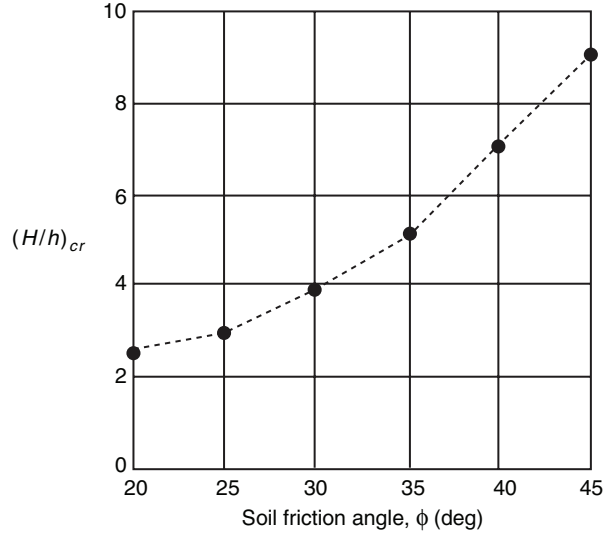

FIGURE 2.17 Variation of $(H/h)_{cr}$ with soil friction angle for square and circular anchors based on the recommendation of Meyerhof and Adams (1968)

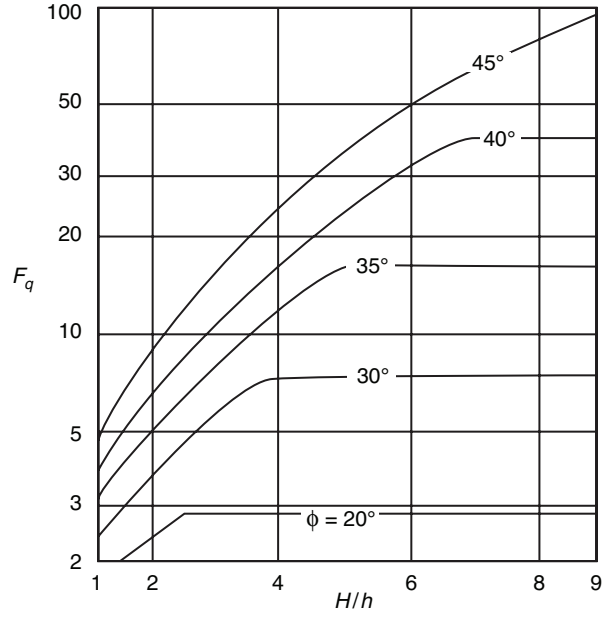

FIGURE 2.18 Plot of F_q (Equations 2.25 and 2.30) for square and circular anchors

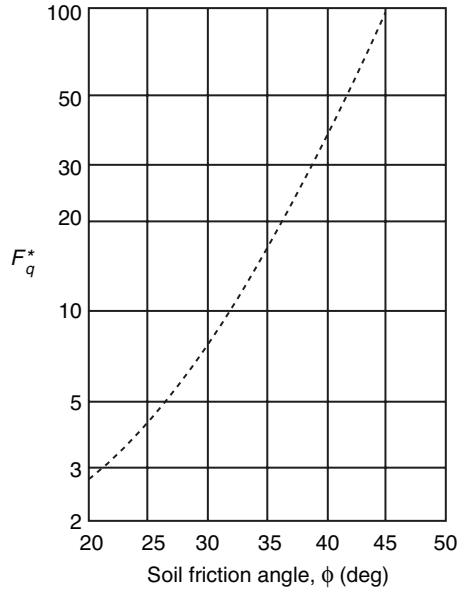

FIGURE 2.19 Plot of F_q^* for deep square and circular anchors

Laboratory experimental observations have shown that the critical embedment ratio for a given soil friction angle ϕ increases with the B/h ratio. Meyerhof (1973) has indicated that for a given value of ϕ:

$$\frac{\left(\frac{H}{h}\right)_{cr\text{-strip}}}{\left(\frac{H}{h}\right)_{cr\text{-square}}} \approx 1.5 \tag{2.31}$$

Based on laboratory model test results, Das and Jones (1982) gave an empirical relationship for the critical embedment ratio of rectangular anchors in the form

$$\left(\frac{H}{h}\right)_{cr\text{-}R} = \left(\frac{H}{h}\right)_{cr\text{-}S} \left[0.133\left(\frac{B}{h}\right) + 0.867\right] \leq 1.4\left(\frac{H}{h}\right)_{cr\text{-}S} \tag{2.32}$$

where

$\left(\frac{H}{h}\right)_{cr\text{-}R}$ = critical embedment ratio of a rectangular anchor with dimensions $B \times h$

$\left(\frac{H}{h}\right)_{cr\text{-}S}$ = critical embedment ratio of a square anchor with dimensions $h \times h$

Using Equation 2.32 and the $(H/h)_{cr\text{-}S}$ values given in Table 2.2, the magnitude of $(H/h)_{cr\text{-}R}$ for rectangular anchors can be estimated. These values of $(H/h)_{cr\text{-}R}$ can be substituted into Equation 2.30 to determine the variation of $F_q = F_q^*$ with the soil friction angle ϕ. Thus, the uplift capacity of shallow and deep anchors can be summarized as follows: For *shallow anchors*:

$$Q_{u(g)} = F_q \gamma A H + W_a \tag{2.33}$$

and for *deep anchors*:

$$Q_{u(g)} = F^* \gamma A H + K_0 p (H - H_{cr}) \overline{\sigma}_0' \tan \phi + W_a \tag{2.34}$$

where

p = perimeter of the anchor shaft
$H - H_{cr}$ = effective length of the anchor shaft (Figure 2.20)
$\overline{\sigma}_0'$ = average effective stress between $z = 0$ to $z = H - H_{cr}$

$$= \frac{1}{2} \gamma (H - H_{cr})$$

K_0 = at-rest earth pressure coefficient ($\approx 1 - \sin \phi$)

The term $K_0 p (H - H_{cr}) \overline{\sigma}_0' \tan \phi$ in Equation 2.34 is the frictional resistance of the shaft. Thus:

$$K_0 p (H - H_{cr}) \overline{\sigma}_0' \tan \phi = \frac{1}{2} \gamma (H - H_{cr})^2 p (1 - \sin \phi) \tan \phi \tag{2.35}$$

Combining Equations 2.34 and 2.35:

$$Q_{u(g)} = F_q^* \gamma A H + \frac{1}{2} \gamma (H - H_{cr})^2 p (1 - \sin \phi) \tan \phi + W_a \tag{2.36}$$

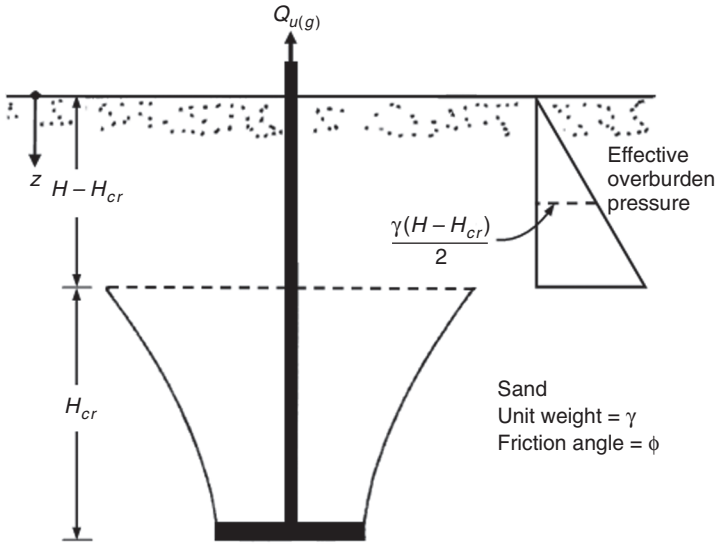

FIGURE 2.20 Deep horizontal plate anchor

2.7 VEESAERT AND CLEMENCE'S THEORY

Based on laboratory model test results, Veesaert and Clemence (1977) suggested that for *shallow circular anchors* the failure surface at ultimate load may be approximated as a truncated cone with an apex angle, as shown in Figure 2.21. With this type of failure surface, the net ultimate uplift capacity can be given as:

$$Q_u = \gamma V + \pi\gamma K(\tan\phi)\left(\cos^2\frac{\phi}{2}\right)\left[\frac{hH^2}{2} + \frac{H^3\tan\left(\frac{\phi}{2}\right)}{3}\right] \quad (2.37)$$

where

V = volume of the truncated cone above the anchor
K = coefficient of lateral earth pressure

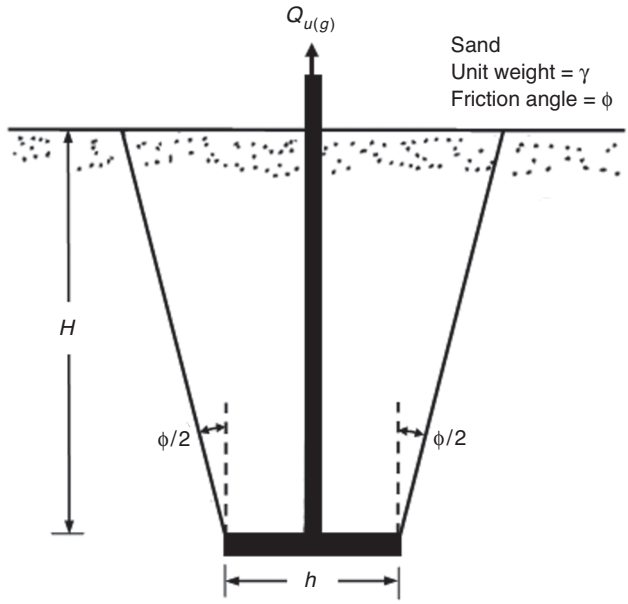

FIGURE 2.21 Assumption of the failure surface in sand for a circular horizontal plate anchor from Veesaert and Clemence's theory (1977)

$$V = \frac{\pi H}{12}\left\{h^2 + \left[h + 2H\tan\left(\frac{\phi}{2}\right)\right]^2 + h\left[h + 2H\tan\left(\frac{\phi}{2}\right)\right]\right\}$$

$$= \frac{\pi H}{12}\left[3h^2 + 4H^2\tan^2\left(\frac{\phi}{2}\right) + 6Hh\tan\left(\frac{\phi}{2}\right)\right] \tag{2.38}$$

Substituting Equation 2.38 into Equation 2.37, we obtain:

$$Q_u = \frac{\pi\gamma H}{3}\left[3h^2 + 4H^2\tan^2\left(\frac{\phi}{2}\right) + 6Hh\tan\left(\frac{\phi}{2}\right)\right]$$

$$+ \pi\gamma K(\tan\phi)\left(\cos^2\frac{\phi}{2}\right)\left[\frac{hH^2}{2} + \frac{H^3\tan\left(\frac{\phi}{2}\right)}{3}\right] \tag{2.39}$$

The breakout factor can now be determined as:

$$F_q = \frac{Q_u}{\gamma AH} = \frac{Q_u}{\gamma\left(\frac{\pi}{4}h^2\right)H} \tag{2.40}$$

Combining Equations 2.39 and 2.40:

$$F_q = \left\{ 4K(\tan\phi)\left[\cos^2\left(\frac{\phi}{2}\right)\right]\left(\frac{H}{h}\right)^2 \times \left[\frac{0.5}{\left(\frac{H}{h}\right)} + \frac{\tan\left(\frac{\phi}{2}\right)}{3}\right]\right\} + \left[1 + 2\left(\frac{H}{h}\right)\tan\left(\frac{\phi}{2}\right) + 1.333\left(\frac{H}{h}\right)^2\tan^2\left(\frac{\phi}{2}\right)\right] \tag{2.41}$$

Veesaert and Clemence (1977) suggested that the magnitude of K_0 may vary between 0.6 to 1.5, with an average value of about 1. Figure 2.22 shows the plot of F_q versus H/h with $K_0 = 1$. In this plot it is assumed that $(H/h)_{cr}$ is the same as that proposed by Meyerhof and Adams (1968) and given in Table 2.2. For $H/h \leq (H/h)_{cr}$, the magnitude of $F_q = F_q^* =$ constant. A comparison of the plots shown in Figures 2.18 and 2.22 reveals the following:

1. For ϕ up to about 35° with $K = 1$, Equation 2.41 yields higher values of F_q compared to those calculated by using Equation 2.30.
2. For $\phi = 40°$ and similar H/h ratios, Equations 2.30 and 2.41 yield practically the same values of F_q.
3. For $\phi > 40°$, the values of F_q calculated by using Equation 2.41 are smaller than those calculated by using Equation 2.30.

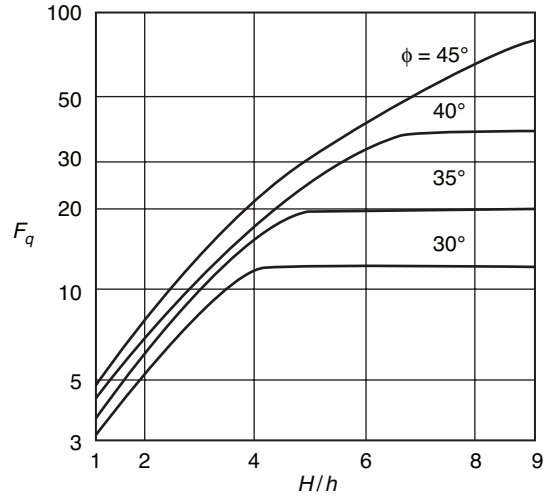

FIGURE 2.22 Variation of F_q for shallow circular anchors (Equation 2.41)

2.8 VESIC'S THEORY

Vesic (1965) studied the problem of an explosive point charge expanding a spherical cavity close to the surface of a semi-infinite, homogeneous, isotropic solid (in this case, the soil). Referring to Figure 2.23, it can be seen that if the distance H is small enough, there will be an ultimate pressure p_0 that will shear away the soil located above the cavity. At that time, the diameter of the spherical

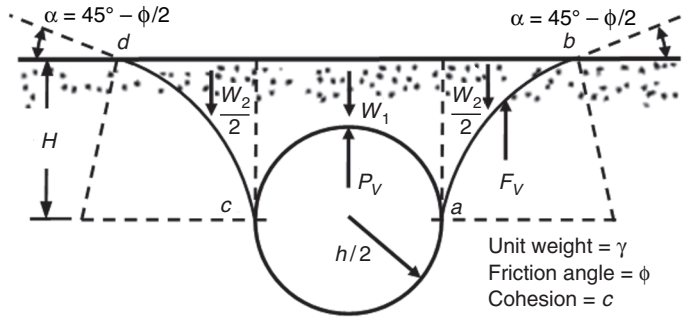

FIGURE 2.23 Vesic's theory (1965) of expansion of cavities

cavity is equal to h. The slip surfaces ab and cd will be tangent to the spherical cavity at a and c. At points b and d, they make an angle $\alpha = 45° - \phi/2$. Now, for equilibrium, summing the components of forces in the vertical direction, we can determine the ultimate pressure p_0 in the cavity. Forces that will be involved are

1. Vertical component of the force inside the cavity, P_V
2. Effective self-weight of the soil, $W = W_1 + W_2$
3. Vertical component of the resultant of internal forces, F_V

For a c-ϕ soil, we can thus determine that

$$p_0 = C\bar{F}_c + \gamma H\bar{F}_q \tag{2.42}$$

where

$$\bar{F}_q = 1.0 - \frac{2}{3}\left[\frac{\left(\frac{h}{2}\right)}{H}\right] + A_1\left[\frac{H}{\left(\frac{h}{2}\right)}\right] + A_2\left[\frac{H}{\left(\frac{h}{2}\right)}\right]^2 \tag{2.43}$$

$$\bar{F}_c = A_3\left[\frac{H}{\left(\frac{h}{2}\right)}\right] + A_4\left[\frac{H}{\left(\frac{h}{2}\right)}\right] \tag{2.44}$$

where

A_1, A_2, A_3, A_4 = functions of the soil friction angle ϕ

For granular soils, $c = 0$. Thus:

$$p_0 = \gamma H\bar{F}_q \tag{2.45}$$

Vesic (1971) applied the preceding concept to determine the ultimate uplift capacity of shallow circular anchors. In Figure 2.23, consider that the circular anchor plate ab, with a diameter h, is located at a depth H below the ground

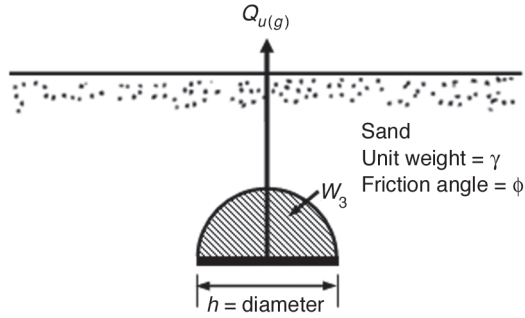

FIGURE 2.24 A hemispherical cavity filled with soil above the anchor plate

surface. If the hemispherical cavity above the anchor plate is filled with soil, it will have a weight of (Figure 2.24):

$$W_3 = \frac{2}{3}\pi\left(\frac{h}{2}\right)^3\gamma \tag{2.46}$$

This weight of soil will increase the pressure by p_1, which can be given as:

$$p_1 = \frac{W_3}{\pi\left(\frac{h}{2}\right)^2} = \frac{\left(\frac{2}{3}\right)\pi\left(\frac{h}{2}\right)^3\gamma}{\pi\left(\frac{h}{2}\right)^2} = \frac{2}{3}\gamma\left(\frac{h}{2}\right)$$

If the anchor is embedded in a cohesionless soil ($c = 0$), then the pressure p_1 should be added to Equation 2.43 to obtain the force per unit area of the anchor, q_u, needed for complete pullout. Thus:

$$q_u = \frac{Q_u}{A} = \frac{Q_u}{\pi\left(\frac{h}{2}\right)^2} = p_0 + p_1 = \gamma H\overline{F}_q + \frac{2}{3}\gamma\left(\frac{h}{2}\right)$$

$$= \gamma H\left[\overline{F}_q + \frac{\frac{2}{3}\left(\frac{h}{2}\right)}{H}\right] \tag{2.47}$$

TABLE 2.3 Vesic's (1971) breakout factor F_q for circular anchors

	H/h				
Soil friction angle, ϕ (deg)	0.5	1.0	1.5	2.5	5.0
0	1.0	1.0	1.0	1.0	1.0
10	1.18	1.37	1.59	2.08	3.67
20	1.36	1.75	2.20	3.25	6.71
30	1.52	2.11	2.79	4.41	9.89
40	1.65	2.41	3.30	5.45	13.0
50	1.73	2.61	3.56	6.27	15.7

or

$$q_u = \frac{Q_u}{A} = \gamma H \left\{ 1 + A_1 \left[\frac{H}{\left(\frac{h}{2}\right)} \right] + A_2 \left[\frac{H}{\left(\frac{h}{2}\right)} \right]^2 \right\} = \gamma H F_q \qquad (2.48)$$

Breakout factor

The variation of the breakout factor F_q for shallow *circular anchor plates* is given in Table 2.3 (and also Figure 2.25). In a similar manner, using the analogy of the expansion of the long cylindrical cavities, Vesic determined the variation of the breakout factor F_q for *shallow strip anchors*. These values are given in Table 2.4 and are also plotted in Figure 2.26.

2.9 SAEEDY'S THEORY

An ultimate holding capacity theory for *circular plate anchors* embedded in sand was proposed by Saeedy (1987) in which the trace of the failure surface was assumed to be an arc of a logarithmic spiral, as shown in Figure 2.27. According to this solution, for shallow anchors the failure surface extends to the ground surface. However, for deep anchors (that is, $H > H_{cr}$), the failure surface extends to a distance of H_{cr} above the anchor plate. Based on this analysis, Saeedy (1987) proposed the net ultimate uplift capacity in a nondimensional form ($Q_u/\gamma H h^2$) for various values of ϕ and the H/h ratio. The authors have converted the solution into a plot of breakout factor $F_q = Q_u/\gamma AH$ (A = area of the anchor

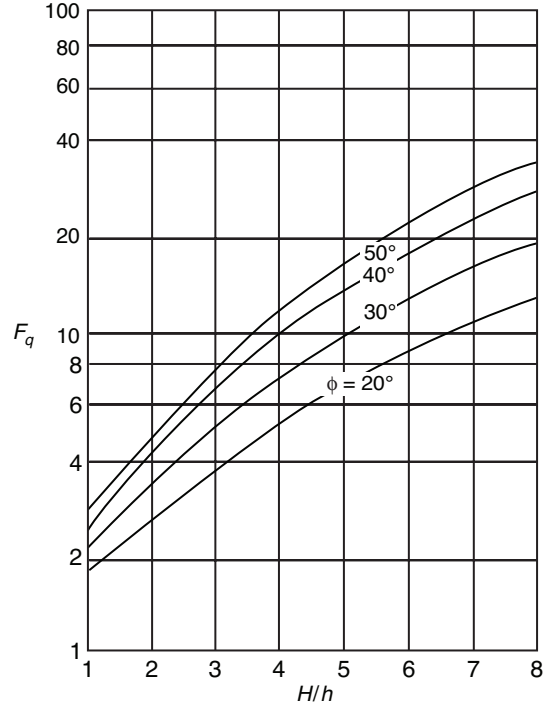

FIGURE 2.25 Vesic's (1971) breakout factor F_q for shallow circular anchors

TABLE 2.4 Vesic's (1971) breakout factor F_q for strip anchors

	H/h				
Soil friction angle, ϕ (deg)	0.5	1.0	1.5	2.5	5.0
0	1.0	1.0	1.0	1.0	1.0
10	1.09	1.16	1.25	1.42	1.83
20	1.17	1.33	1.49	1.83	2.65
30	1.24	1.47	1.71	2.19	3.38
40	1.30	1.58	1.87	2.46	3.91
50	1.32	1.64	2.04	2.6	4.2

plate) versus the soil friction angle ϕ, as shown in Figure 2.28. According to Saeedy (1987), during the anchor pullout, the soil located above the anchor gradually becomes compacted, in turn increasing the shear strength of the soil and, hence, the net ultimate uplift capacity. For that reason, he introduced an empirical *compaction factor,* which is given in the form

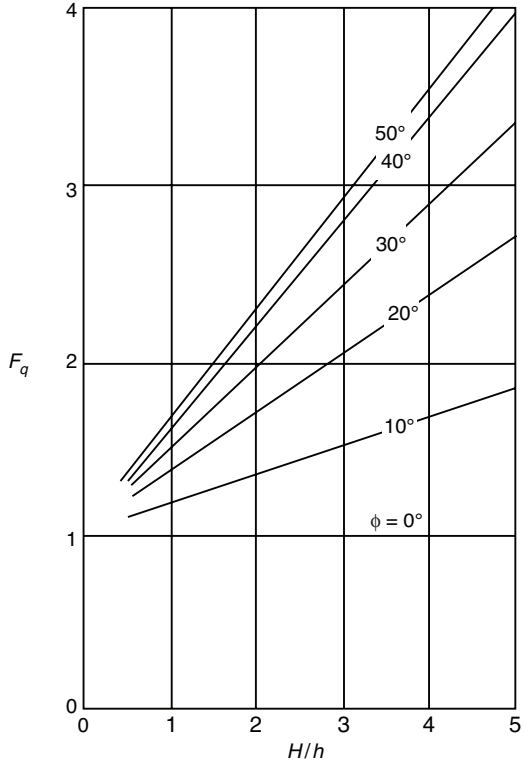

FIGURE 2.26 Vesic's (1971) breakout factor F_q for shallow strip anchors

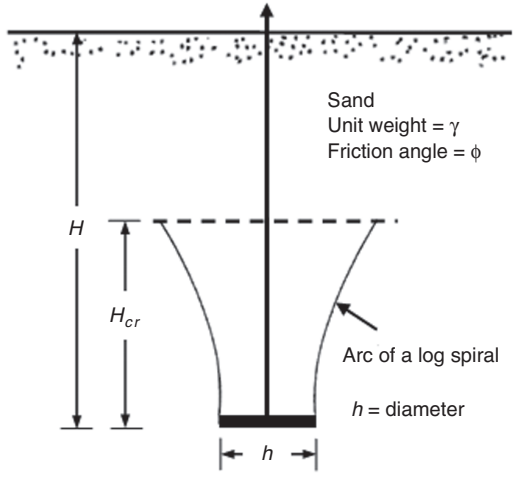

FIGURE 2.27 Saeedy's theory (1987) for circular plate anchors

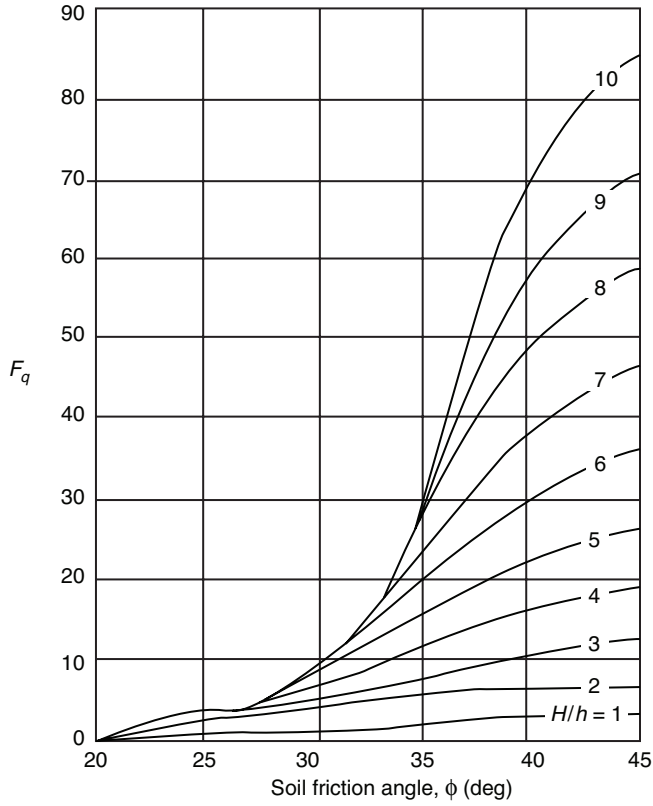

FIGURE 2.28 Plot of F_q based on Saeedy's theory (1987)

$$\mu = 1.044 D_r + 0.44 \tag{2.49}$$

where

μ = compaction factor
D_r = relative density of compaction

Thus, the actual net ultimate capacity can be expressed as:

$$Q_{u(\text{actual})} = \mu F_q \gamma A H \tag{2.50}$$

2.10 DISCUSSION OF VARIOUS THEORIES

Based on various theories presented in the previous sections, we can make some general observations:

1. All of the preceding theories presented, except that of Meyerhof and Adams (1968), are for the axisymmetric case (that is, for use in the case of *circular* anchors). Meyerhof and Adams's theory addresses the case of *rectangular* anchors.
2. Most theories assume that the shallow anchor condition exists for $H/B \leq 5$. Meyerhof and Adams's theory provides a critical embedment ratio $(H/h)_{cr}$ for *square* and *circular* anchors as a function of the soil friction angle.
3. Experimental observations generally tend to show that for shallow anchors embedded in loose sand, Balla's theory (1961) overestimates the net ultimate uplift capacity. However, better agreement is obtained for anchors embedded in dense soil.
4. Vesic's theory (1971) is generally fairly accurate in estimating the net ultimate uplift capacity for shallow anchors in loose sand. However, laboratory experimental observations have shown that for shallow anchors embedded in dense sand, this theory can underestimate the actual capacity by as much as 100% or more.
5. Mariupol'skii's theory (1965) suggests that for calculation of the net ultimate uplift capacity, the lower of the two values obtained from Equations 2.14 and 2.15 should be used. The reason for such recommendation is due to the fact that the critical embedment was not clearly established in the theory.

Figure 2.29 shows a comparison of some published laboratory experimental results for the net ultimate uplift capacity of *circular anchors* with the theories of Balla, Vesic, and Meyerhof and Adams. Table 2.5 gives the references to the laboratory experimental curves shown in Figure 2.29. In developing the theoretical plots for $\phi = 30°$ (loose sand condition) and $\phi = 45°$ (dense sand condition), the following procedures have been used:

1. According to Balla's theory (1961), from Equation 2.9 for circular anchors:

$$Q_u = H^3\gamma(F_1 + F_3)$$

Figure 2.7

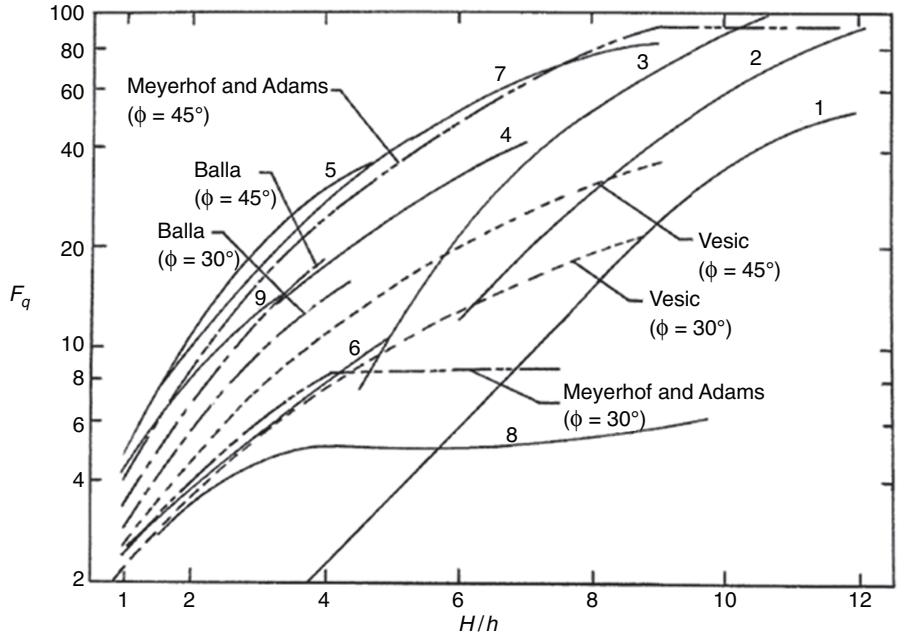

FIGURE 2.29 Comparison of theories with laboratory experimental results for circular anchor plates

TABLE 2.5 References to laboratory experimental curves shown in Figure 2.29

Curve no.	Reference	Circular anchor diameter, h (mm)	Soil properties
1	Baker and Kondner (1966)	25.4	$\phi = 42°$, $\gamma = 17.61$ kN/m^3
2	Baker and Kondner (1966)	38.1	$\phi = 42°$, $\gamma = 17.61$ kN/m^3
3	Baker and Kondner (1966)	50.8	$\phi = 42°$, $\gamma = 17.61$ kN/m^3
4	Baker and Kondner (1966)	76.2	$\phi = 42°$, $\gamma = 17.61$ kN/m^3
5	Sutherland (1965)	38.1–152.4	$\phi = 45°$
6	Sutherland (1965)	38.1–152.4	$\phi = 31°$
7	Esquivel-Diaz (1967)	76.2	$\phi \approx 43°$, $\gamma = 14.81$–15.14 kN/m^3
8	Esquivel-Diaz (1967)	76.2	$\phi \approx 33°$, $\gamma = 12.73$–12.89 kN/m^3
9	Balla (1961)	61–119.4	Dense sand

Thus:

$$F_1 + F_3 = \frac{Q_u}{\gamma H^3} = \frac{\left(\frac{\pi}{4} h^2\right) Q_u}{\gamma H^3 \left(\frac{\pi}{4} h^2\right)} = \frac{\left[\frac{\pi}{4} \left(\frac{h}{H}\right)^2\right] Q_u}{\gamma AH}$$

or

$$F_q = \frac{Q_u}{\gamma AH} = \frac{F_1 + F_3}{\frac{\pi}{4} \left(\frac{h}{H}\right)^2} \tag{2.51}$$

Thus, for a given soil friction angle, the sum of $F_1 + F_3$ has been obtained from Figure 2.7 and the breakout factor has been calculated for various values of H/h, and they have been plotted in Figure 2.29.

2. For Vesic's theory (1971), the variations of F_q versus H/h for circular anchors have been given in Table 2.3. These values of F_q have also been plotted in Figure 2.29.
3. The breakout factor relationship for circular anchors based on Meyerhof and Adams's theory (1968) is given in Equation 2.25. Using $K_u \approx 0.95$, the variations of F_q with H/h have been calculated and are plotted in Figure 2.29.

Based on the comparison between the theories and the laboratory experimental results shown in Figure 2.29, it appears that Meyerhof and Adams's theory (1968) is more applicable to a wide range of anchors and it provides as good an estimate as any for the net ultimate uplift capacity. Therefore, this theory is recommended for use. However, it needs to be kept in mind that the majority of the experimental results presently available in the literature for comparison with the theory are from laboratory model tests. When applying these results to the design of an actual foundation, the *scale effect* needs to be taken into consideration. For that reason, a judicious choice is necessary in selecting the value of the soil friction angle ϕ.

Example 2.1

Consider a circular anchor plate embedded in sand. For the anchor, diameter $h = 0.3$ m and depth of embedment $H = 1.2$ m. For the sand, unit weight $\gamma = 17.4$ kN/m^3 and friction angle $\phi = 35°$. Using Balla's theory, calculate the net ultimate uplift capacity.

Solution

From Equation 2.9:

$$Q_u = H^3\gamma(F_1 + F_3)$$

From Figure 2.7, for $\phi = 35°$ and $H/h = 1.2/0.3 = 4$, the magnitude of $F_1 + F_3 \approx 0.725$. Thus:

$$Q_u = (1.2)^3\,(17.4)\,(0.725) = \mathbf{21.8\ kN}$$

Example 2.2

Redo Example 2.1 using Vesic's theory (1965).

Solution

From Equation 2.48:

$$Q_u = \gamma AHF_q$$

From Figure 2.25, for $\phi = 35°$ and $H/h = 4$, F_q is about 9. Therefore:

$$Q_u = \left[\left(\frac{\pi}{4}\right)(0.3)^2\right](17.4)\,(1.2)\,(9) = \mathbf{13.28\ kN}$$

Example 2.3

Redo Example 2.1 using Meyerhof and Adams's theory (1968).

Solution

From Equation 2.25:

$$F_q = 1 + 2\left[1 + m\left(\frac{H}{h}\right)\right]\left(\frac{H}{h}\right)K_u \tan\phi$$

For $\phi = 35°$, $m = 0.25$ (Table 2.1). Hence:

$$F_q = 1 + 2\,[1 + (0.25)\,(4)]\,(4)\,(0.95)\,(\tan 35°) = 11.64$$

Therefore:

$$Q_u = F_q \gamma AH = (11.64)\,(17.4)\left[\left(\frac{\pi}{4}\right)(0.3)^2\right](1.2) = \mathbf{17.18\ kN}$$

Example 2.4

Redo Example 2.1 using Veesaert and Clemence's theory (1977). Use $K = 1$.

Solution

From Equation 2.41:

$$F_q = \left\{4K(\tan\phi)\left[\cos^2\left(\frac{\phi}{2}\right)\right]\left(\frac{H}{h}\right)^2\left[\frac{0.5}{\left(\frac{H}{h}\right)} + \frac{\tan\left(\frac{\phi}{2}\right)}{3}\right]\right\}$$

$$+ \left[1 + 2\left(\frac{H}{h}\right)\tan\left(\frac{\phi}{2}\right) + 1.333\left(\frac{H}{h}\right)^2 \tan^2\left(\frac{\phi}{2}\right)\right]$$

Using $\phi = 35°$, $H/h = 4$, and $K = 1$:

$$F_q = \left\{ (4)(1)(\tan 35°)[\cos^2(17.5°)](4)^2 \left[\frac{0.5}{4} + \frac{\tan(17.5°)}{3} \right] \right\}$$

$$+ \{1 + (2)(4)[\tan(17.5°)] + (1.333)(4)^2[\tan^2(17.5°)]\}$$

$$= 15$$

Therefore:

$$Q_u = F_q \gamma A H = (15)(17.4)\left[\left(\frac{\pi}{4} \right)(0.3)^2 \right](1.2) = \mathbf{22.14\ kN}$$

2.11 LOAD-DISPLACEMENT RELATIONSHIP

In order to determine the allowable net ultimate uplift capacity of plate anchors, two different procedures can be adopted:

1. Use of a *tentative factor of safety* F_s, based on the uncertainties of determination of the soil shear strength parameters and other associated factors. For this type of analysis:

$$Q_{u(\text{all})} = \frac{Q_u}{F_s} \tag{2.52}$$

2. Use of a *load-displacement relationship*. In this method, the allowable net ultimate uplift capacity is calculated which corresponds to a predetermined allowable vertical displacement of the anchor.

Das and Puri (1989) investigated the load-displacement relationship of *shallow horizontal square and rectangular plate anchors* embedded in medium and dense sands. For these laboratory model tests, the width of the anchor plate (h) was kept at 50.8 mm. The length-to-width ratios of the anchors (B/h) were varied from 1 to 3, and the H/h ratios were varied from 1 to 5. Based on their laboratory observations, the net load Q versus vertical displacement Δ plots can

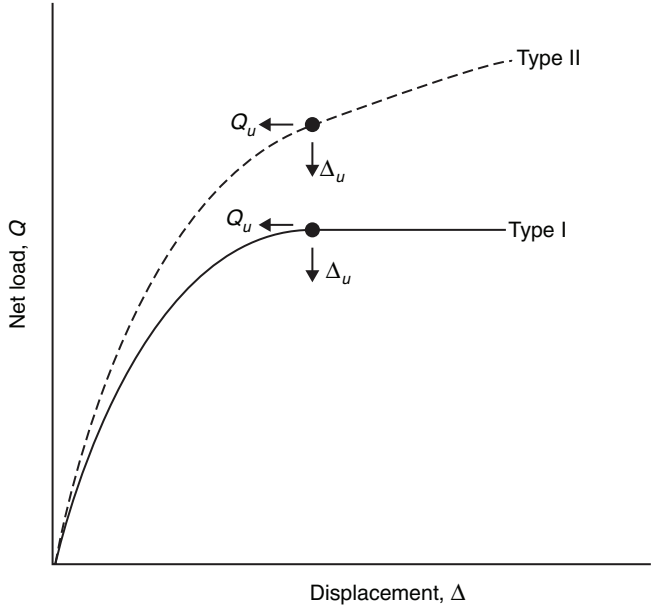

FIGURE 2.30 Nature of load versus displacement plots

be of two types, as shown in Figure 2.30. In Type I, the net load increases with displacement up to a maximum value at which sudden pullout occurs. The maximum load in this case is the net ultimate uplift capacity Q_u. In Type II, the net load increases with the vertical displacement fairly rapidly up to a certain point, beyond which the load-displacement relationship becomes practically linear. For this case, the net ultimate uplift capacity is defined as the point where the slope of the Q versus Δ plot becomes minimum. The vertical displacement which corresponds to load Q_u is defined as Δ_u in Figure 2.30.

Figure 2.31 shows the magnitudes of Δ_u for anchors with various B/h ratios placed at varying embedment ratios (H/h). It needs to be pointed out that for tests conducted in medium sand, the relative density of compaction D_r was about 48%. Similarly, for tests conducted in dense sand, the average value of D_r was about 73%. With their experimental results, Das and Puri (1989) proposed a nondimensional empirical load-displacement relationship for shallow plate anchors which is of the form

$$\overline{Q} = \frac{\overline{\Delta}}{a + b\overline{\Delta}} \tag{2.53}$$

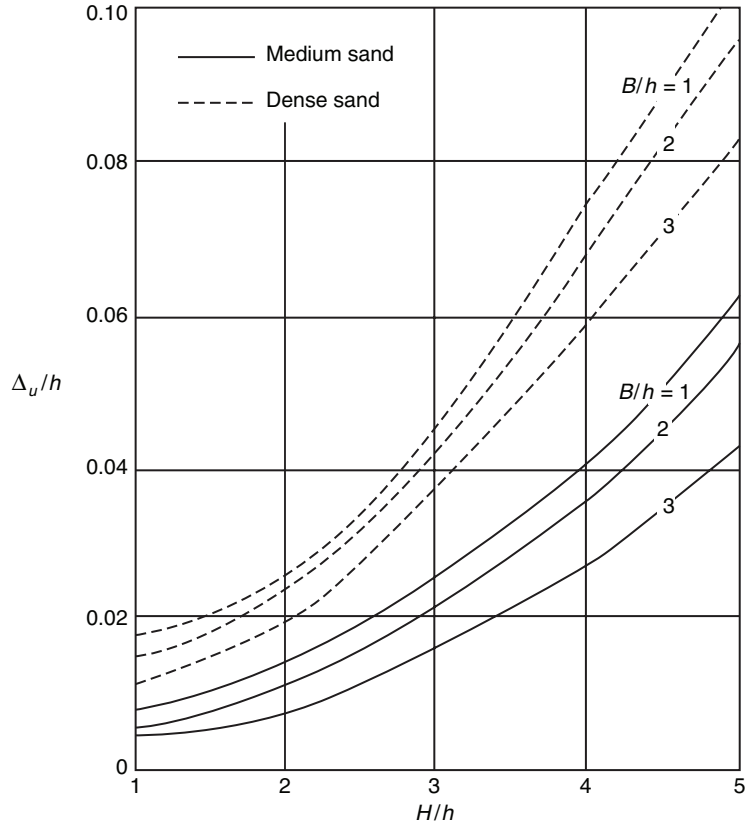

FIGURE 2.31 Variation of Δ_u/h with H/h based on the model tests of Das and Puri (1989) (h = 50.8 mm)

where

$$\overline{Q} = \frac{Q}{Q_u} \tag{2.54}$$

$$\overline{\Delta} = \frac{\Delta}{\Delta_u} \tag{2.55}$$

Δ = anchor displacement at net uplifting load Q
a, b = constants

The constants a and b are approximately equal to 0.175 and 0.825, respectively, and they are not functions of the relative density of compaction. From Equation 2.53, it follows that:

$$\frac{\overline{\Delta}}{Q} = a + b\overline{\Delta} \tag{2.56}$$

The preceding equation implies that a plot of $\overline{\Delta}/\overline{Q}$ versus $\overline{\Delta}$ will be approximately linear.

Example 2.5

Consider a shallow rectangular anchor embedded in sand where $h = 0.3$ m, $B = 0.9$ m, and $H = 1.2$ m. For the sand, $\gamma = 18$ kN/m^3 and $\phi = 35°$. Estimate:

a. The net ultimate uplift capacity using the theory of Meyerhof and Adams (1968)
b. The anchor displacement at ultimate load
c. The net load Q at an anchor displacement of $0.5\Delta_u$

Solution

Part a. For this case:

$$\frac{B}{h} = \frac{0.9}{0.3} = 3; \qquad \frac{H}{h} = \frac{1.2}{0.3} = 4$$

From Table 2.2, $H/h < (H/h)_{cr}$ for $\phi = 35°$. Therefore, it is a shallow anchor. From Equations 2.29 and 2.30:

$$Q_u = F_q \gamma B h H$$

$$F_q = 1 + \left\{ \left[1 + 2m\left(\frac{H}{h}\right) \right] \left(\frac{h}{B}\right) + 1 \right\} \left(\frac{H}{h}\right) K_u \tan\phi$$

For $\phi = 35°$, the value of m is 0.25. Assuming $K_u \approx 0.95$, we can calculate F_q. Hence:

$$F_q = 1 + \left\{ [1 + (2)\,(0.25)\,(4)] \left(\frac{1}{3}\right) + 1 \right\} (4)\,(0.95)\,(\tan 35°) = 6.32$$

Therefore:

$$Q_u = F_q \gamma B h H = (6.32)\,(18)\,(0.9)\,(0.3)\,(1.2) = \mathbf{36.86\ kN}$$

Part b. Consider the sand as loose. From Figure 2.31, for $B/h = 3$ and $H/h = 4$, the value of $\Delta_u/h \approx 0.06$. Therefore:

$$\Delta_u \approx (0.06)\,(0.3) = 0.18\ \text{m} = \mathbf{180\ mm}$$

Part c. From Equation 2.53:

$$\overline{Q} = \frac{\overline{\Delta}}{a + b\overline{\Delta}}; \qquad \overline{\Delta} = \frac{\Delta}{\Delta_u} = 0.5$$

Thus:

$$\overline{Q} = \frac{0.5}{0.175 + (0.825)\,(0.5)} = 0.851; \qquad \overline{Q} = \frac{Q}{Q_u} = 0.851$$

Therefore:

$$Q = (0.851)\,(36.86) = \mathbf{31.37\ kN}$$

Liu et al. (2012) presented a laboratory experimental investigation on soil deformation around plate anchors during uplift in sand by using digital image correlation. This study shows that the soil deformation and the pullout resistance of horizontal plate anchors are substantially influenced by soil density and anchor embedment depth, whereas particle size within the studied range (fine to coarse sand) has limited influence. For the same embedment ratio of 3 in loose sand, the anchor deforms 6.30 mm to reach its peak pullout resistance of

24.8 N compared with the values of 0.76 mm and 61.3 N, respectively, in dense sand. In dense sand, the shape of the failure surface changes from a truncated cone above a shallow anchor to a combined shape of a curved cone and a truncated cone for a deep anchor. In contrast, in loose sand, a cone-shaped failure surface is formed within the soil mass above a shallow anchor; however, no failure surface is observed for a deep anchor, where the compressibility of soil is the dominating factor that influences the behavior of deep plate anchors in loose sand.

2.12 ANCHORS SUBJECTED TO REPEATED LOADING

Horizontal anchors are sometimes used to moor surface vessels or buoys as well as semi-submersible or submersible structures. These anchors may be subjected to a combination of sustained and repeated loads. The application of repeated loads may create a progressive accumulative cyclic strain that will ultimately lead to the uplift of the anchor. Very few studies are available to evaluate the effect of repeated loads on anchors. Andreadis et al. (1978) studied the behavior of model circular anchor plates embedded in saturated dense sand and subjected to cyclic loading. For this study, the embedment ratio H/h was kept as 12 (that is, deep anchor condition). The cyclic load was sinusoidal in nature with 10-second duration cycles (Figure 2.32a). In some tests, the cyclic load Q_c was applied alone, as shown in Figure 2.32b. Also, some tests were conducted with an initial application of a sustained static load Q_s and then a cyclic load of magnitude Q_c, and the results of these tests are shown in Figure 2.33. In Figure 2.33, the relative anchor movement is defined as:

$$\Delta\lambda = \frac{\Delta}{h} \tag{2.57}$$

where

Δ = uplift of anchor
h = anchor diameter

It can be seen from Figure 2.33 that for a given magnitude of Q_c/Q_u, the relative anchor displacement $\Delta\lambda$ increased with the number of cycles.

Based on their model tests, Andreadis et al. (1978) suggested that when the cyclic relative anchor displacement is kept below about half the relative movement to failure in static pullout tests, there is essentially no reduction in strength

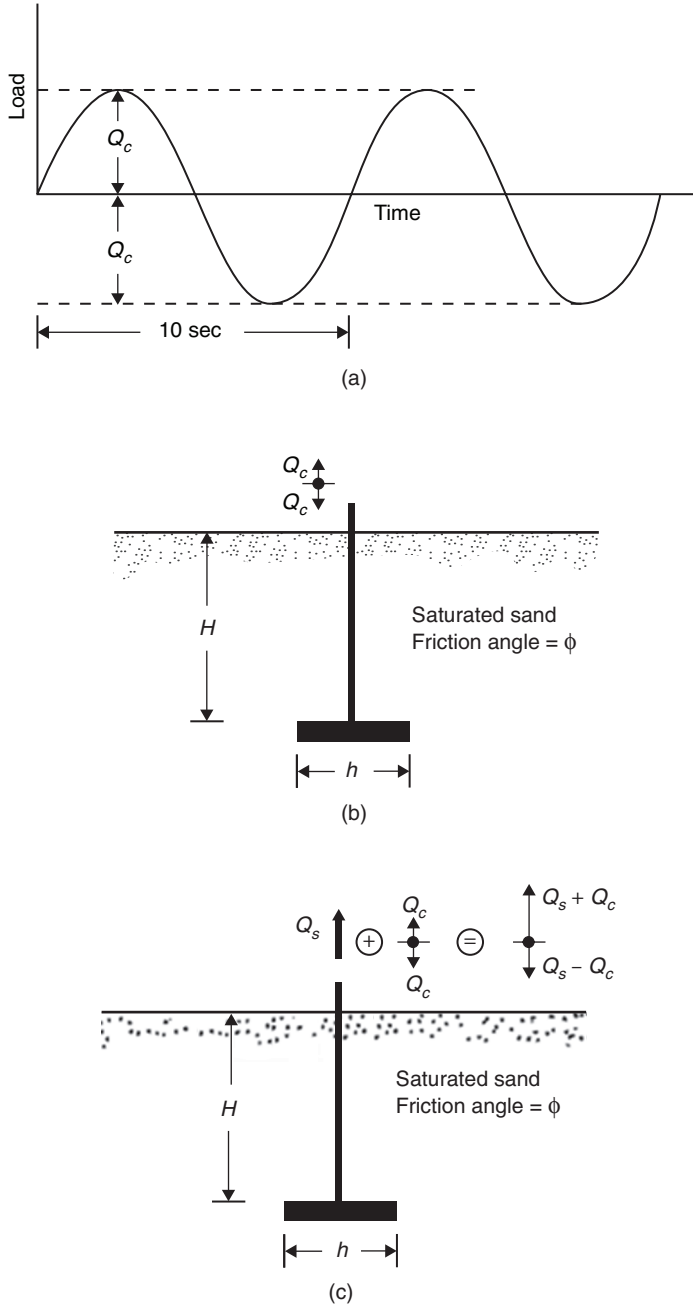

FIGURE 2.32 Details of the model tests of Andreadis et al. (1978) on deep circular anchor plates

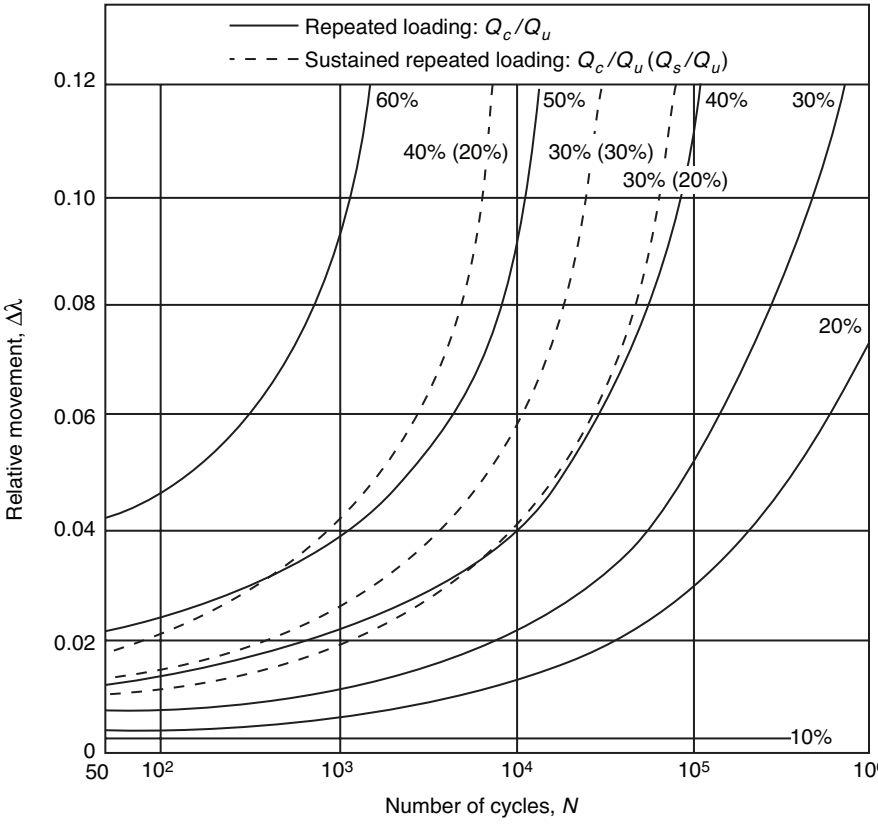

FIGURE 2.33 Relative anchor movement versus number of cycles in dense sand (H/h = 12, circular anchor) (after Andreadis et al., 1978)

due to cyclic loading. For that reason, a plot of Q_c/Q_u versus number of cyclic load applications for various values of $\Delta\lambda$ is shown in Figure 2.34, essentially obtained from the experimental results shown in Figure 2.33. Therefore, if the ultimate displacement Δ_u at ultimate static load Q_u is known, one can calculate the allowable maximum value $\Delta\lambda$ as:

$$\Delta\lambda_{(\text{allowable})} \approx \frac{1}{2}\Delta_u \tag{2.58}$$

Once $\Delta\lambda_{(\text{allowable})}$ is known, the magnitude of Q_c/Q_u and thus Q_c, corresponding to the number of load application cycles during the life span of the anchor, can be estimated.

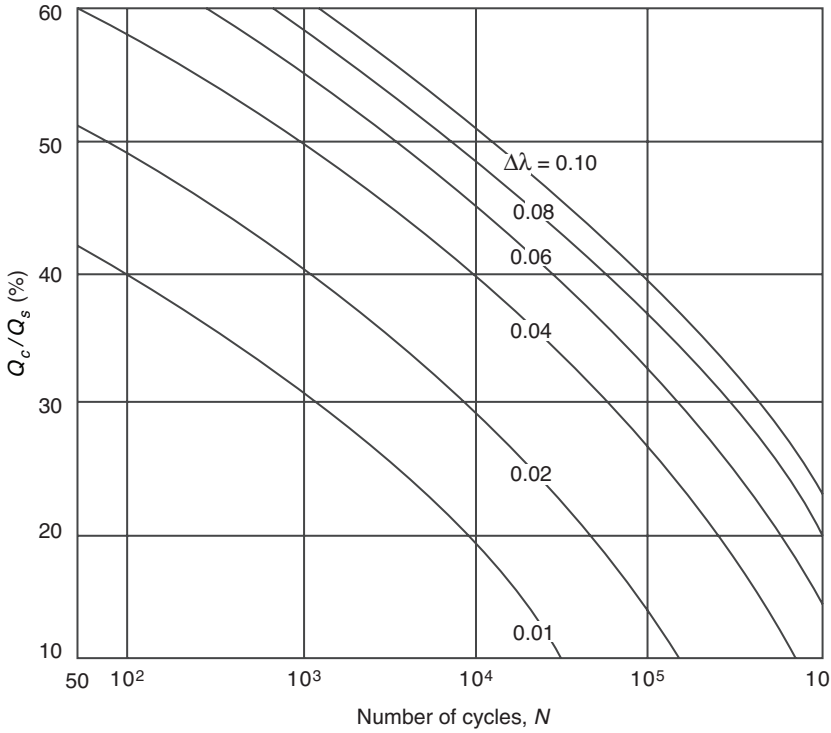

FIGURE 2.34 Relative cyclic load versus number of cycles in dense sand (H/h = 12, circular anchor) (adapted from Andreadis et al., 1978)

2.13 UPLIFT CAPACITY OF SHALLOW GROUP ANCHORS

When anchors placed in a group are subjected to an uplifting load, the net ultimate uplift capacity of the group may possibly be smaller than the net ultimate uplift capacity of a single anchor times the number of anchors in the group. This condition arises when the center-to-center spacing of the anchor is small and when, during the anchor uplift, there is interference of the failure zones in soil. Figure 2.35 shows a group of anchors located at a shallow depth H. All of the anchors are circular in shape, and the center-to-center spacing of the anchors is equal to s. In the plan of the anchor group, there are m number of rows and n columns. The gross ultimate uplift capacity of the anchor group, $Q_{ug(g)}$, can be given as:

$$Q_{ug(g)} = Q_{ug} + W_g \tag{2.59}$$

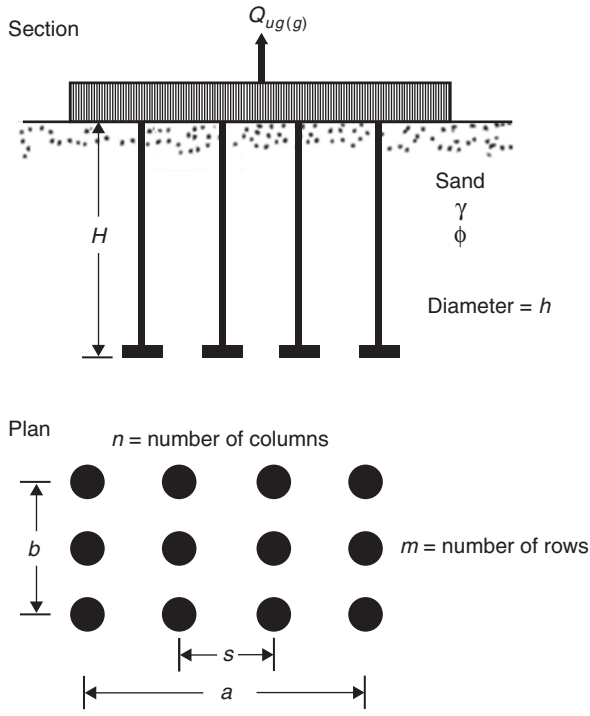

FIGURE 2.35 Group anchors

where

Q_{ug} = net ultimate uplift capacity of the group
W_g = effective self-weight of anchors and the shafts

Meyerhof and Adams (1968) derived a theoretical relationship for the net ultimate capacity of group anchors, according to which

$$Q_{ug} = \gamma H^2 \left[a + b + S_F \left(\frac{\pi}{2} \right) h \right] K_u \tan \phi + W_s \qquad (2.60)$$

where

S_F = shape factor
K_u = nominal uplift coefficient

W_s = effective weight of the sand located above the anchor group
$a = s(n - 1)$ (see Figure 2.35)
$b = s(m - 1)$ (see Figure 2.35)

The shape factor S_F is given by the same relationship as in Equation 2.23, or:

$$S_F = 1 + m\left(\frac{H}{h}\right)$$

Table 2.1

The nominal uplift coefficient K_u is the same as shown in Figure 2.13 and may be taken as approximately 0.95 for all values of the soil friction angle ϕ. In deriving Equation 2.60, it is assumed that the passive pressure along the curved portion of the perimeter of the group is governed by the shape factor S_F, and the passive earth pressure along the straight portions is the same as for strip anchors.

In the conventional manner, the group efficiency η can now be defined as:

$$\eta = \frac{Q_{ug}}{mnQ_u} \tag{2.61}$$

Thus, combining Equations 2.60, 2.61, and 2.22, we obtain:

$$\eta\,(\%) = \left\{ \frac{\gamma H^2 \left[a + b + S_F\left(\frac{\pi}{2}\right)h\right] K_u \tan\phi + W_s}{mn\left[\left(\frac{\pi}{2}\right) S_F \gamma h H^2 K_u \tan\phi + W\right]} \right\} (100) \leq 100\% \tag{2.62}$$

In order to investigate the applicability of the preceding equation, Das and Jin-Kaun (1987) conducted a limited number of laboratory model tests in compacted sand at a relative density of 68% with an angle of friction of 37°. Figures 2.36 and 2.37 show the model test results for group efficiency for the cases of $H/h = 4$ and 6, respectively. The theoretical variations of the group efficiency with the center-to-center spacing of anchors are also shown in Figures 2.36 and 2.37. A comparison of the theoretical and experimental results shows that for a given anchor configuration and H/h, the s/h ratio at which $\eta = 100\%$ is approximately twice that predicted by the theory. However, the general trend

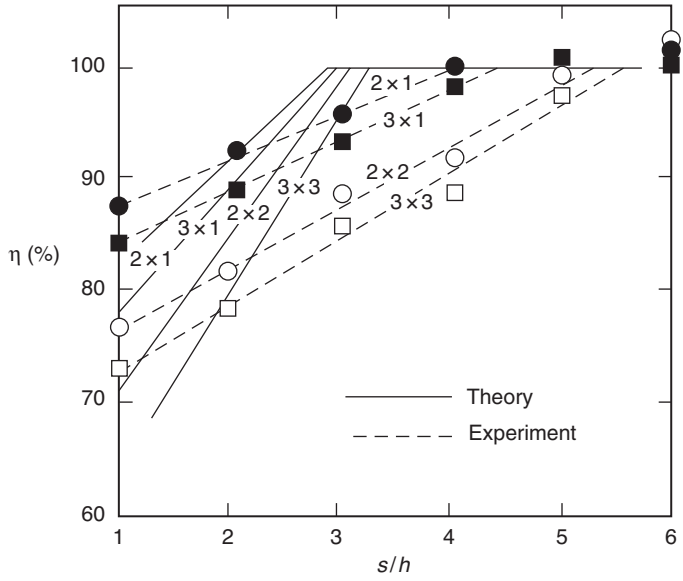

FIGURE 2.36 Variation of η versus s/h for group piles (relative density = 68%, H/h = 4) (adapted from Das and Jin-Kaun, 1987)

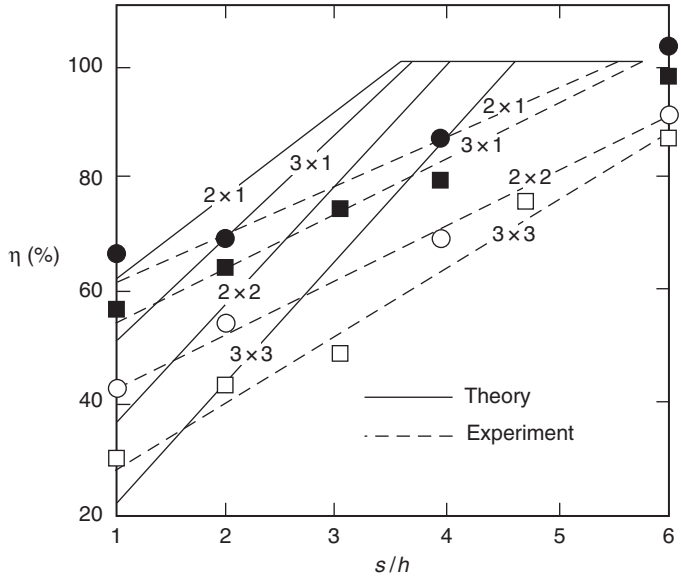

FIGURE 2.37 Variation of η versus s/h for group piles (relative density = 68°, H/h = 6) (adapted from Das and Jin-Kaun, 1987)

of the actual variation of η versus s/h for a given anchor configuration is similar to that predicted by the theory.

Kumar and Kouzer (2008a) analyzed the effect of spacing of a group of two and multiple rough strip anchors, with equal widths and placed horizontally in sand, on the magnitude of the vertical uplift resistance. The analysis was carried out by using an upper bound limit analysis with the employment of a simple rigid wedge mechanism bounded by planar rupture surfaces. It has been reported that when the clear spacing S $(= s - h)$ between the anchors is greater than $2H \tan \phi$, no interference of the anchors occurs. On the other hand, for $S < 2H \tan \phi$, the uplift resistance of the anchors reduces substantially with a decrease in S. The uplift resistance for a group of interfering multiple anchors was found to be smaller than that for a group of two anchors installed at a large spacing.

2.14 SPREAD FOUNDATIONS UNDER UPLIFT

Spread foundations constructed for electric transmission towers are subjected to uplifting force. The uplift capacity of such foundations can be estimated by using the same relationship described in this chapter. During the construction of such foundations, the embedment ratio H/h is usually 3 or less. The native soil is first excavated for foundation construction. Once the foundation construction is finished, the excavation is backfilled and compacted. The degree of compaction of the backfill material plays an important role in the actual net ultimate uplift capacity of the foundation. Kulhawy et al. (1987) conducted several laboratory model tests to observe the effect of the degree of compaction of the backfill compared to the native soil. According to their observations, in most cases, at ultimate load, failure in soil takes place by side shear, as shown in Figure 2.38. However, wedge or combined shear failure occurs for foundations with $H/h <$ about 2 in medium to dense native soil where the backfill is at least 85% as dense as the native soil (Figure 2.39). Figure 2.40 shows the effect of backfill compaction on the breakout factor F_q when the native soil is loose. Similarly, Figure 2.41 shows the effect where the native soil is dense. Based on the observations of Kulhawy et al. (1987), this study shows that the compaction of the backfill has a great influence on the breakout factor of the foundation, and the net ultimate uplift capacity is greatly increased with the degree of backfill compaction.

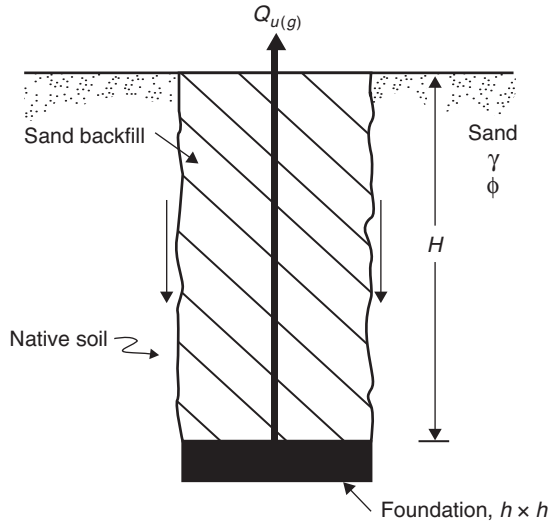

FIGURE 2.38 Failure by side shear

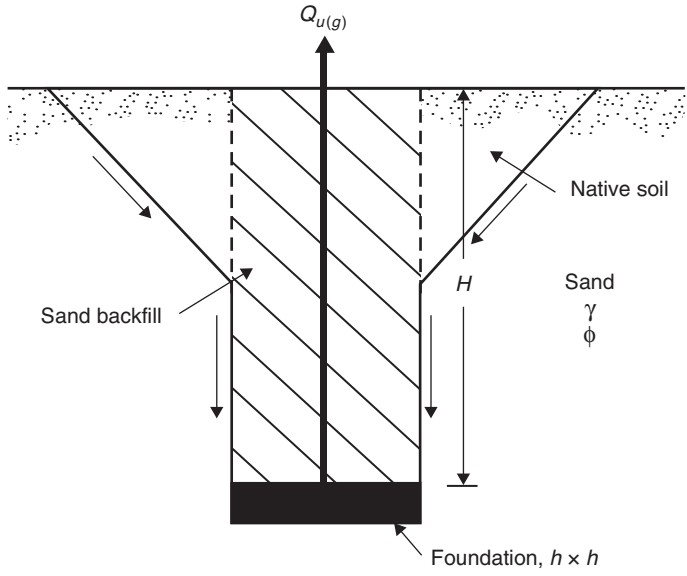

FIGURE 2.39 Wedge or combined shear failure

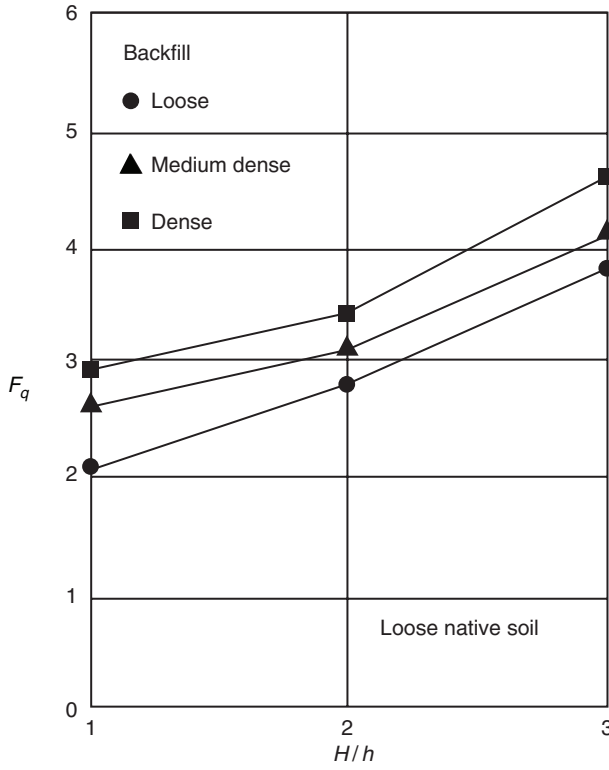

FIGURE 2.40 Effect of backfill on breakout factor for square foundation in loose native soil (adapted from Kulhawy et al., 1987)

2.15 INCLINED LOAD RESISTANCE OF HORIZONTAL PLATE ANCHORS

Das and Seeley (1975b) conducted a limited number of model tests to observe the nature of variation of the ultimate uplifting load of *horizontal square plate anchors* embedded in loose sand and subjected to inclined pull. The plate anchor used for the tests was 61 mm × 61 mm. The friction angle of the sand for the density of compaction at which tests were conducted was 31°. For this study, the pullout load on the anchor was applied by a cable that can allow full rotation of the anchor during pullout. Such conditions may arise to moor surface vessels or buoys and also semi-submersible or submerged structures. Figure 2.42 shows an anchor plate embedded at a depth H and subjected to a gross ultimate uplift

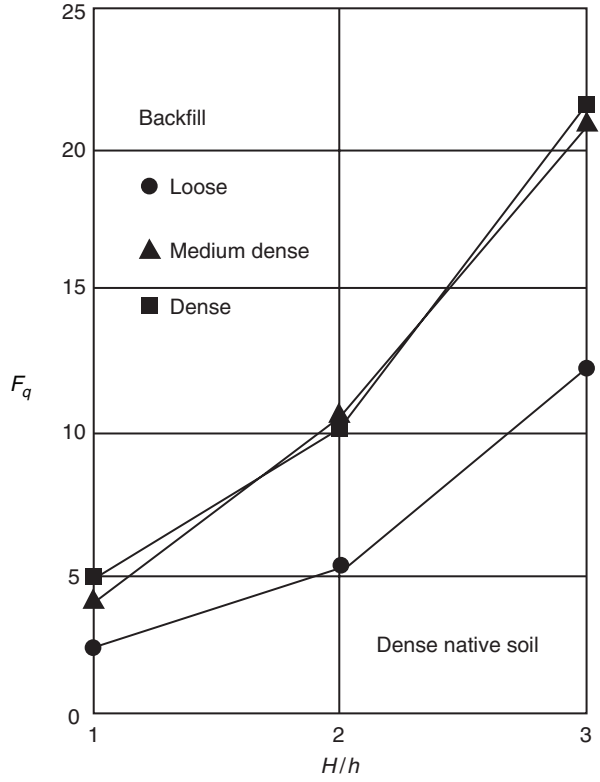

FIGURE 2.41 Effect of backfill on breakout factor for square foundation in dense native soil (adapted from Kulhawy et al., 1987)

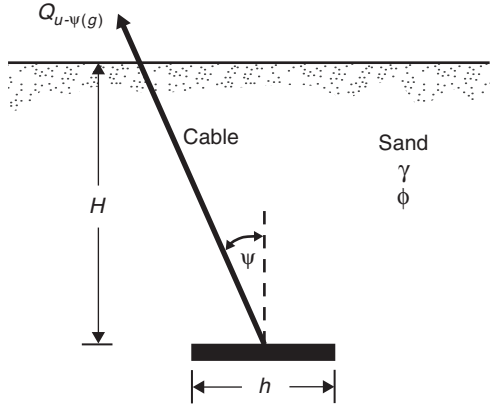

FIGURE 2.42 Inclined uplifting load on horizontal plate anchor

load $Q_{u\text{-}\psi(g)}$, with the load inclined at an angle ψ with respect to the vertical. The net ultimate uplift capacity can thus be given as:

$$Q_{u\text{-}\psi} = Q_{u\text{-}\psi(g)} - W_a \cos\psi \tag{2.63}$$

where

$Q_{u\text{-}\psi}$ = net ultimate uplift capacity measured in the direction of the load application
W_a = effective weight of the anchor

Figure 2.43 shows the variation of $Q_{u\text{-}\psi}$ with the angle of load inclination ψ for $H/h = 1$, 2, 2.5, and 4.5. From this figure it can be seen that for $\psi \leq 45°$,

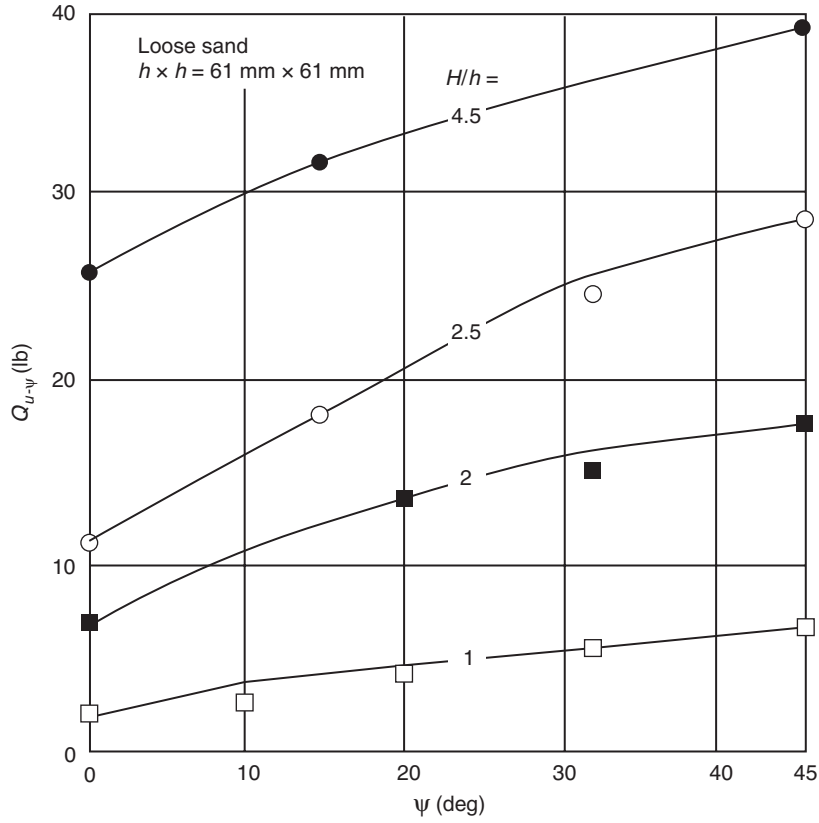

FIGURE 2.43 Effect of load inclination on $Q_{u\text{-}\psi}$ (adapted from Das and Seeley, 1975b)

the magnitude of $Q_{u\text{-}\psi}$ increases with the increase of the load inclination. Also, as the embedment ratio H/h increases, the ratio $Q_{u\text{-}\psi}/Q_{u\text{-}\psi=0}$ decreases (for a given value of ψ).

2.16 OTHER STUDIES

Some more analytical and numerical studies have been carried out by researchers until the recent past to estimate the ultimate pullout load of horizontal plate anchors in sands (Rowe and Davis, 1982; Tagaya et al., 1983, 1988; Smith, 1988, 2012; Merifield and Sloan, 2006; Kumar and Kouzer, 2008b; White et al., 2008; Deshmukh et al., 2011).

Merifield and Sloan (2006) presented rigorous lower and upper bound solutions for the ultimate capacity of horizontal strip anchors in frictional soils. They have reported that the failure mode for horizontal anchors consists of the upward movement of a rigid column of soil immediately above the anchor, accompanied by lateral deformation extending out and upward from the anchor edge. As the anchor is pulled vertically upward, the material above the anchor tends to lock up as it attempts to dilate during deformation. The effect of anchor interface roughness was found to have little or no effect on the calculated pullout capacity for horizontal anchors at all embedment depths and friction angles analyzed.

Merifield et al. (2006) studied the effect of anchor shape upon the ultimate capacity of horizontal anchors by developing lower bound solutions for the ultimate capacity of horizontal square and circular anchors in sand. It has been reported that the breakout factors for circular and square anchors increase nonlinearly with increasing embedment ratio. The rate of increase is greatest for medium to dense cohesionless soils where the effective soil friction angle $\phi' \geq 30°$. The capacity of both square and circular anchors is significantly greater than that of strip anchors at the same embedment ratio.

Kumar and Kouzer (2008b) examined the vertical uplift capacity of strip anchors embedded horizontally at shallow depths in sand by using an upper bound limit analysis in conjunction with finite elements and linear programming. They have reported that the uplift capacity increases substantially with increase in the embedment ratio of the anchor and the friction angle of the soil mass. The influence of friction angle ϕ on the pullout resistance is found to be greater at higher embedment ratios. Even though the analysis considers the development of plastic strains within elements, it has been noticed that the soil mass lying above the anchor remains rigid and a planar rupture surface emanating from the rupture edge and making an angle ϕ with the vertical develops.

White et al. (2008) described a limit equilibrium solution for predicting the uplift resistance of plate and pile anchors buried in sand by assuming that an inverted trapezoidal block is lifted above the pipe. The shear planes on each side of the block are inclined at the angle of dilation. The uplift resistance is equal to the weight of the lifted soil block plus the shear resistance along the two inclined failure surfaces. It is also assumed that the normal stress on the sliding planes is equal to the *in situ* value inferred from at-rest earth pressure conditions. The developed analytical expression requires the friction and dilation angles, which vary with density and stress level. It has been shown that the solution for uplift resistance based on the limit theorems of plasticity is generally very unconservative, which can be attributed to the assumption of normality that is required by the limit theorems. Normality leads to unrealistically high dilation, which imposes an improbable uplift mechanism involving uplift of a far wider zone of soil than is seen in model tests.

Deshmukh et al. (2011) presented the details of the theoretical analysis of net uplift capacity of horizontal strip anchors in cohesionless soils by assuming a plane failure surface inclined at $90° - \phi/2$ to the horizontal. The vertical soil reaction on the failure surface was evaluated using Kotter's equation. It has been reported that this analysis demonstrates a successful application of Kotter's equation and is reliable for embedment ratios less than 8.

The information about the vertical uplift capacity of horizontal plate anchors under seismic loads is limited. Kumar (2001) theoretically examined the influence of horizontal earthquake acceleration on the vertical uplift capacity of shallow strip anchors buried in cohesionless material by using the upper bound theorem of limit analysis and with the assumption of planar rupture surfaces. It has been reported that the pseudo-static horizontal seismic forces induce a progressive reduction in the uplift resistance of shallow anchors. The reduction becomes greater with increase in the magnitude of the earthquake acceleration coefficient and is found to be more significant for smaller values of soil friction angle ϕ and higher values of embedment ratio H/h.

2.17 SUMMARY OF MAIN POINTS

1. Horizontal plate anchors are used in the construction of foundations subjected to uplifting load.
2. The embedment ratio of the anchor is the ratio of the depth of embedment (H) to the width of the anchor (h), that is, H/h, which governs the anchor condition as shallow or deep. For greater values of H/h, the deep condition occurs where the failure surface does not extend to the ground surface.

3. The net ultimate uplift capacity is the sum of the effective weight of the soil located in the failure zone and the shearing resistance developed along the failure surface.
4. The soil cone and friction cylinder methods are the early uplift capacity theories used to determine the net ultimate uplift capacity of shallow circular plate anchors.
5. Balla's theory (1961) is generally in good agreement for the uplift capacity of anchors embedded in dense sand at an embedment ratio of $H/h \leq 5$. However, for anchors located in loose and medium sand, the theory overestimates the net ultimate uplift capacity.
6. The breakout factor, defined by Equation 2.10, increases with H/h up to a maximum value at $H/h = (H/h)_{cr}$. For $H/h > (H/h)_{cr}$, the breakout factor remains practically constant. Anchors located at an embedment ratio of $H/h \leq (H/h)_{cr}$ are shallow anchors, and those located at $H/h > (H/h)_{cr}$ are deep anchors. Most theories assume that the shallow anchor condition exists for $H/B \leq 5$. Meyerhof and Adams's theory (1968) provides a critical embedment ratio $(H/h)_{cr}$ for *square* and *circular* anchors as a function of the soil friction angle.
7. Meyerhof and Adams (1968) proposed a semi-theoretical relationship for estimation of the ultimate uplift capacity of *strip, rectangular,* and *circular* anchors. This is the only theory presently available for estimation of the net ultimate uplift capacity for rectangular anchors.
8. Vesic's theory (1971) is generally fairly accurate in estimating the net ultimate uplift capacity for shallow anchors in loose sand. Meyerhof and Adams's theory (1968) is more applicable to a wide range of anchors and it provides as good an estimate as any for the net ultimate uplift capacity.
9. The model tests suggest that when the cyclic relative anchor displacement is kept below about half the relative movement to failure in static pullout tests, there is essentially no reduction in strength due to cyclic loading.
10. The net ultimate uplift capacity of a group of anchors may possibly be smaller than the net ultimate uplift capacity of a single anchor times the number of anchors in the group when the center-to-center spacing of the anchor is small and when there is interference of the failure zones in the soil during anchor uplift.
11. The compaction of the backfill above the anchor plate has a great influence on the breakout factor of the foundation, and the net ultimate uplift capacity is greatly increased with the degree of backfill compaction.
12. The recent numerical studies with their limitations show that the anchor interface roughness has little or no effect on the calculated pullout capacity for horizontal anchors at all embedment depths and friction angles. The

pseudo-static horizontal seismic forces induce a progressive reduction in the uplift resistance of shallow anchors.

SELF-ASSESSMENT QUESTIONS

Select the most appropriate answer to each multiple-choice question

2.1. The sum of the effective self-weight of the horizontal plate anchor, the effective weight of the soil located in the failure zone, and the shearing resistance developed along the failure surface is called:
   a. ultimate capacity
   b. net ultimate capacity
   c. gross ultimate capacity
   d. none of the above

2.2. The soil cone method of determining the net ultimate uplift capacity of a horizontal plate anchor assumes that the failure surface in soil at ultimate load may be approximated as a truncated cone having an apex angle, where ϕ is the soil friction angle, of:
   a. $45° - \phi/2$
   b. $45° + \phi/2$
   c. $90° - \phi/2$
   d. $90° + \phi/2$

2.3. The breakout factor:
   a. always increases with increase in embedment ratio
   b. increases with increase in embedment ratio up to a maximum value
   c. always decreases with increase in embedment ratio
   d. decreases with increase in embedment ratio up to a minimum value

2.4. Which of the following is not required for the calculation of the net ultimate uplift capacity of a horizontal plate anchor embedded in sand:
   a. area of the anchor plate
   b. depth of the anchor plate below the ground
   c. unit weight of the soil above the anchor plate
   d. unit weight of the soil below the anchor plate

2.5. Estimation of the net ultimate uplift capacity of a horizontal plate anchor embedded in sand for rectangular anchors can be done by:
   a. Balla's theory (1961)
   b. Vesic's theory (1971)
   c. Mariupol'skii's theory (1965)
   d. Meyerhof and Adams's theory (1968)

2.6. Horizontal plate anchors for transmission line towers are usually constructed with an embedment depth ratio of:
   a. 3
   b. 3 or less
   c. greater than 3
   d. 1

2.7. For a given embedment depth ratio, the inclined load resistance of a horizontal plate anchor:
   a. increases with increase in inclination of the load with respect to vertical
   b. decreases with increase in inclination of the load with respect to vertical
   c. increases with increase in inclination of the load with respect to horizontal
   d. remains unaffected with variation of inclination of the load with respect to vertical or horizontal

2.8. The net allowable ultimate uplift capacity of horizontal plate anchors can be determined by using:
   a. a tentative factor of safety
   b. a load displacement relationship
   c. both a and b
   d. none of the above

2.9. With increase in friction angle of the soil backfill above the horizontal plate anchor, the breakout factor of the anchor:
   a. increases linearly
   b. increases nonlinearly
   c. decreases linearly
   d. decreases nonlinearly

2.10. For a circular plate anchor embedded in sand with diameter $h = 1$ m, depth of embedment $H = 1$ m, unit weight of sand above the plate anchor $\gamma = 15$ kN/m^3, and sand friction angle $\phi = 20°$, the net ultimate uplift capacity calculated from Balla's theory (1961) will be:
   a. 7.5 kN
   b. 15 kN
   c. 30 kN
   d. 300 kN

Answers

2.1: c 2.2: d 2.3: b 2.4: d 2.5: d 2.6: b 2.7: a 2.8: c 2.9: b 2.10: c

REFERENCES

Andreadis, A., Harvey, R.C., and Burley, E. (1978). Embedment anchors subjected to repeated loading. *J. Geotech. Eng. Div. ASCE,* 104(7):1033–1036.

Baker, W.H. and Kondner, R.L. (1966). Pullout load capacity of a circular earth anchor buried in sand. *Highw. Res. Rec.,* No. 108, National Academy of Sciences, Washington, D.C., 1–10.

Balla, A. (1961). The resistance to breaking-out of mushroom foundations for pylons. *Proc. 5th Int. Conf. Soil Mech. Found. Eng.,* Paris, 1, 569–576.

Caquot, A. and Kerisel, L. (1949). *Traite de Mecanique des Sols,* Gauthier-Villars, Paris.

Das, B.M. and Jin-Kaun, Y. (1987). Uplift capacity of model group anchors in sand. *Foundations for Transmission Line Towers,* Geotech. Spec. Publ. 8, ASCE, 57–71.

Das, B.M. and Jones, A.D. (1982). Uplift capacity of rectangular foundations in sand. *Transp. Res. Rec.,* No. 884, National Academy of Sciences, Washington, D.C., 54–58.

Das, B.M. and Puri, V.K. (1989). Load displacement relationship for horizontal rectangular anchors in sand. *Proc. 4th Int. Conf. Civil Struct. Eng. Computing,* London, Civil-Comp Press, 2, 207–212.

Das, B.M. and Seeley, G.R. (1975a). Breakout resistance of horizontal anchors. *J. Geotech. Eng. Div. ASCE,* 101(9):999–1003.

Das, B.M. and Seeley, G.R. (1975b). Inclined load resistance of anchors in sand. *J. Geotech. Eng. Div. ASCE,* 101(9):995–998.

Deshmukh, V.B., Dewaikar, D.M., and Choudhary, D. (2011). Uplift capacity of horizontal strip anchors in cohesionless soil. *Geotech. Geol. Eng.,* 29:977–988.

Downs, D.I. and Chieurzzi, R. (1966). Transmission tower foundations. *J. Power Div. ASCE,* 88(2):91–114.

Esquivel-Diaz, R.F. (1967). Pullout Resistance of Deeply Buried Anchors in Sand, M.S. thesis, Duke University, Durham, NC.

Ireland, H.O. (1963). Discussion, uplift resistance of transmission tower footing. *J. Power Div. ASCE,* 89(1):115–118.

Kulhawy, F.H., Trautmann, C.H., and Nicolaides, C.N. (1987). Spread foundations in uplift: experimental study. *Foundations for Transmission Line Towers,* Geotech. Spec. Publ. 8, ASCE, 110–127.

Kumar, J. (2001). Seismic vertical uplift capacity of strip anchors. *Geotechnique,* 51(3):275–279.

Kumar, J. and Kouzer, K.M. (2008a). Vertical uplift capacity of a group of shallow horizontal anchors in sand. *Geotechnique,* 58(10):821–823.

Kumar, J. and Kouzer, K.M. (2008b). Vertical uplift capacity of horizontal anchors using upper bound limit analysis and finite elements. *Can. Geotech. J.,* 45:698–704.

Liu, J., Liu, M., and Zhu, Z. (2012). Sand deformation around an uplift plate anchor. *J. Geotech. Geoenviron. Eng.,* 138(6):728–737.

Mariupol'skii, L.G. (1965). The bearing capacity of anchor foundations (English translation). *Soil Mech. Found. Eng.* (in Russian), 26–37.

Merifield, R.S. and Sloan, S.W. (2006). The ultimate pullout capacity of anchors in frictional soils. *Can. Geotech. J.,* 43:852–868.

Merifield, R.S., Lyamin, A.V., and Sloan, S.W. (2006). Three-dimensional lower-bound solutions for the stability of plate anchors in sand. *Geotechnique,* 56(2): 123–132.

Meyerhof, G.G. (1973). Uplift resistance of inclined anchors and piles. *Proc. 8th Int. Conf. Soil Mech. Found.,* Moscow, 167–172.

Meyerhof, G.G. and Adams, J.I. (1968). The ultimate uplift capacity of foundations. *Can. Geotech. J.,* 5(4):225–244.

Mors, H. (1959). The behavior of mast foundations subjected to tensile forces. *Bautechnik,* 36(10):367–378.

Rowe, R.K. and Davis, H. (1982). The behaviour of anchor plates in sand. *Geotechnique,* 32(1):25–41.

Saeedy, H.S. (1987). Stability of circular vertical earth anchors. *Can. Geotech. J.,* 24(3):452–456.

Smith, C. (1998). Limit loads for an anchor/trapdoor embedded in an associative Coulomb soil. *Int. J. Num. Anal. Meth. Geomech.,* 22(11):855–865.

Smith, C.C. (2012). Limit loads for a shallow anchor/trapdoor embedded in a non-associative Coulomb soil. *Geotechnique,* 62(7):563–571.

Sutherland, H.B. (1965). Model studies for shaft raising through cohesionless soils. *Proc. 6th Int. Conf. Soil Mech. Found. Eng.,* Montreal, 2, 410–413.

Tagaya, K., Tanaka, A., and Aboshi, H. (1983). Application of finite element method to pullout resistance of buried anchor. *Soils Found.,* 23(3):91–104.

Tagaya, K., Scott, R.F., and Aboshi, H. (1988). Pullout resistance of buried anchor in sand. *Soils Found.,* 28(3):114–130.

Veesaert, C.J. and Clemence, S.P. (1977). Dynamic pullout resistance of anchors. *Proc. Int. Symp. Soil-Structure Interaction,* Rourkee, India, Vol. 1, 389–397.

Vesic, A.S. (1965). Cratering by explosives as an earth pressure problem. *Proc. 6th Int. Conf. Soil Mech. Found. Eng.,* Montreal, 427–431.

Vesic, A.S. (1971). Breakout resistance of objects embedded in ocean bottom. *J. Soil Mech. Found. Div. ASCE,* 97(9):1183–1205.

White, D.J., Cheuk, C.Y., and Bolton, M.D. (2008). The uplift resistance of pipes and plate anchors buried in sand. *Geotechnique,* 58(10):771–779.

3

HORIZONTAL PLATE ANCHORS IN CLAY

This chapter describes the theoretical and experimental research results presently available for determination of the net ultimate uplift capacity of horizontal plate anchors embedded in saturated clay. In the recent past, some numerical investigations including three-dimensional lower bound study of the behavior of horizontal plate anchors in clays have been reported in the research literature. This chapter also summarizes such works briefly.

3.1 INTRODUCTION

Figure 3.1 shows a plate anchor embedded in a saturated clay at a depth H below the ground surface. The width of the anchor plate is equal to h, and the undrained cohesion of the clay is c_u. In soft saturated clay, when the anchor is subjected to an uplift force, the soil located above the anchor will be compressed and, at the same time, the soil below the anchor will be relieved of some stress. This will, in turn, result in an increase in the pore water pressure above the anchor accompanied by a decrease in the pore water pressure below the anchor. The difference will result in a suction force. This suction force will increase the short-term uplift capacity of the anchor. Thus, the uplift capacity can be given by the expression

$$Q_{u(g)} = Q_u + W_a + U \tag{3.1}$$

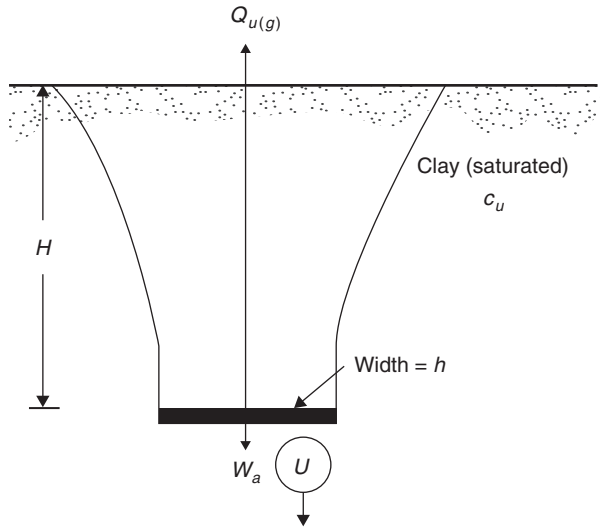

FIGURE 3.1 Horizontal anchor in saturated clay

where

$Q_{u(g)}$ and Q_u = gross and net ultimate uplift capacity, respectively
W_a = effective weight of the anchor
U = suction force below the anchor

Very little is known at the present time about the magnitude of the suction force and its variation with depth and type of clay soil. However, for design purposes, the suction force can be neglected and the net ultimate uplift capacity can be taken as:

$$Q_u = Q_{u(g)} - W_a \tag{3.2}$$

In the following sections, the existing theories for estimation of the net uplift capacity Q_u are summarized.

3.2 VESIC'S THEORY

In Section 2.8, it was shown that for anchors embedded in sand ($c = 0$):

$$Q_u = A\gamma HF_q \tag{3.3}$$

where

A = area of the anchor plate

The preceding relation was derived by Vesic (1971) using the analogy of expansion of cavities. In a similar manner, it can be shown that in a c-ϕ soil

$$Q_u = A(\gamma H F_q + c F_c) \tag{3.4}$$

where

F_q, F_c = breakout factors
c = cohesion of the soil

For the undrained condition, $\phi = 0$ and $c = c_u$. It was shown in Tables 2.3 and 2.4 that for $\phi = 0$, the value of F_q is equal to 1. Thus:

$$Q_u = A(\gamma H + c_u F_c) \tag{3.5}$$

Vesic (1971) presented the theoretical variation of the breakout factor F_c (for $\phi = 0$ condition) with the embedment ratio H/h, and these values are given in Table 3.1. In Table 3.1, B is the dimension of the anchor at right angle to the cross section shown in Figure 3.1. A plot of these same values of F_c against H/h is also shown in Figure 3.2. Based on the laboratory model test results available, it appears that Vesic's theory gives a closer estimate only for shallow anchors embedded in softer clay.

In general, the breakout factor increases with embedment ratio up to a maximum value and remains constant thereafter, as shown in Figure 3.3. The maximum value of $F_c = F_c^*$ is reached at $H/h = (H/h)_{cr}$. Anchors located at $H/h > (H/h)_{cr}$ are referred to as deep anchors. For these anchors, at ultimate uplifting load, local shear failure in soil located around the anchor takes place. Anchors located at $H/h \leq (H/h)_{cr}$ are shallow anchors.

TABLE 3.1 Variation of F_c ($\phi = 0$ condition)

	H/h				
Anchor type	0.5	1.0	1.5	2.5	5.0
Circular (diameter = h)	1.76	3.80	6.12	11.6	30.3
Strip ($h/B \approx 0$)	0.81	1.61	2.42	4.04	8.07

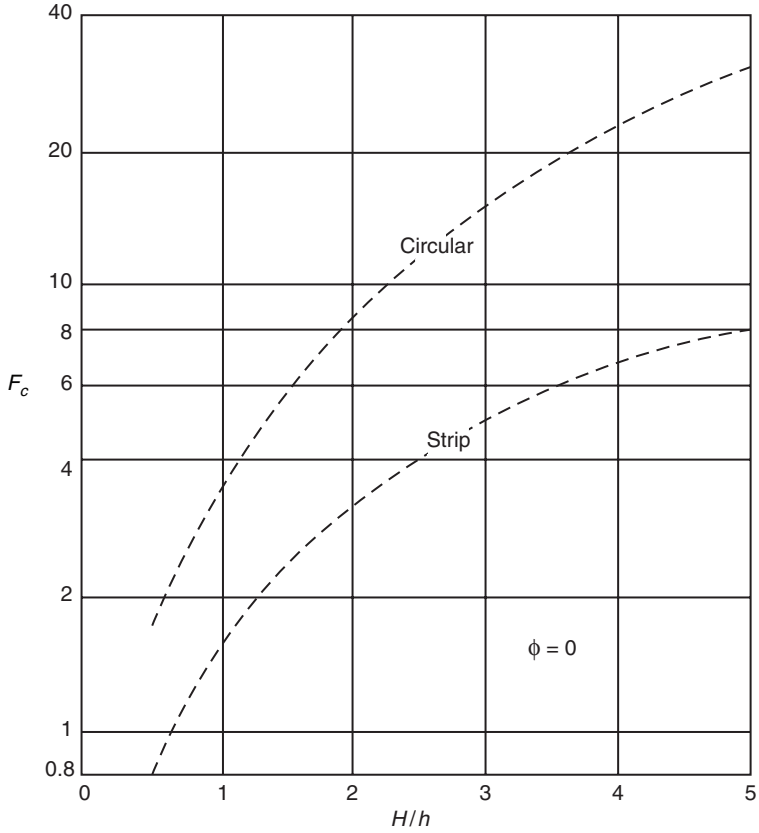

FIGURE 3.2 Variation of Vesic's (1971) breakout factor F_c

3.3 MEYERHOF'S THEORY

Based on experimental results, Meyerhof (1973) proposed a relationship the same as Equation 3.5. For *circular* and *square* anchors:

$$F_c = 1.2\left(\frac{H}{h}\right) \leq 9 \tag{3.6}$$

and for *strip* anchors:

$$F_c = 0.6\left(\frac{H}{h}\right) \leq 8 \tag{3.7}$$

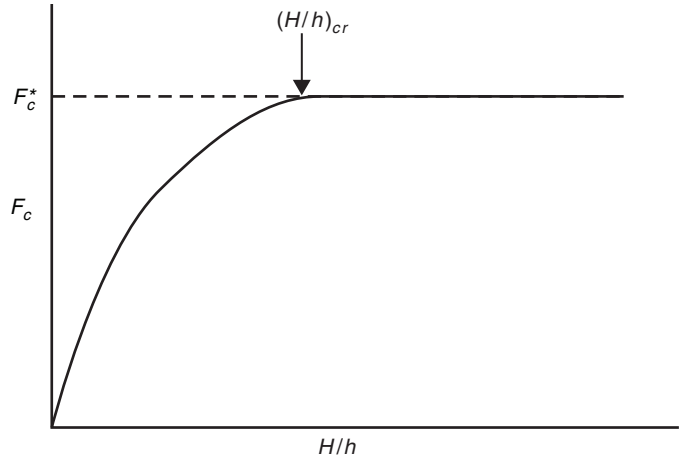

FIGURE 3.3 Nature of variation of F_c with H/h

Equations 3.6 and 3.7 imply that for *circular* and *square* anchors:

$$\left(\frac{H}{h}\right)_{cr} = \frac{9}{1.2} = 7.5 \tag{3.8}$$

and for *strip* anchors:

$$\left(\frac{H}{h}\right)_{cr} = \frac{8}{0.6} \approx 13.5 \tag{3.9}$$

The breakout factor variations with embedment ratio according to Equations 3.6 and 3.7 are shown in Figure 3.4. Based on the experimental results, it appears that Equations 3.6 and 3.7 are reasonable estimates for anchors embedded in stiff clay.

3.4 DAS'S THEORY

Das (1978) compiled a number of laboratory model test results on *circular* anchors embedded in saturated clay with the undrained cohesion c_u varying from 5.18 kN/m^2 to about 172.5 kN/m^2. Figure 3.5 shows the average plots of F_c versus H/h obtained from these studies, along with the critical embedment ratios. The details relating to curves *a, b, c, d,* and *e* shown in Figure 3.5 are given in Table 3.2.

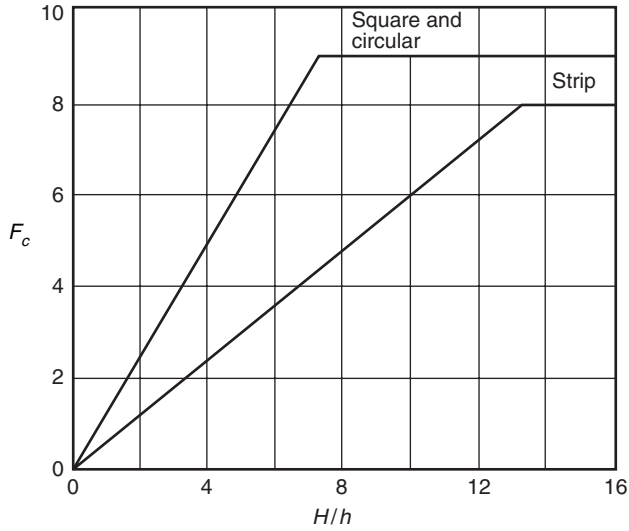

FIGURE 3.4 Variation of F_c with H/h (Equations 3.6 and 3.7)

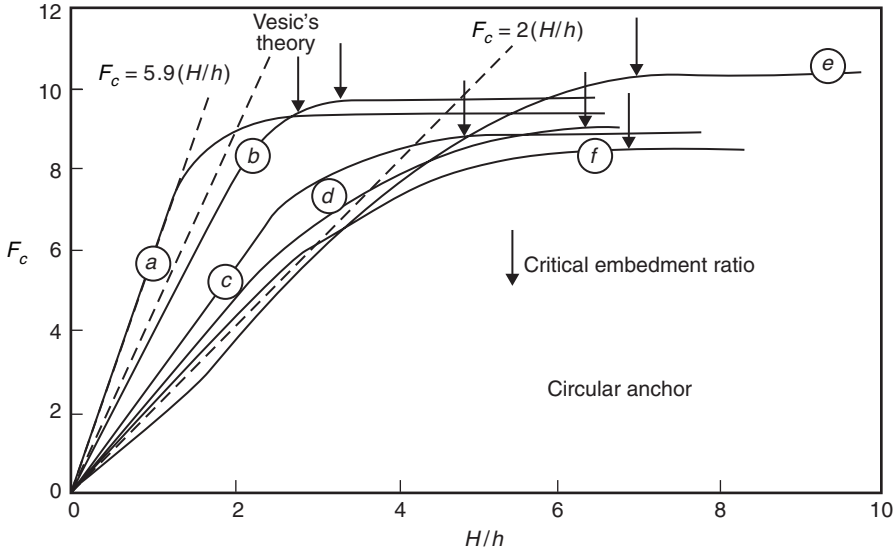

FIGURE 3.5 Variation of breakout factor with H/h for various experimental observations

TABLE 3.2 Details for the curves shown in Figure 3.5

Curve	Reference	Year	c_u (kPa)
a	Ali	1968	5.18
b	Kupferman	1971	6.9
c	Adams and Hayes	1967	10.35–13.8
d	Bhatnagar	1969	53.17
e	Adams and Hayes	1967	96.6–172.5

From Figure 3.5, it can be seen that for shallow anchors:

$$F_c \approx n\left(\frac{H}{h}\right) \leq 8 \text{ to } 9 \tag{3.10}$$

where

n = a constant

The magnitude of n varies between 5.9 to 2.0 and is a function of the undrained cohesion c_u. Since n is a function of c_u and $F_c = F_c^*$ is about 8 to 9 in all cases, it is obvious that the critical embedment ratio $(H/h)_{cr}$ will be a function of c_u.

Das (1978) also reported some model test results conducted with *square* and *rectangular* anchors of width $h = 50.8$ mm. Based on these model test results, the variation of F_c with H/h is shown in Figure 3.6. Using the critical embedment ratios obtained from Figures 3.5 and 3.6, it was proposed that

$$\left(\frac{H}{h}\right)_{cr\text{-}S} = 0.107c_u + 2.5 \leq 7 \tag{3.11}$$

where

$(H/h)_{cr\text{-}S}$ = critical embedment ratio of *square* anchor (or *circular* anchor)
c_u = undrained cohesion in kN/m^2

A plot based on Equation 3.11 is shown in Figure 3.7. It was also observed by Das (1980) that

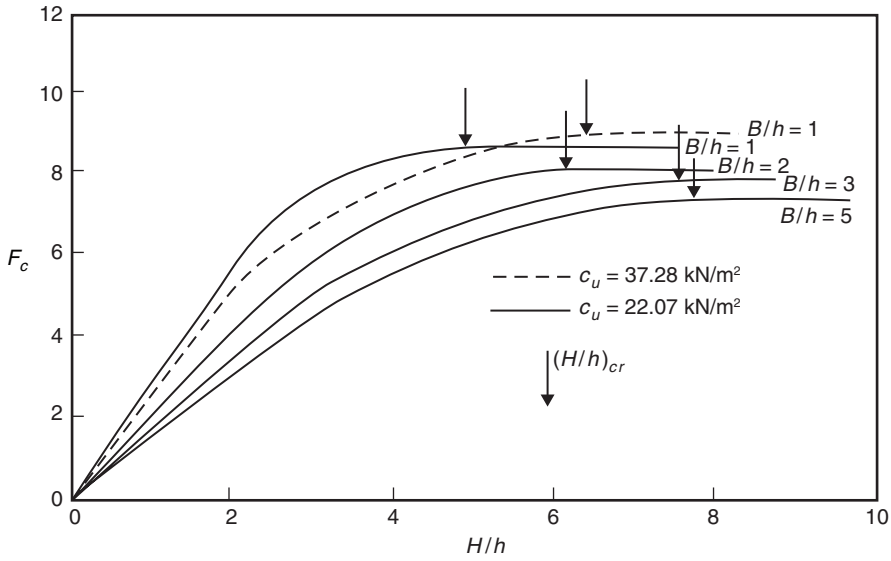

FIGURE 3.6 Model test results of Das (1978) for variation of F_c with H/h

$$\left(\frac{H}{h}\right)_{cr\text{-}R} = \left(\frac{H}{h}\right)_{cr\text{-}S}\left[0.73 + 0.27\left(\frac{B}{h}\right)\right] \leq 1.55\left(\frac{H}{h}\right)_{cr\text{-}S} \tag{3.12}$$

where

$(H/h)_{cr\text{-}R}$ = critical embedment ratio of rectangular anchors (Figure 3.8)

Based on these model test results, Das (1980) proposed an empirical procedure to obtain the breakout factors for shallow and deep anchors. According to this procedure, α' and β' are two nondimensional factors defined as:

$$\alpha' = \frac{\dfrac{H}{h}}{\left(\dfrac{H}{h}\right)_{cr}} \tag{3.13}$$

and

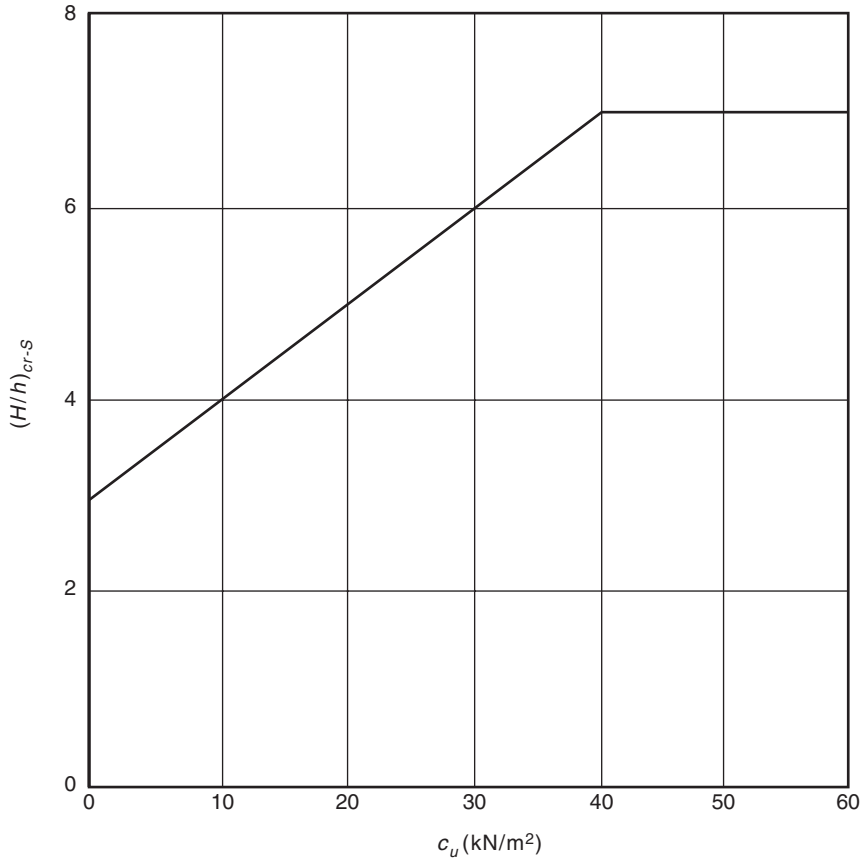

FIGURE 3.7 Plot of $(H/h)_{cr\text{-}S}$ versus c_u (in kN/m^2) from Equation 3.11

$$\beta' = \frac{F_c}{F_c^\star} \tag{3.14}$$

For a given anchor (that is, circular, square, or rectangular), the critical embedment ratio can be calculated by using Equations 3.11 and 3.12. The magnitudes of $F_c^\star$ can be given by the following empirical relationship:

$$F_{c\text{-}R}^\star = 7.56 + 1.44\left(\frac{h}{B}\right) \tag{3.15}$$

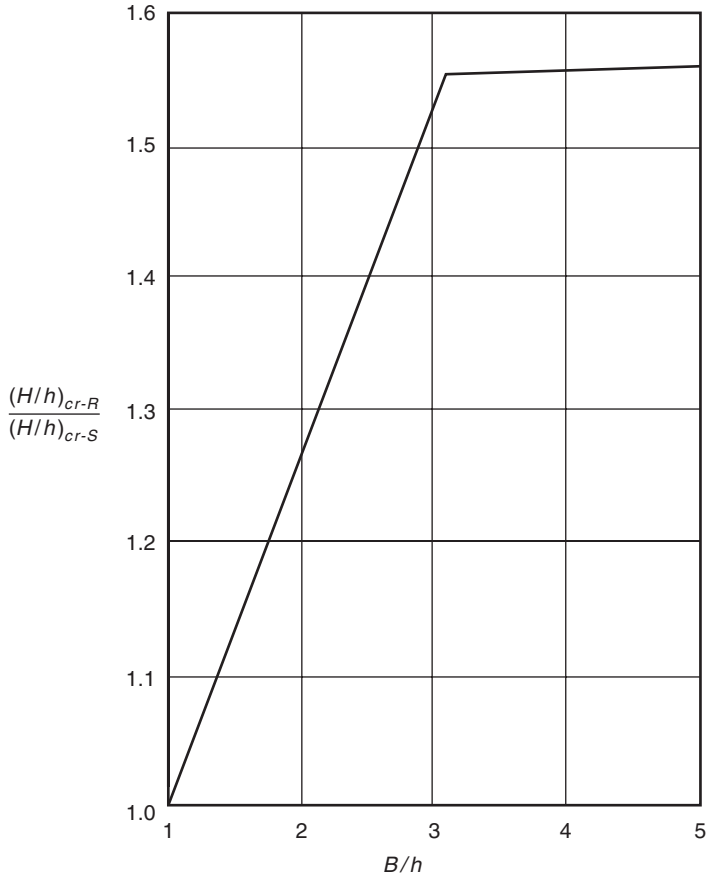

FIGURE 3.8 Plot of $(H/h)_{cr\text{-}R}/(H/h)_{cr\text{-}S}$ against B/h from Equation 3.12

where

$F^{\star}_{c\text{-}R}$ = breakout factor for deep rectangular anchor

It can be seen from Equation 3.15 that for *square* and *circular* anchors $F^{\star}_{c\text{-}R}$ is equal to 9. Using all the experimental curves shown in Figures 3.5 and 3.6, when the nondimensional breakout factor β' is plotted against the nondimensional embedment ratio α', they appear to fall in a rather narrow range, as

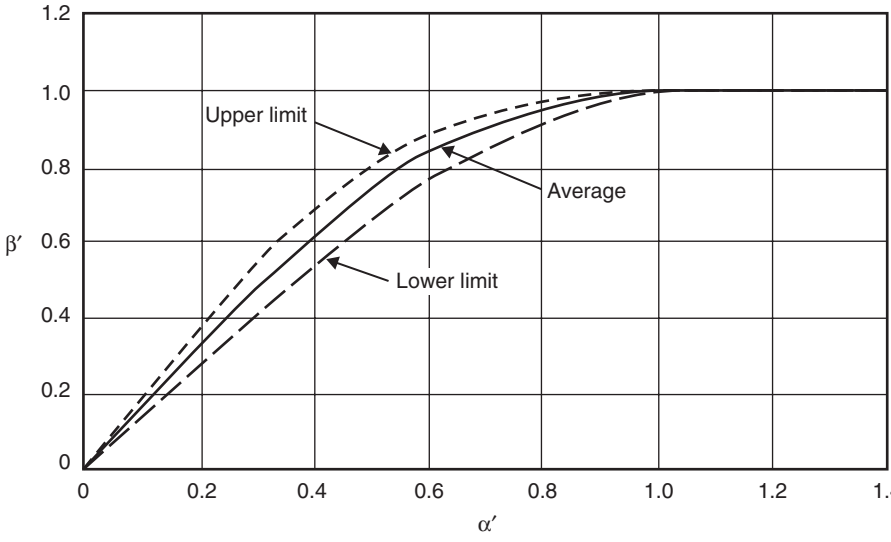

FIGURE 3.9 Plot of β′ versus α′ (adapted from Das, 1980)

shown in Figure 3.9. The average plot of β' versus α' is also shown in Figure 3.9. Hence, the following is a step-by-step procedure for estimation of the net ultimate uplift capacity:

1. Determine the representative value of the undrained cohesion c_u.
2. Determine the critical embedment ratio using Equations 3.11 and 3.12.
3. Determine the H/h ratio for the anchor.
4. If $H/h > (H/h)_{cr}$ as determined by Step 2, it is a deep anchor. However, if $H/h \leq (H/h)_{cr}$, it is a shallow anchor.
5. For $H/h > (H/h)_{cr}$:

$$F_c = F_c^* = 7.56 + 1.44\left(\frac{h}{B}\right)$$

Thus:

$$Q_u = A\left\{\left[7.56 + 1.44\left(\frac{h}{B}\right)\right]c_u + \gamma H\right\} \tag{3.16}$$

where

A = area of the anchor

6. For $H/h \le (H/h)_{cr}$:

$$Q_u = A(\beta' F_c^* c_u + \gamma H)$$

$$= A\left\{\beta'\left[7.56 + 1.44\left(\frac{h}{B}\right)\right]c_u + \gamma H\right\} \tag{3.17}$$

The value of β' can be obtained from the average curve of Figure 3.9. The procedure outlined above gives fairly good results in estimating the net ultimate holding capacity of anchors.

Example 3.1

A plate anchor that measures 0.4 m × 0.6 m is embedded at a depth of 1.8 m. The undrained cohesion of the clay is 42 kN/m^2, and its saturated unit weight γ is 18.9 kN/m^3. Estimate the net ultimate uplift capacity.

Solution

From Equation 3.11:

$$\left(\frac{H}{h}\right)_{cr\text{-}S} = 0.107c_u + 2.5 = (0.107)(42) + 2.5 \approx 7$$

Again, from Equation 3.12:

$$\left(\frac{H}{h}\right)_{cr\text{-}R} = \left(\frac{H}{h}\right)_{cr\text{-}S}\left[0.73 + 0.27\left(\frac{B}{h}\right)\right]$$

$$= (7)\left[0.73 + 0.27\left(\frac{0.6}{0.4}\right)\right] \approx 7.95$$

The actual embedment ratio is $H/h = 1.8/0.4 = 4.5$. Hence this is a shallow anchor.

$$\alpha' = \frac{\dfrac{H}{h}}{\left(\dfrac{H}{h}\right)_{cr}} = \frac{4.5}{7.95} = 0.566$$

Referring to Figure 3.9, for $\alpha' = 0.566$, the magnitude of β' is 0.82. From Equation 3.17:

$$Q_u = A\left\{\beta'\left[7.56 + 1.44\left(\frac{h}{B}\right)\right]c_u + \gamma H\right\}$$

$$= (0.4)(0.6)\left\{(0.82)\left[7.56 + (1.44)\left(\frac{0.4}{0.6}\right)\right](42) + (18.9)(1.8)\right\}$$

$$= \mathbf{78.6\ kN}$$

3.5 THREE-DIMENSIONAL LOWER BOUND SOLUTION

Merifield et al. (2003) presented three-dimensional numerical limit analysis to evaluate the effect of anchor shape on the pullout capacity of horizontal anchors in undrained clay. The anchor was idealized as either square, circular, or rectangular in shape. Estimates of the ultimate pullout load were obtained by using a newly developed three-dimensional numerical procedure based on a finite element formulation of the lower bound theorem of limit analysis. The formulation assumed a perfectly plastic soil model with a Tresca yield criterion. Consideration has been given to the effect of anchor embedment depth, anchor roughness, and overburden pressure. It has been reported that the breakout factors for square, circular, and rectangular anchors in weightless soil are always greater than those obtained for strip anchors at corresponding embedment ratios. Rectangular anchors with aspect ratios (B/h) greater than 10 can be considered to behave essentially as a strip anchor. The ultimate capacity of horizontal square, circular, or rectangular anchors is not likely to be affected noticeably by anchor roughness.

The following list enumerates the suggested procedure for estimating the uplift capacity of circular and square anchors in homogeneous soil profiles:

1. Determine representative values of material parameters, c_u and γ.
2. Knowing the anchor size (h = diameter or width, B = length) and embedment depth H, calculate the embedment ratio H/h.
3. Determine the overburden ratio $\gamma H/c_u$.
4. Adopt a limiting value of the breakout factor $F_c^\star = 12.56$ for circular anchors and $F_c^\star = 11.9$ for square anchors.
5. A. Calculate the breakout factor F_{c0} for a homogeneous soil profile with no unit weight ($\gamma = 0$) as:

$$F_{c0} = S\left\{2.56 \ln\left[2\left(\frac{H}{h}\right)\right]\right\} \tag{3.18}$$

where S is a shape factor illustrated in Figure 3.10 for circular anchors and in Figure 3.11 for square anchors.

B. Calculate the breakout factor $F_c = F_{c\gamma}$ for a homogenous soil profile with unit weight ($\gamma \neq 0$) as:

$$F_c = F_{c\gamma} = F_{c0} + \frac{\gamma H}{c_u} \tag{3.19}$$

C. If $F_c \geq F_c^\star$, then the anchor is a deep anchor. The ultimate pullout load is given by:

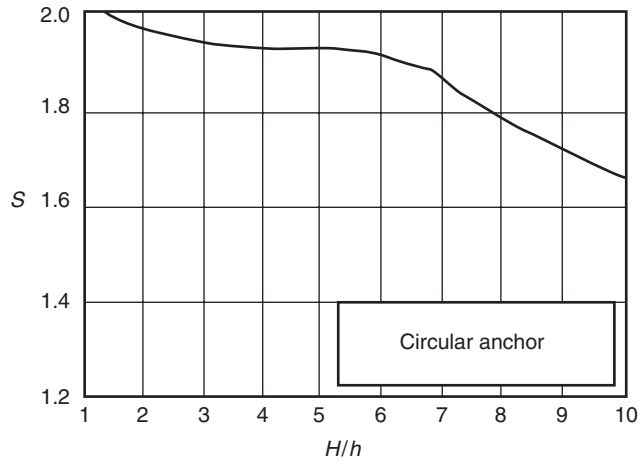

FIGURE 3.10 Shape factor S for circular anchor (adapted from Merifield et al., 2003)

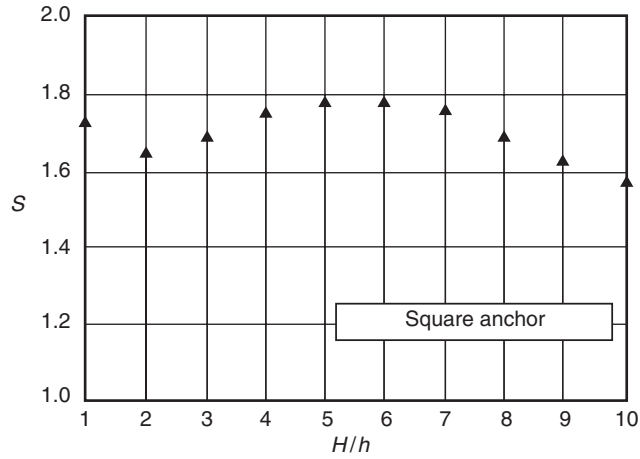

FIGURE 3.11 Shape factor *S* for square anchor (adapted from Merifield et al., 2003)

$$Q_u = c_u A F_c^{\star} \tag{3.20}$$

D. If $F_c \leq F_c^{\star}$, then the anchor is a shallow anchor. The ultimate pullout load is given by:

$$Q_u = c_u A F_{c\gamma} \tag{3.21}$$

Example 3.2

A square horizontal plate anchor 0.25 m wide is to be embedded 1.75 m in a homogeneous clay. Determine the ultimate pullout capacity given that the clay has a shear strength $c_u = 60$ kPa and unit weight $\gamma = 15.3$ kN/m^3.

Solution

The embedment ratio is

$$\frac{H}{h} = \frac{1.75}{0.25} = 7.0$$

The overburden ratio is

$$\frac{\gamma H}{c_u} = \frac{(15.3 \times 1.75)}{60} = 0.45$$

For a square anchor, $F_c^\star = 11.9$. From Figure 3.11, $S \approx 1.75$. Using Equation 3.18:

$$F_{c0} = 1.75\{2.56 \ln[2(7.0)]\} = 11.82$$

Using Equation 3.19:

$$F_c = F_{c\gamma} = 11.82 + 0.45 = 12.27$$

Since $F_c > F_c^\star$, the anchor is deep, and using Equation 3.20:

$$Q_u = (60)(0.25 \times 0.25)(11.9) = \mathbf{44.6\ kN}$$

It is important to note that the study by Wang et al. (2010) shows that for square and circular deep anchors under immediate breakaway conditions, the maximum uplift capacity increases with soil elastic modulus. This fact suggests that the lower bound limit analysis and small-strain finite element analysis may overestimate the pullout capacity of horizontal plate anchors during vertical pullout. Therefore, for design purpose, it becomes important to reduce the estimated value of the ultimate uplift capacity suitably to arrive at the allowable ultimate uplift capacity.

3.6 FACTOR OF SAFETY

In most cases of anchor design, it is recommended that a factor of safety of 2 to 2.5 be used to arrive at the net allowable ultimate uplift capacity.

3.7 UPLIFT CAPACITY OF ANCHORS IN LAYERED SOIL

The uplift capacity of anchors embedded in a saturated clay layer overlain by a compact sand deposit was studied by Stewart (1985) using laboratory model tests. The basic conclusions of this study can qualitatively be summarized by referring to Figure 3.12. In Figure 3.12a, a plate anchor is embedded in a satu-

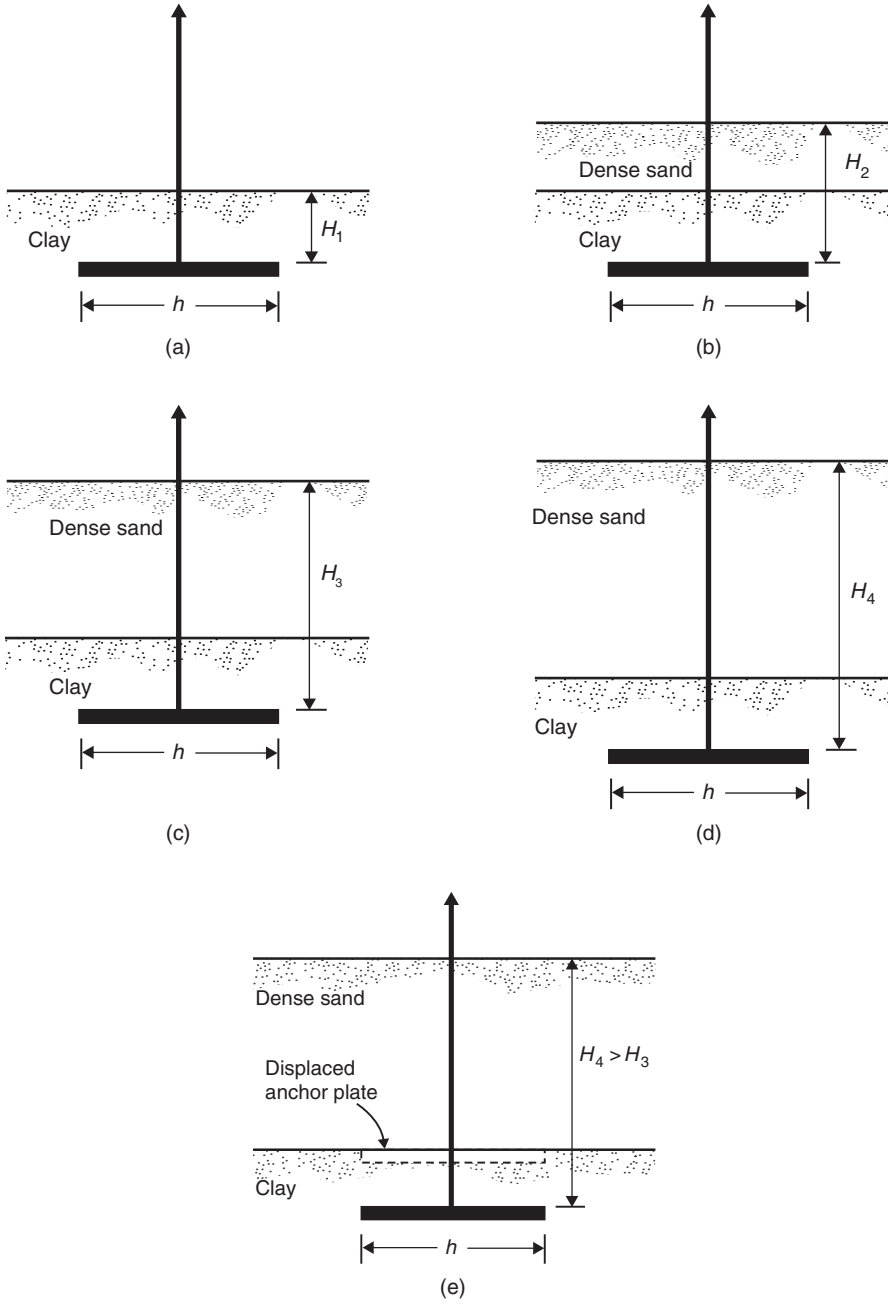

FIGURE 3.12 Plate anchor in saturated clay overlain by dense sand

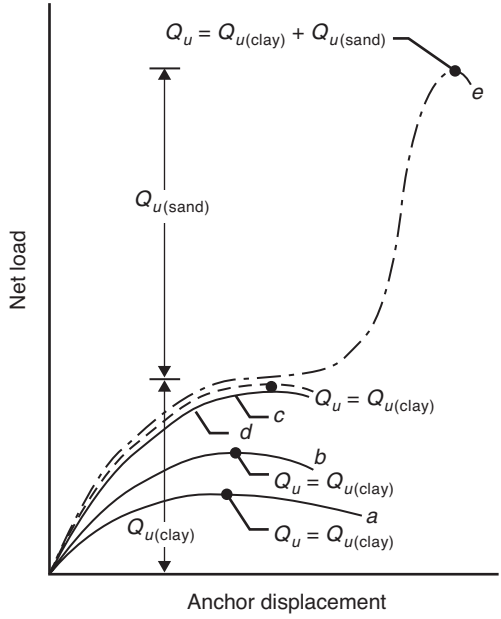

FIGURE 3.13 Nature of net load versus anchor displacement plots for plate anchor in clay overlain by dense sand

rated clay at a depth $H = H_1$. When subjected to an uplifting load, the nature of the plot of the net load Q versus anchor uplift Δ will be of the type shown by curve *a* in Figure 3.13. If H_1 is relatively small, then the failure surface will extend to the top of the clay layer, indicating a shallow anchor condition. If a layer of dense sand is now placed on the clay layer, the total thickness of the soil above the anchor will be equal to H_2 (Figure 3.12b). For this condition, the nature of the Q versus Δ plot will be as shown by curve *b* in Figure 3.13. For this condition, the sand acts as a surcharge on the clay layer and increases the net ultimate uplift capacity. If the thickness of the clay layer is gradually increased, depending on the relative value of c_u, the angle of friction of sand, γ_{clay}, and γ_{sand}, there will be a condition when the anchor will behave like a deep anchor located in clay. For this condition, let the thickness of the sand and clay above the anchor be equal to H_3, as shown in Figure 3.12c. Curve *c* in Figure 3.13 represents the Q versus Δ plot for this condition. If the thickness of the sand layer is further increased (Figure 3.12d) and an uplifting load is applied to the anchor, the load-displacement plot will follow the path shown by curve *d* in Figure 3.13, which is the same path as shown by curve *c* in Figure 3.13. However, if sufficient upward anchor displacement is allowed such that the anchor reaches

the top of the sand (Figure 3.12e), then the load resistance increases again and follows the path shown by curve *e* in Figure 3.13. Based on this, we can draw the following conclusions:

1. The sand overlay can significantly increase the net ultimate uplift capacity.
2. The net ultimate uplift capacity is composed of two parts:

$$Q_u = Q_{u(\text{clay})} + Q_{u(\text{sand})} \tag{3.22}$$

where

$Q_{u(\text{clay})}$ = clay component
$Q_{u(\text{sand})}$ = sand component

The magnitude of $Q_{u(\text{clay})}$ increases with H/h ratio up to a maximum value at $H/h = H_3/h$ (Figure 3.12c). A further increase in H/h has no effect on the magnitude of $Q_{u(\text{clay})}$. The sand component, $Q_{u(\text{sand})}$, is mobilized only when the anchor plate punches through the clay layer and reaches the sand-clay interface.

3.8 OTHER STUDIES

Some more analytical and numerical analyses have been carried out by researchers in the recent past to estimate the ultimate pullout load of horizontal plate anchors in clays.

Rowe and Davis (1982) reported a finite element study of the undrained behavior of horizontal anchor plates in homogeneous, isotropic saturated clay. This study shows that in many cases, ultimate collapse is preceded by significant anchor displacement, and therefore a definition of failure which allows reasonable displacement predictions to be made at working loads should be considered. They defined the failure load as the load which would give rise to a displacement four times that predicted by an elastic analysis. The failure loads defined on this basis are largely insensitive to elastic parameters of the soil and to the depth of soil beneath the anchor. It has been reported that for the limiting conditions of immediate or no breakaway of the soil behind the anchor, an anchor can be considered deep at an embedment ratio of 3 to 4; increasing the embedment beyond this has no effect on anchor capacity. Anchor capacity for the intermediate case in which breakaway occurs during loading is dependent on overburden pressure, which is a function of anchor depth. It was reported

that the anchor roughness was of little importance for shallow horizontal anchor plates. The anchor capacity of circular anchors was found to be up to twice that of a strip for very shallow anchors.

Merifield et al. (2001) applied numerical limit analysis to rigorously evaluate the stability of horizontal strip anchors in both homogeneous and inhomogeneous undrained clays. Rigorous bounds on the ultimate pullout capacity were obtained by using two numerical procedures that were based on finite element formulations of the upper and lower bound theorems of limit analysis. These formulations followed standard procedure by assuming a rigid perfectly plastic clay model with a Tresca yield criterion and generated large linear programming problems. The analysis considered the effect of anchor embedment depth, anchor roughness, material homogeneity, and overburden pressure. In this approach, the true pullout capacity can be bracketed by obtaining both upper and lower bound estimates of the pullout capacity. Results were presented for the case where no suction forces exist between the anchor and the soil, which constitutes what is known as the *immediate breakaway* condition. The study shows that for most cases they considered, the exact anchor capacity can be predicted to within $\pm 5\%$ using numerical finite element formulations of the lower and upper bound limit theorems. The ultimate capacity increases linearly with overburden pressure up to a limiting value, which reflects the transition from shallow to deep anchor behavior where the mode of failure becomes localized around the anchor. At a given embedment depth, an anchor may behave as shallow or deep, depending on the dimensionless overburden ratio $\gamma H/c_u$. The ultimate capacity of horizontal anchors is less affected by anchor roughness.

Song et al. (2008) studied the behavior of strip and circular plate anchors with fully attached and vented rear faces during vertical pullout in uniform and normally consolidated clays by means of small-strain and large-deformation finite element analyses. Suction behind the anchor was ignored for the vented case so that separation occurs when the normal stress reduces to zero. From small-strain analysis of fully attached anchors, the transitional embedment depth from shallow to deep failure mechanisms was found to be $(H/h)_{cr} = 2$ for strip anchors and $(H/h)_{cr} = 1$ for circular anchors. Soil unit weight had no effect on the pullout response of an attached anchor. The ultimate pullout capacity factors for deeply embedded and fully attached anchors were found to be $F_c^\star = 11.6$ and 11.7, respectively, for smooth and rough strip anchors; $F_c^\star = 13.1$ and 13.5 for smooth and rough circular anchors, both for a thickness ratio (thickness t of the anchor plate to its width or diameter h) of 0.05. In large-deformation analysis of plate anchors in uniform soil, the pullout response of an attached anchor formed a unique curve regardless of soil unit weight, soil strength, and

anchor size for any anchor embedded to a depth of at least half of the anchor size initially. However, the transitional embedment depth from shallow to deep embedment was reduced to $(H/h)_{cr} = 1.4$ for strip anchors and $(H/h)_{cr} = 0.75$ for circular anchors due to the soil heave formed during continuous pullout. For a vented anchor in uniform soil, the anchor broke away from the soil below the anchor at a certain embedment depth, called the separation embedment depth (H_s). The separation embedment depth ratio (H_s/h) was found to increase linearly with the undrained shear strength ratio of soil, $c_u/\gamma h$. When the anchor embedment reached H_s, the pullout capacity decreased rapidly and linearly. The increasing pullout capacity factor for an attached anchor during continuous pullout was due to the stronger soil from the initial embedment depth trapped around the anchor and also due to the increasing effect of soil weight above the anchor.

3.9 SUMMARY OF MAIN POINTS

1. Horizontal plate anchors are used in the construction of foundations in clays subjected to uplifting load.
2. In general, the breakout factor F_c increases with embedment depth ratio H/h up to a maximum value and remains constant thereafter. The embedment depth ratio H/h corresponding to the maximum F_c is called the critical embedment depth ratio $(H/h)_{cr}$, the lower and higher values of which categorize the anchors as shallow and deep, respectively.
3. Vesic's theory (1971) gives a closer estimate of the uplift capacity only for shallow horizontal plate anchors embedded in softer clays.
4. The critical embedment ratio $(H/h)_{cr}$ is a function of undrained shear strength c_u of clays.
5. The ultimate capacity of horizontal square, circular, or rectangular anchors is not likely to be affected noticeably by anchor roughness.
6. The breakout factors for square, circular, and rectangular anchors in weightless soil are always greater than those obtained for strip anchors at corresponding embedment ratios.
7. A rectangular anchor with an aspect ratio (length-to-width ratio) greater than 10 can be considered to behave essentially as a strip anchor.
8. The lower bound limit analysis and small-strain finite element analysis may overestimate the pullout capacity of horizontal plate anchors during vertical pullout.
9. The sand overlay on a clay layer can significantly increase the net ultimate uplift capacity of the horizontal plate anchor.

SELF-ASSESSMENT QUESTIONS

Select the most appropriate answer to each multiple-choice question

3.1. A horizontal plate anchor located at an embedment depth ratio greater than the critical embedment depth ratio is called:
   a. a shallow anchor
   b. a deep anchor
   c. an inclined anchor
   d. none of the above

3.2. For undrained clays, the angle of internal friction is equal to:
   a. 0°
   b. 45°
   c. 90°
   d. 180°

3.3. According to Meyerhof's theory (1973), the critical embedment depth ratio for horizontal circular plate anchors in clays is approximately:
   a. 7.5
   b. 8.0
   c. 9.0
   d. 13.5

3.4. For a given embedment depth ratio, a horizontal strip anchor in clay has a breakout factor of 3. Which of the following can be a possible value of the breakout factor for a horizontal circular anchor for the same embedment depth ratio and the same clay:
   a. 1
   b. 2
   c. 3
   d. 4

3.5. Select the correct statement:
   a. The ultimate pullout capacity of horizontal square, circular, or rectangular anchors is likely to be affected noticeably by anchor roughness
   b. The ultimate pullout capacity of only horizontal square anchors is likely to be affected noticeably by anchor roughness
   c. The ultimate pullout capacity of horizontal square, circular, or rectangular anchors is not likely to be affected noticeably by anchor roughness
   d. The ultimate pullout capacity of vertical square, circular, or rectangular anchors is not likely to be affected noticeably by anchor roughness

3.6. In most cases of anchor design, the recommended factor of safety is about:
   a. 1 to 1.5
   b. 2 to 2.5
   c. 3 to 3.5
   d. 4 to 5.5

3.7. Das's theory (1978) is applicable to:
   a. circular anchors only
   b. square anchors only
   c. rectangular anchors only
   d. circular, square, and rectangular anchors

3.8. The breakout factor for a deep rectangular anchor (width = h, length = B) is:
   a. directly proportional to (h/B)
   b. directly proportional to $(h/B)^2$
   c. inversely proportional to (h/B)
   d. inversely proportional to $(h/B)^2$

3.9. According to three-dimensional lower bound solution, the limiting value of the breakout factor for circular anchors is approximately:
   a. 0
   b. 11.9
   c. 12.56
   d. none of the above

3.10. With the presence of a sand overlay on the clay layer, the net ultimate uplift capacity of a horizontal plate anchor:
   a. decreases
   b. increases
   c. becomes extremely small
   d. remains unaffected

Answers

3.1: b 3.2: a 3.3: a 3.4: d 3.5: c 3.6: b 3.7: d 3.8: a 3.9: c 3.10: b

REFERENCES

Adams, J.I. and Hayes, D.C. (1967). The uplift capacity of shallow foundations. *Ont. Hydro Res. Q.,* 19(1):1–13.

Ali, M. (1968). Pullout Resistance of Anchor Plates in Soft Bentonite Clay, M.S. thesis, Duke University, Durham, NC.

Bhatnagar, R.S. (1969). Pullout Resistance of Anchors in Silty Clay, M.S. thesis, Duke University, Durham, NC.

Das, B.M. (1978). Model tests for uplift capacity of foundations in clay. *Soils Found.,* 18(2):17–24.

Das, B.M. (1980). A procedure for estimation of ultimate uplift capacity of foundations in clay. *Soils Found.,* 20(1):77–82.

Kupferman, M. (1971). The Vertical Holding Capacity of Marine Anchors in Clay Subjected to Static and Cyclic Loading, M.S. thesis, University of Massachusetts, Amherst.

Merifield, R.S., Sloan, S.W., and Yu, H.S. (2001). Stability of plate anchors in undrained clay. *Geotechnique,* 51(2):141–153.

Merifield, R.S., Lyamin, A.V., Sloan, S.W., and Yu, H.S. (2003). Three-dimensional lower bound solutions for stability of plate anchors in clay. *J. Geotech. Geoenviron. Eng.,* 129(3):243–253.

Meyerhof, G.G. (1973). Uplift resistance of inclined anchors and piles. *Proc. VIII Int. Conf. Soil Mech. Found.,* Moscow, 167–172.

Rowe, R.K. and Davis, E.H. (1982). The behaviour of anchor plates in clay. *Geotechnique,* 31(1):9–23.

Song, Z., Hu, Y., and Randolph, F. (2008). Numerical simulation of vertical pullout of plate anchors in clay. *J. Geotech. Geoenviron. Eng.,* 134(6):866–875.

Stewart, W. (1985). Uplift capacity of circular plate anchors in sand. *Can. Geotech. J.,* 22(4):589–592.

Vesic, A.S. (1971). Breakout resistance of objects embedded in ocean bottom. *J. Soil Mech. Found. Div. ASCE,* 97(9):1183–1205.

Wang, D., Hu, Y., and Randolph, M.F. (2010). Three-dimensional large deformation finite-element analysis of plate anchors in uniform clay. *J. Geotech. Geoenviron. Eng.,* 136(2):355–365.

4

VERTICAL PLATE ANCHORS

In this chapter, the holding capacity of vertical anchors is analyzed in detail. A number of theoretical and experimental studies conducted to define the actual failure surface in soil around an anchor at ultimate load also are included. The discussion is divided into two major parts: behavior of anchors in sand and behavior of anchors in clay (undrained condition).

4.1 INTRODUCTION

The use of vertical plate anchors to resist horizontal loading in the construction of sheet pile walls was discussed in Chapter 1 (see Figure 1.4). Inadequate design of anchors has been the cause of failure of many sheet pile walls. Sheet pile walls are flexible structures, and due to the outward bulging of these walls, the lateral earth pressure produced is quite different than that calculated for rigid structures using the classical Rankine or Coulomb earth pressure theories. In conducting laboratory measurements, Rowe (1952) showed that the bending moment to which an anchored sheet pile wall is subjected can be substantially reduced when the anchor movement is less than about 0.1% of the height of the wall. The movement of 0.1% of the anchor includes the elongation of the tie-rod connecting the vertical plate anchors and the wall. Hence, it is important to properly estimate the ultimate and allowable holding capacities of plate anchors

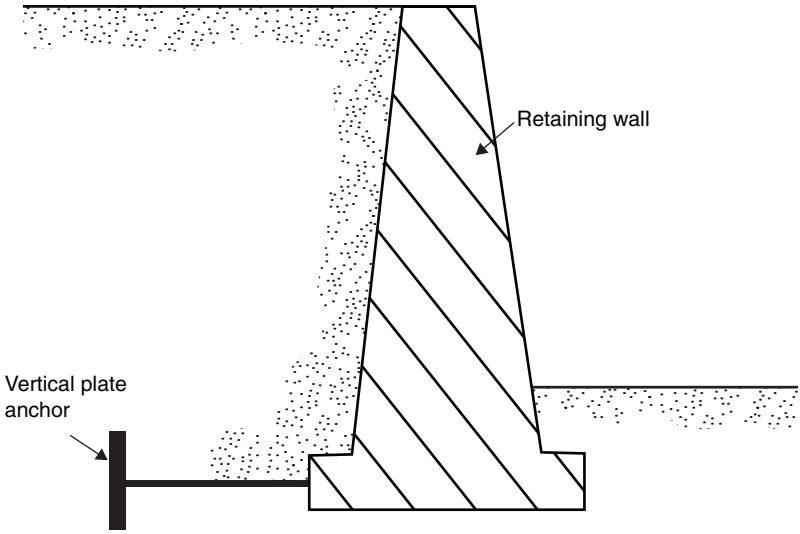

FIGURE 4.1 Vertical plate anchor at the base of a retaining wall to resist sliding

and also the corresponding displacements. Vertical plate anchors can also be used at pressure pipeline bends, at the base of retaining walls to resist sliding (Figure 4.1), and also where it is necessary to control thermal stresses.

Figure 4.2 shows the geometric parameters of a vertical anchor plate. The height and width of the anchor plate are h and B, respectively. The depth of the embedment of the anchor plate (that is, the distance from the ground surface to the bottom of the plate) is H. In most practical cases, the anchor can be considered as a strip anchor (two-dimensional plane strain case) if the B/h ratio is greater than about 6.

The holding capacity of an anchor is primarily derived from the passive force imposed by the soil in front of the anchor slab. If the embedment ratio H/h of the anchor is relatively small, at ultimate pullout load on the anchor the passive failure surface developed in soil in front of the anchor will intersect the ground surface. This is referred to (as in the case of horizontal anchors, discussed in Chapters 2 and 3) as the *shallow anchor condition*. Figure 4.3 shows the failure surface in front of a shallow square plate anchor (that is, $h = B$) embedded in sand as observed by Hueckel (1957). At greater embedment ratios, the *local shear failure* in soil will take place at ultimate load, and these anchors are called *deep anchors*. Thus the ultimate holding capacity Q_u is a function of several parameters:

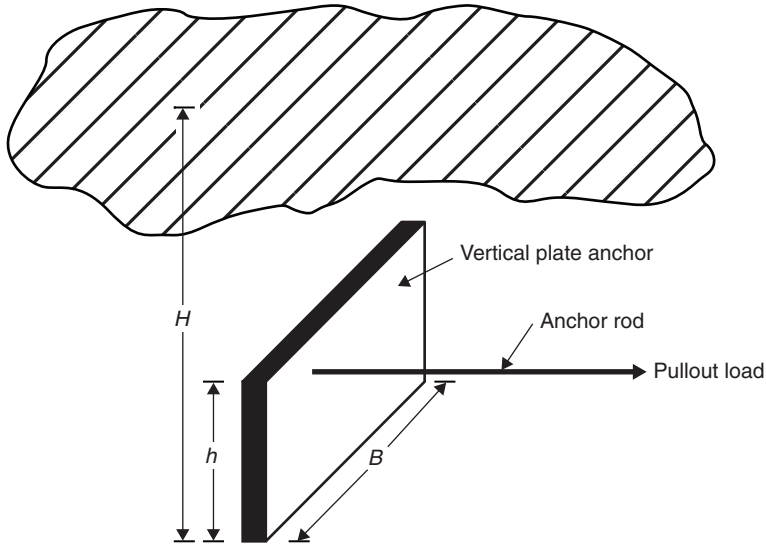

FIGURE 4.2 Geometric parameters of a vertical plate anchor

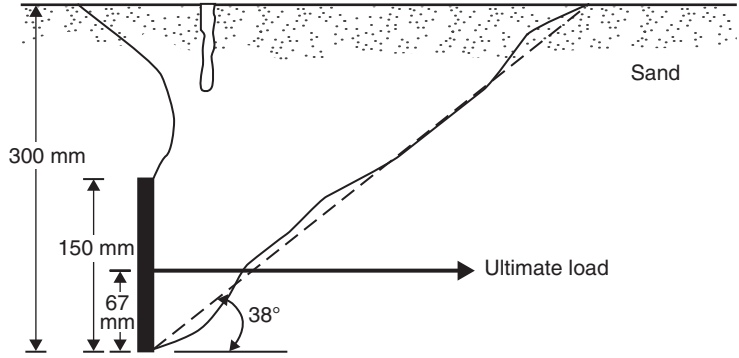

FIGURE 4.3 Failure surface in front of a square anchor slab (150 mm × 150 mm) embedded in sand at $H/h = 2$ (soil friction angle $\phi = 34°$) as observed by Hueckel (1957)

1. H/h ratio
2. Width-to-height ratio, B/h
3. Shear strength parameters of the soil (soil friction angle, ϕ, and cohesion, c)
4. The angle of friction of the anchor-soil interface, δ

It is important to note that for vertical anchors, the gross ultimate holding capacity $Q_{u(g)}$ is equal to the net ultimate holding capacity Q_u.

4.2 ANCHORS IN SAND

4.2.1 Ultimate Holding Capacity from Rankine's Theory

One of the earlier methods for estimation of the holding capacity of vertical anchors used the theory of *Rankine's lateral earth pressure* (Teng, 1962). Figure 4.4a shows a vertical strip anchor embedded in a granular soil, at a relatively shallow depth. The relatively *shallow depth condition* refers to the case where

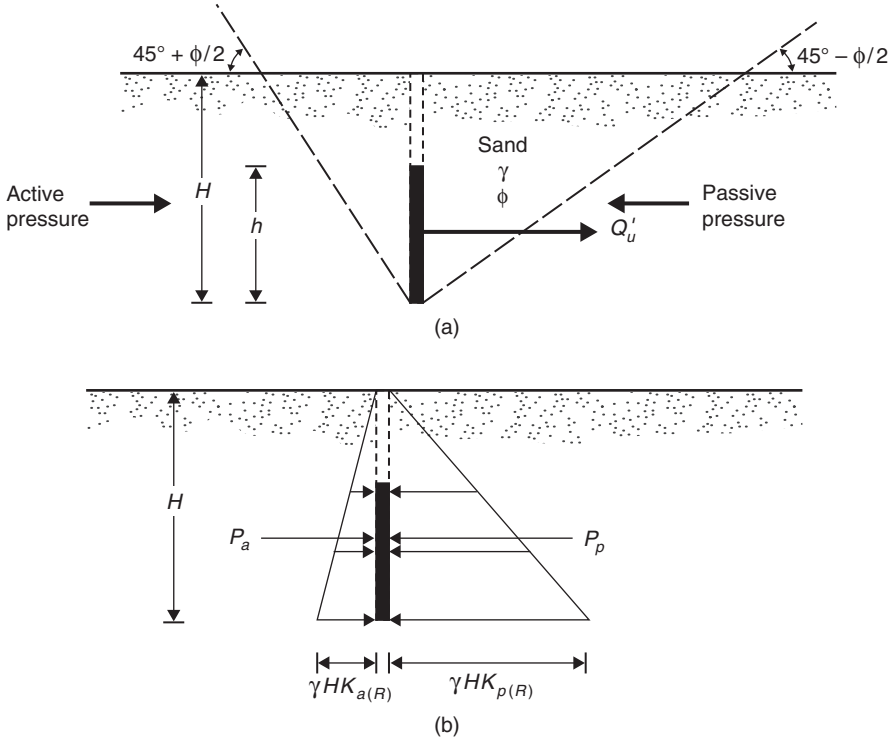

FIGURE 4.4 Ultimate holding capacity of strip vertical anchor as derived by Teng (1962)

$h/H < ⅓$ to ½. Assuming that the Rankine state exists, the failure surface in soil around the anchor at ultimate load also is shown in Figure 4.4a.

According to this procedure, for a strip anchor, the ultimate holding capacity per unit width (that is, at right angles to the cross section shown in Figure 4.4b) can be given as:

$$Q'_u = P_p - P_a \tag{4.1}$$

where

Q'_u = ultimate holding capacity per unit width
P_p = passive force in front of the anchor per unit width (Figure 4.4b)
P_a = active force at the back of the anchor per unit width (Figure 4.4b)

The relationships for P_p and P_a are as follows:

$$P_p = \frac{1}{2}\gamma H^2 \tan^2\left(45° + \frac{\phi}{2}\right) \tag{4.2a}$$

$$P_a = \frac{1}{2}\gamma H^2 \tan^2\left(45° - \frac{\phi}{2}\right) \tag{4.2b}$$

where

γ = unit weight of soil
ϕ = soil friction angle
$\tan^2\left(45° + \frac{\phi}{2}\right) = K_{p(R)}$ = Rankine passive earth pressure coefficient
$\tan^2\left(45° - \frac{\phi}{2}\right) = K_{a(R)}$ = Rankine active earth pressure coefficient

For anchors with a limited width B, the frictional resistance developed along the vertical faces of the failure surface must be taken into account (Figure 4.5). Following the procedure of Teng (1962), the total earth pressure normal to *abc* and *def* is

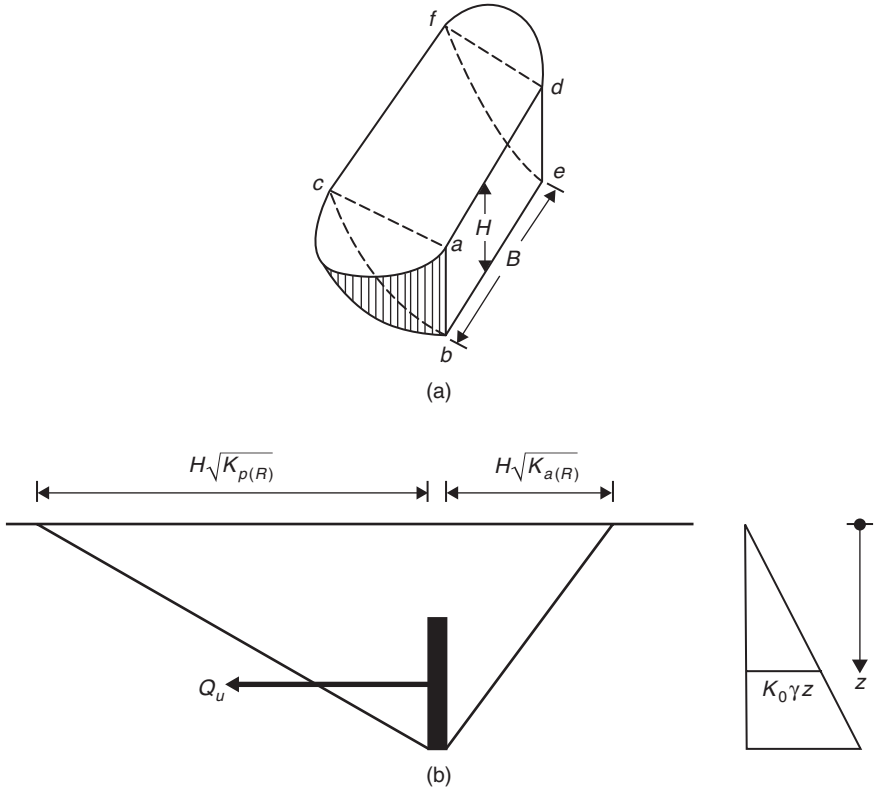

FIGURE 4.5 Frictional resistance developed along the vertical faces of the failure surface: Teng's method (1962)

$$N = 2\int_0^H \left(\frac{H - z}{H}\right)\left[H\sqrt{K_{p(R)}} + H\sqrt{K_{a(R)}}\right](dz)\,(\gamma K_0)$$

$$= \frac{1}{3}K_0\gamma\left[\sqrt{K_{p(R)}} + \sqrt{K_{a(R)}}\right]H^3 \qquad (4.3a)$$

where

K_0 = earth pressure coefficient at rest ≈ 0.4

Hence, the total frictional resistance at the ends is

$$F = N \tan \phi = \frac{1}{3} K_0 \left[\sqrt{K_{p(R)}} + \sqrt{K_{a(R)}} \right] H^3 \tan \phi \qquad (4.3b)$$

Hence, the ultimate holding capacity can be given as:

$$Q_u = Q'_u B + F$$

$$= B(P_p - P_a) + \frac{1}{3} K_0 \left[\sqrt{K_{p(R)}} + \sqrt{K_{a(R)}} \right] H^3 \tan \phi \qquad (4.4)$$

Example 4.1

For a vertical plate anchor, assume the following values: $h = 2$ ft, $B = 5$ ft, $H = 4$ ft, $\gamma = 105$ lb/ft^3, and $\phi = 32°$. Determine the ultimate holding capacity, Q_u.

Solution

$$K_{p(R)} = \tan^2 \left(45° + \frac{\phi}{2} \right) = \tan^2 \left(45° + \frac{32°}{2} \right) = 3.25$$

$$K_{a(R)} = \tan^2 \left(45° - \frac{\phi}{2} \right) = \tan^2 \left(45° - \frac{32°}{2} \right) = 0.307$$

$$P_p = \frac{1}{2} \gamma H^2 K_{p(R)} = \left(\frac{1}{2} \right) (105) (4)^2 (3.25) = 2730 \text{ lb/ft}$$

$$P_a = \frac{1}{2} \gamma H^2 K_{a(R)} = \left(\frac{1}{2} \right) (105) (4)^2 (0.307) = 257.9 \text{ lb/ft}$$

$$F = \frac{1}{3} K_0 \gamma \left[\sqrt{K_{p(R)}} + \sqrt{K_{a(R)}} \right] H^3 \tan \phi$$

$$= \left(\frac{1}{3} \right) (0.4) (105) \left(\sqrt{3.25} + \sqrt{0.307} \right) (4)^3 \tan 32°$$

$$= 699.25 \text{ lb}$$

Therefore:

$$Q_u = B(P_p - P_a) + F = (5)(2730 - 257.9) + 699.25 \approx \mathbf{13{,}060\ lb}$$

4.2.2 Analysis of Ovesen and Stromann

In 1964, Ovesen reported the results of several model tests conducted for shallow anchors in sand at the Danish Geotechnical Institute. The method of analysis developed in this section (Ovesen and Stromann, 1972) is primarily based on those model tests and also on the following concepts:

1. Determination of the holding capacity per unit width of a continuous anchor plate, $Q'_{u(B)}$, of height H, as shown in Figure 4.6a. This is known as the *basic case.*

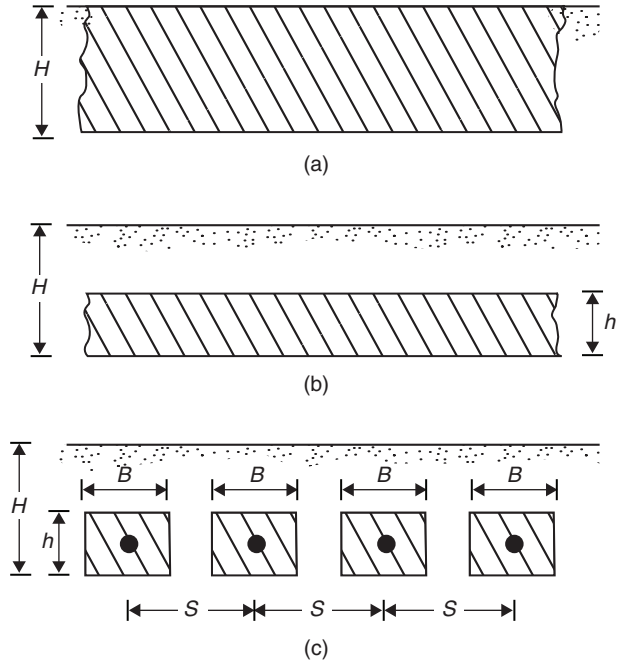

FIGURE 4.6 Ovesen and Stromann's analysis (1972): (a) basic case, (b) strip case, and (c) actual case

2. Estimation of the holding capacity per unit width of an anchor whose height is h (Figure 4.6b) and has an embedment depth of $H (h \leq H)$. This is known as the *strip case*.
3. Estimation of the holding capacity of an anchor with limited width-to-height ratio, B/h (Figure 4.6c). This is known as the *actual case*.

4.2.2.1 Basic Case

Figure 4.7 shows the basic case for a vertical anchor embedded in sand. The assumed failure surface in soil for translation of the anchor at ultimate load $Q'_{u(B)}$ (load per unit width) is also shown in this figure. For a rough anchor surface, P_a is the active force per unit width. The horizontal and vertical components of P_a can be given as:

$$P_{a(H)} = P_a \cos \phi \tag{4.5}$$

$$P_{a(V)} = P_a \sin \phi \tag{4.6}$$

where

$P_{a(H)}$, $P_{a(V)}$ = horizontal and vertical components of P_a, respectively
ϕ = soil friction angle

The passive failure surface in front of the anchor slab consists of (a) straight rupture line *BC*, (b) Prandtl radial shear zone *ACD*, and (c) Rankine passive zone *ADE*. (Note: Angles *EAD* and *AED* are both equal to $45° - \phi/2$).

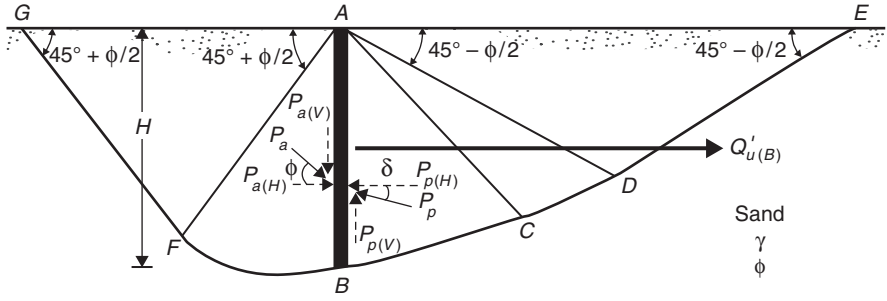

FIGURE 4.7 Basic case for failure surface at ultimate load

The horizontal and vertical components of the passive force P_p are

$$P_{p(H)} = \frac{1}{2}\gamma H^2 K_{pH} \tag{4.7}$$

$$P_{p(V)} = \frac{1}{2}\gamma H^2 K_{pH} \tan\delta \tag{4.8}$$

where

γ = unit weight of the soil
K_{pH} = horizontal component of the passive earth pressure coefficient
δ = anchor-soil friction angle

For vertical equilibrium:

$$P_{a(V)} + W = P_{p(V)} \tag{4.9}$$

where

W = weight of anchor per unit width

From Equations 4.8 and 4.9:

$$K_{pH} \tan\delta = \frac{P_{a(V)} + W}{\frac{1}{2}\gamma H^2} \tag{4.10}$$

Figure 4.8 shows the variation of $K_{pH} \tan\delta$ and ϕ from which K_{pH} can be estimated. Now, for horizontal equilibrium:

$$Q'_{u(B)} = P_{p(H)} - P_{a(H)} = \frac{1}{2}\gamma H^2 K_{pH} - P_{a(H)} \tag{4.11}$$

The magnitudes of $P_{a(V)}$ and $P_{a(H)}$ can be determined using any ordinary active earth pressure theory. Figure 4.9 shows the variation of the active earth pressure coefficient K_a according to Caquot and Kerisel (1949). Note that:

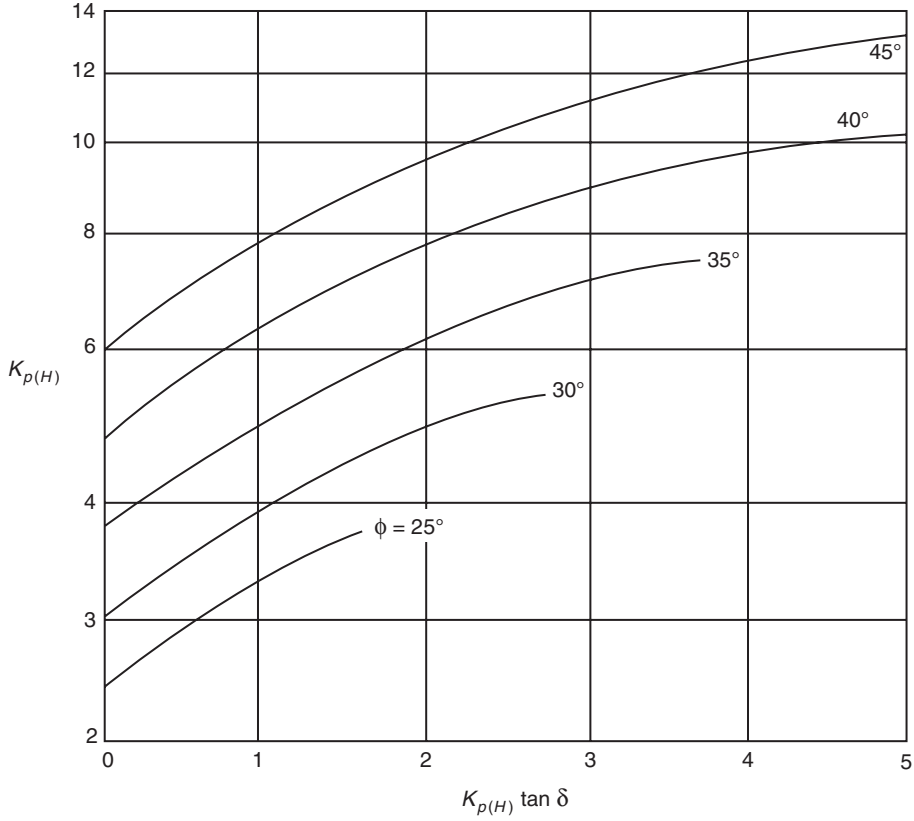

FIGURE 4.8 Variation of $K_{p(H)}$ with $K_{p(H)}$ tan δ and ϕ (after Ovesen and Stromann, 1972)

$$P_a = \frac{1}{2}\gamma H^2 K_a \tag{4.12}$$

4.2.2.2 Strip Case

Based on the experimental evidence of Ovesen (1964), the ultimate holding capacity of a *strip anchor* can be given as:

$$Q'_u = R_{ov} Q'_{u(B)} \tag{4.13}$$

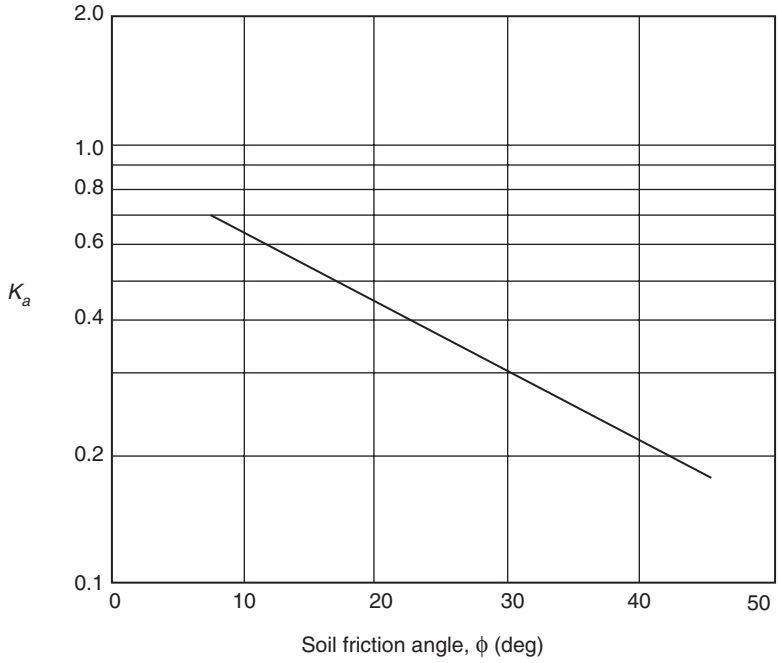

FIGURE 4.9 Variation of K_a with ϕ

where

Q'_u = ultimate holding capacity per unit width for strip anchor

The variation of R_{ov} with the ratio h/H is shown in Figure 4.10. Note that:

$$R_{ov} = \frac{C_{ov} + 1}{C_{ov} + \dfrac{H}{h}} \tag{4.14}$$

where

C_{ov} = 19 for dense sand and 14 for loose sand

Equation 4.14 was developed by Dickin and Leung (1985) from Figure 4.10.

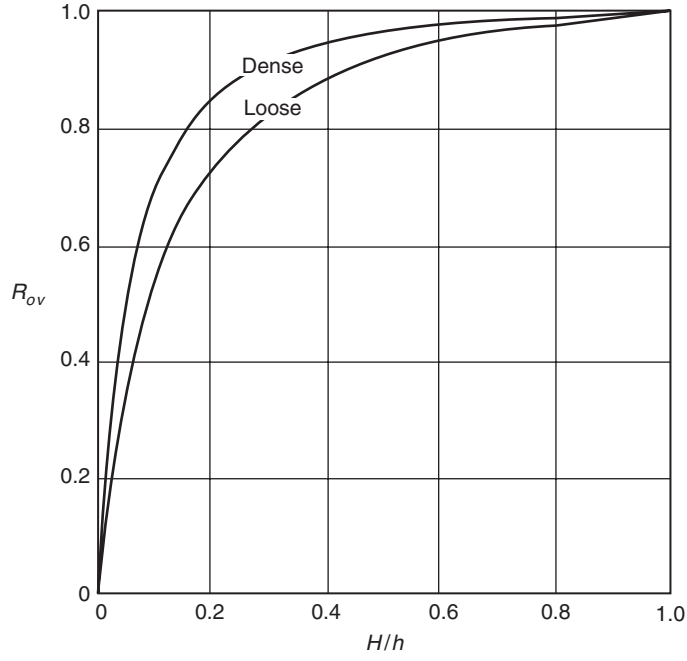

FIGURE 4.10 Variation of R_{ov} with H/h (after Ovesen and Stromann, 1972)

4.2.2.3 Anchor with Limited B/h Ratio (Actual Case)

When an anchor has a limited width-to-height ratio (B/h), the failure surface in soil will be three-dimensional, as shown in Figure 4.5. Hence, the ultimate holding capacity of an anchor, Q_u, can be given by Equation 4.4 as $Q_u = Q'_u + F$. However, if a number of vertical anchors are used in a row, depending on the S/B ratio (S = center-to-center spacing of the anchor, as shown in Figure 4.11), the failure surface may overlap. In that case, $Q_u = Q'_u B + F'$, where F' is the friction resistance $\leq F$.

Hueckel (1957) conducted a number of laboratory model tests on three square anchors (Figure 3.11) to determine the S/B ratio at which $F = F'$, and these results are shown in Figure 4.12. Note that Q_{ug} is the notation for the holding capacity of the anchor group. In this case, the group consists of three anchors, each measuring 100 mm × 100 mm. From this figure, it can be seen that at $S/B \approx 3$ to 4, the effect of interference practically disappears.

Ovesen and Stromann (1972) expressed Q_u as:

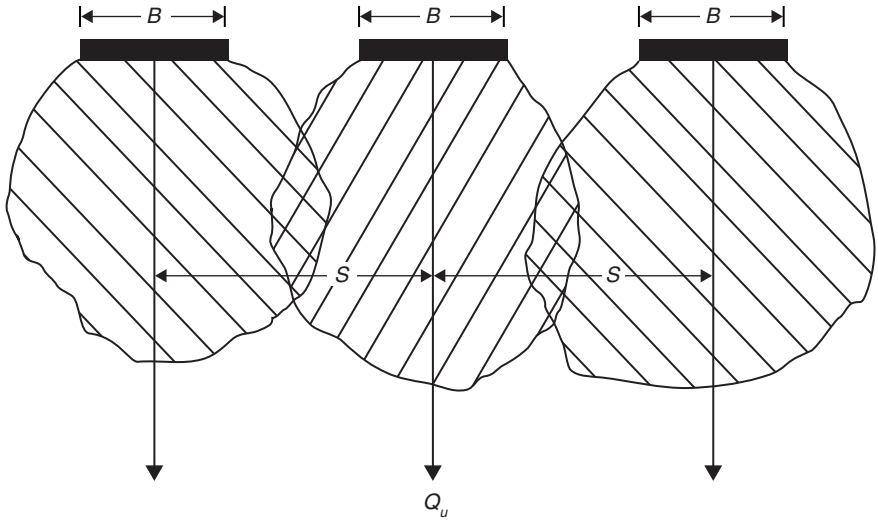

FIGURE 4.11 Overlapping of failure surface in soil in front of a row of vertical anchors

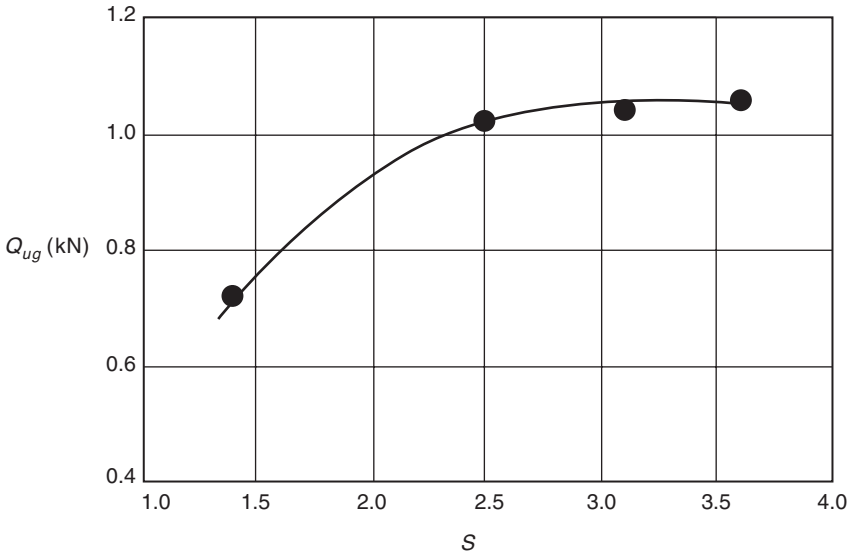

FIGURE 4.12 Variation of the ultimate group capacity with center-to-center spacing of anchor as observed by Hueckel (1957) ($B = h = 100$ mm, $H/h = 2$, number of anchors = 3, $\phi = 36°$)

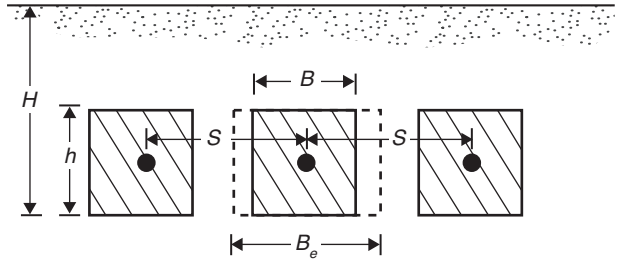

FIGURE 4.13 Definition of equivalent width

$$Q_u = Q'_u B_e \tag{4.15}$$

where

B_e = equivalent width $\leq B$ (Figure 4.13)

The variation of B_e can be obtained from Figure 4.14.

In the case of a single anchor (that is, $S = \infty$), we can also write that:

$$Q_u = Q'_u B S_f \tag{4.16}$$

where

$S_f = B_e/B$ = shape factor

From Figure 4.14, it can be shown that with $S = \infty$ (also see Dickin and Leung, 1983):

$$S_f = 0.42 \left(\frac{\frac{H}{h} + 1}{\frac{B}{h}} \right) + 1 \qquad \text{(for dense sand)} \tag{4.17}$$

and

$$S_f = 0.26 \left(\frac{\frac{H}{h} + 1}{\frac{B}{h}} \right) + 1 \qquad \text{(for loose sand)} \tag{4.18}$$

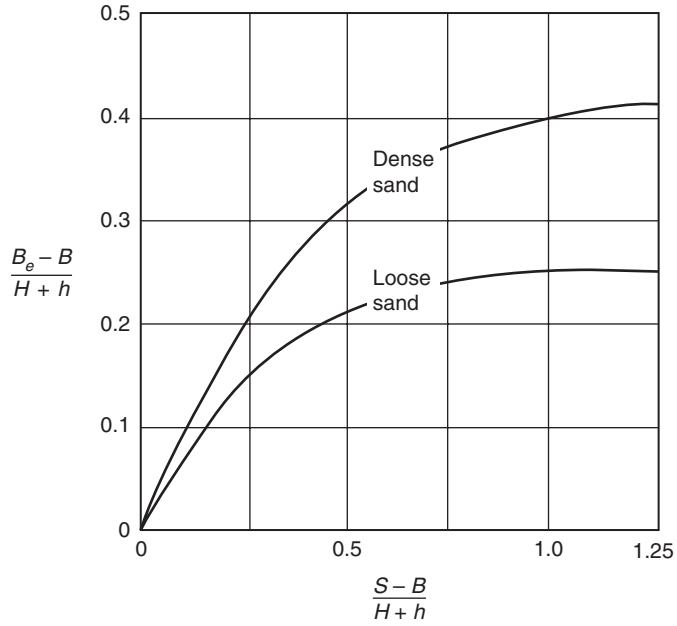

FIGURE 4.14 Variation of $(B_e - B)/(H + h)$ with $(S - B)/(H + h)$ (after Ovesen and Stromann, 1972)

Hence, for single anchors with limited width-to-height ratio, combining Equations 4.11, 4.14, 4.17, and 4.18, we obtain:

$$Q_u = B\left[\frac{1}{2}\gamma H^2 K_{pH} - P_{a(H)}\right]\left(\frac{C_{ov} + 1}{C_{ov} + \frac{H}{h}}\right) \times \left[F\left(\frac{\frac{H}{h} + 1}{\frac{B}{h}}\right) + 1\right] \tag{4.19}$$

where for dense sand $C_{ov} = 19$ and $F = 0.42$, and for loose sand $C_{ov} = 14$ and $F = 0.26$.